TECHNISCHE UNIVERSITÄT WIEN
Vienna | Austria

institute of telecommunications

DISSERTATION

Signal Processing for Fourth Generation Wired Broadband Access Networks

Conducted for the purpose of receiving the academic title
"Doktor der technischen Wissenschaften"

Sanda Drakulić, MSc.
born in Zagreb, Croatia, Sept. 27th, 1986
Matriculation number: 1028381
Siebenbrunnengasse 66/27, 1050 Vienna

March 20, 2017 ....

Submitted to the TU Wien, Faculty of Electrical Engineering and Information Technology

Advisor

Univ.Prof. Ing. Dipl.-Ing. Dr.-Ing. Christoph Mecklenbräuker
TU Wien, Austria
Institute of Telecommunications

Examiners

Prof. Dr. Per Ödling
Lund University, Sweden
Prof. Dr. Tomas Nordström
Halmstad University, Sweden

to my grandfather Milorad

ABSTRACT

With the demand for more bandwidth, driven by the end user requirements and the competition among network operators, it is inevitable that fibre-to-the-home (FTTH) deployments will become reality for most customers. However, FTTH represents an expensive and slow solution for delivering broadband speeds due to the expensive labour, scattered population, problems with home fiber wiring, and slow roll-outs. As an FTTH alternative, hybrid fiber-copper access is proposed where fiber is brought as close as possible to housing complexes and then existing twisted copper cables are used to bridge the last 20 to 250 m. Currently deployed copper-based technologies, i.e., digital subscriber line (DSL), are capable of delivering up to 100 Mbps over 17 MHz spectrum and long loop lengths (up to 1 km). For delivering even higher (broadband) bit-rates the International Telecommunication Union (ITU) has standardized in 2014 a new (fourth) DSL technology, called G.fast, which extends bandwidth up to 212 MHz and allows network operators to deliver speeds of up to 1 Gbps over short copper wires ($<$250 m). Furthermore, crosstalk cancellation (also known as vectoring) represents a mandatory feature for G.fast to achieve the foreseen bit-rates.

In the first part of this thesis, I address the issues relevant to ITU, i.e., I focus on the achievable bit-rates of both linear and non-linear vectoring schemes for the 212 MHz profile in order to show which vectoring scheme is more suitable for 212 MHz profile. More precisely, the ITU has agreed that for the lower-bandwidth profile (up to 106 MHz) linear vectoring schemes will be used whereas there is an ongoing discussion whether linear or non-linear vectoring schemes shall be used for the 212 MHz profile. I also take into account the impact of channel state information (CSI) errors since vectoring efficiency heavily depends on the CSI accuracy. Simulation results reveal that even with 99.9 % accurate channel estimation bit-rate losses are considerably high (for realistic scenarios up to 18 % loss compared to bit-rates under perfect CSI). Furthermore, vectoring requires joint signal processing among the users at the receiver side for upstream transmission or at the transmitter side for downstream transmission. However, in many deployment scenarios joint signal processing is feasible among groups of users only, referred to as partial vectoring. For previous DSL systems, such as very high speed digital subscriber line 2 (VDSL2), spectrum coordination has been proposed to mitigate crosstalk originating among different groups. In this thesis I evaluate spectrum coordination for the case of partial vectoring in a G.fast-compliant simulation setup. I also propose interference alignment (IA) as an alternative to spectrum coordination and show that IA outperforms spectrum coordination when vectoring is not applied, most notably on spectrum above 100 MHz. However, simulations indicate that in case of partial vec-

toring for G.fast, a simple time division multiple access (TDMA) scheme outperforms both spectrum coordination and IA.

The replacement of currently deployed DSL technologies, such as VDSL2, by G.fast equipment will be gradual. Therefore the coexistence of G.fast and legacy DSL systems needs to be investigated before bringing the G.fast technology to the market. G.fast and VDSL2 have different modulation parameters (e.g., carrier spacing and sampling rate) as well as (possibly) asynchronous transmissions which leads to inter-carrier and inter-symbol interference (ICSI) and therefore makes vectoring between these two systems impractical. Second part of this thesis focuses on the question in which scenarios G.fast and legacy DSL produce negligible interference among them. For this purpose, I propose and investigate an analytical ICSI model for asynchronous discrete multi-tone (DMT) systems with various carrier spacings and sampling rates. I also combine the developed ICSI model with a CSI error model in order to obtain a joint performance model. A detailed simulation study is carried out on the impact of ICSI on G.fast and VDSL2 systems which shows that the bit-rate losses in G.fast and VDSL2 systems can be substantial compared to the interference-free performance. Furthermore, the influence of different VDSL2 transmit and receive filters is analyzed focusing on the required spectral separation between these two systems. Based on the investigated scenarios in this thesis, G.fast must start at frequencies above 23 MHz assuming high order filtering at VDSL2 transceivers for negligible interference between G.fast and VDSL2 systems.

ZUSAMMENFASSUNG

Der wachsende Bedarf nach mehr Bandbreite, bedingt durch steigende Nutzeranforderungen und Konkurrenz unter Netzbetreibern, kann langfristig nur durch die Verlegung von Glasfaserkabeln bis zum Endkunden (FTTH) gedeckt werden. Allerdings ist der FTTH-Ausbau aufgrund hoher Arbeitskosten, teils geringer Bevlkerungsdichten, und Erschwernissen in der Hausverkabelung langsam und teuer. Als FTTH-Alternative bieten sich hybride Telefonkabel-Glasfasernetze an. Dabei werden Glasfaserkabel bis nahe zu den Haushalten verlegt und die vorhandenen Kupferleitungen zur Überbrckung der letzten 20 bis 250 Meter genutzt. Herkömmliche Digital Subscriber Line (DSL) Technologien ermöglichen Datenraten von rund 100 Mbps ber ein 17 MHz breites Frequenzspektrum und Kabellängen von bis zu 1 km. Um noch höhere Datenraten (bis zu 1 Gbps) über kurze Kabellängen (<250 m) übertragen zu können hat die Internationale Fernmeldeunion (ITU) 2014 einen neuen (vierten) DSL-Standard namens G.fast verabschiedet. Der Kompensation des Übersprechens zwischen Leitungspaaren (vectoring) kommt bei G.fast eine zentrale Rolle zur Erfüllung der Bandbreitenziele zu. Die Entscheidung ob das zukünftige 212 MHz G.fast Profil lineare oder nichtlineare vectoring Methoden vorsieht ist noch offen. Des Weiteren hngt die Effektivität von vectoring Methoden von der Korrektheit der Kanalzustandsinformation (CSI) ab und erfordert eine gemeinsame Verarbeitung der Signale aller Leitungspaare auf der Sende- oder Empfangsseite. In vielen praktischen Anwendungen ist dies jedoch nur für gewisse Untergruppen von Leitungen möglich (partial vectoring). Das verbleibende Übersprechen zwischen den Untergruppen kann etwa mittels Koordinierung der Sendeleistungsspektren (DSM-L2) reduziert werden.

Diese Dissertation beschäftigt sich daher im ersten Teil mit der Simulation der erreichbaren Datenraten von linearen als auch nichtlinearen vectoring Algorithmen für das 212 MHz G.fast Profil unter Berücksichtigung möglicher Kanalschätzfehler. Meine Ergebnisse zeigen, dass auch kleine Kanalschätzfehlern hohe Datenratenverluste zur Folge haben. Weiters untersuche ich partial vectoring in G.fast und schlage Interference-Alignment (IA) als Alternative zu DSM-L2 vor. Es wird gezeigt dass IA DSM-L2 in Bezug auf die erreichbaren Datenraten übertrifft wenn vectoring nicht möglich ist, insbesondere für Frequenzen ber 100 MHz. Ist jedoch vectoring in den einzelnen Untergruppen möglich so stellt sich ein einfaches Zeitmultiplexverfahren als die bevorzugte Koordinationsmethode heraus.

Der Austausch gegenwrtig genutzter DSL Systeme wie VDSL2 durch G.fast wird schrittweise erfolgen. Damit ist die Untersuchung der Koexistenz beider Technologien vor der Markteinfhrung von G.fast unerlässlich. Unterschiede in Modulationsparametern wie

Trägerabstand und Abtastrate als auch Asynchronität verursachen Interferenzen zwischen Trägern und Symbolen (ICSI). Dies wiederum macht vectoring technisch schwer realisierbar. Der zweite Teil der Arbeit beschftigt sich daher mit der Frage unter welchen Bedingungen G.fast und bestehende DSL-Systeme dennoch frei von Interferenz operieren können. Dazu wird ein analytisches ICSI-Signalmodell entwickelt welches die Unterschiede in Modulationsparametern und Asynchronität berücksichtigt. Dieses wird in weiterer Folge mit einem CSI-Fehlermodell zu einem realistischen Leistungsmodell kombiniert. Eine detaillierte Simulationsstudie zeigt dass die potentiellen Datenratenverluste für G.fast und VDSL2 Systeme im Vergleich zur ICSI-freien Performanz erheblich sind. Des Weiteren wird der Einfluss von verschiedenen VDSL2 Sende- und Empfangsfiltern im Hinblick auf den erforderlichen spektralen Abstand zwischen den beiden Systemen analysiert. Die Simulationsergebnisse zeigen dass G.fast Systeme nur den Frequenzbereich über 23 MHz nutzen sollten um Interferenzen mit VDSL2 Systemen zu vermeiden.

ACKNOWLEDGEMENT

CONTENT

LIST OF FIGURES

LIST OF TABLES

1 INTRODUCTION

Telecommunication operators are examining the capabilities of various access networks to provide a high-speed fixed broadband service. In terms of transmission capacity, fiber-to-the-home (FTTH) networks outperform cable- and copper-twisted-pair-based networks. However, one of the drawbacks of FTTH networks is the cost of deploying fiber to each home, which can be quite high for some network scenarios [4–6]. Moreover, from the viewpoint of implementation, in some cases it can be problematic to roll out fiber in the last mile of the network because of the necessary approvals that are required, especially inside buildings and in customers' apartments. One possibility to overcome this issues is to reuse existing telephone/copper cables for the last mile resulting in a hybrid fiber-copper architecture. In such architectures fiber is rolled out as close as possible to the final user (e.g., up to the distribution point (Dp)) while the rest is then covered with twisted copper lines. Such hybrid architectures are referred to as fiber-to-the-distribution-point (FTTDp) or fiber-to-the-building (FTTB). Digital subscriber line (DSL) is the most widespread technology used over twisted pairs, for which the International Telecommunication Union (ITU) has up to today released four generations. The latest, G.fast, was approved by ITU at the end of 2014 [7, 8] and is exactly tailored for FTTDp/FTTB deployments. G.fast promises to bring aggregate (downstream and upstream) bit-rates up to 1 Gbps [9–11] over a single twisted-pair from the Dp to the customer premises equipment (CPE) over an extended frequency range of up to 106 MHz while in the future releases it is foreseen to additionally extend frequency range up to 212 MHz. The achievable bit-rate over a particular line depends, among other factors, on its length and wire type where the majority of installations are expected to be within 250 meters. By shortening the copper length and increasing the utilized bandwidth, the DSL crosstalk channel (i.e., interference) coupling will strengthen relative to the direct channel [12–14]. Due to this strong crosstalk between twisted copper pairs dynamic spectrum management (DSM) schemes, which mitigate or completely cancel crosstalk, are essential tools which enable G.fast achieving its promised bit-rates. Especially important and powerful is DSM-level 3 also known as vectoring which allows crosstalk cancellation and therefore enables targeted bit-rates by G.fast, cf. Figure 1.1.

There are two vectoring options available for G.fast: linear and non-linear vectoring. The
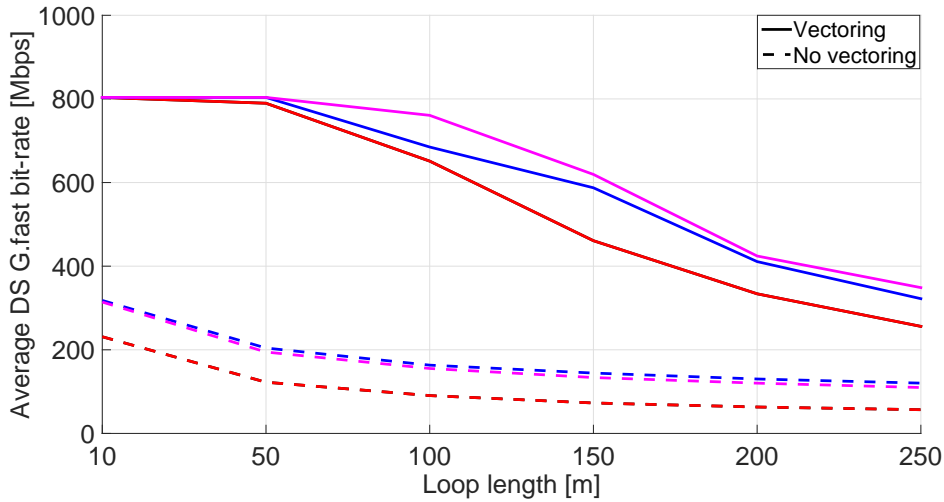
Figure 1.1: Vectoring vs. no vectoring downstream (DS) bit-rates for G.fast 106 MHz
            profile. Presented bit-rates are for linear vectoring and measurements data
            in the [3] (magenta), [2] (red), and [15] (blue).

first version of the G.fast standard (for frequencies up to 106 MHz) uses linear vectoring
schemes. There is still an ongoing discussion whether linear vectoring should also be
used for the future releases (for frequencies up to 212 MHz). Furthermore, the efficiency
of vectoring heavily relies on the accuracy of channel state information (CSI). Although
channel gains in copper access systems are quasi-stationary, they do exhibit dynamic
behaviour. Potentially sources of channel dynamics include slow changes in ambient
conditions [16] or sudden termination changes in coupled loops [17, 18].

Vectoring challenges such as implementation and computational complexity associated
with full signal coordination aries when the number of DSL lines is large or when they
are not co-located at any end. To resolve this problem, users can be divided into a
few vectoring groups. Crosstalk between users in each group (intra-group crosstalk)
can be eliminated using vectoring, however, crosstalk between users in different groups
(inter-group crosstalk) still remains. In legacy DSL systems partial vectoring is usually
combined with dynamic spectrum management level 1 and level 2 (DSM-L1 and DSM-
L2) [19–21] (cf. Section 3.4.2) in order to mitigate inter-group crosstalk while an efficient
crosstalk mitigation technique for partial vectoring in G.fast is still an open issue.

During the transmission process towards (potentially) exclusively G.fast deployments,
G.fast will share the access network with existing DSL systems, particularly with vec-
tored very high speed digital subscriber line 2 (VDSL2) [22]. However, G.fast and
vectored VDSL2 as specified by the ITU recommendations use overlapping spectrum
and different carrier spacing, sampling rates, and different multiplexing schemes (G.fast

uses time division duplex (TDD) while VDSL2 uses frequency division duplex (FDD)). Differences in modulation parameters along with potentially asynchronous transmission among different DSL technologies are source of inter-carrier and inter-symbol interference (ICSI) in DSL coexistence scenarios. ICSI makes crosstalk signals between different tones coupled together and consequently per-tone vectoring between the two systems impractical. In case when vectoring is not practical among all disturbing lines it has been shown that even few uncontrolled interferers can cause significant performance degradation [23–25]. Therefore, G.fast facilitates coexistence by providing a configurable power spectral density mask [8] and G.fast start frequencies [26, 27]. The right selection of these configurable parameters may be a crucial performance factor as shown in [26, 28].

This Chapter is organized as follows. Short history of DSL is given in Section 1.1. In Section 1.2 I describe the main motivation for this work and analyze related work, while in Section 1.3 I summarize the main research questions and objectives that are considered. In Section 1.4 I outline the organization and the contributions of this thesis.

1.1   A Brief History of DSL

The range of DSL technologies is quite broad, and therefore in this Section I briefly describe the different DSL technologies that have been developed or are currently under development. More precisely, I define various DSL generations (similarly as done in [6]) where each new generation was tailored to fulfill the demand for more bandwidth. First DSL generation is mainly based on integrated services digital network (ISDN) [29] which marked the start of data communication beyond dial-up modems. ITU standardized ISDN in 1993 which is able of delivering 128 kbps over a pair of standard telephone copper wires and frequencies up to 3.4 kHz.[1]. Both ISDN and the second DSL generation, which is mainly based on asymmetric DSL (ADSL) [30], are characterized by deployments from central office. As its name indicates, ADSL asymmetrically divides the bandwidth (and correspondingly the bit-rates) for the upstream and downstream transmissions. Due to the asymmetric performance, ADSL became the most popular DSL standard which was standardized by ITU in 1999. The upstream ADSL bands starts at 25 kHz and goes up to 138 kHz. The downstream ADSL band starts at 180 kHz and goes up to 1.104 MHz. ADSL is capable of delivering up to 8 Mbps in downstream and 1 Mbps in upstream. Important variants of ADSL include ADSL2 [31] and ADSL2+ [32] which extend the spectrum up to 1.1 MHz and 2.2 MHz, respectively, and consequently achieve higher bit-rates (i.e., 12 Mbps and 24 Mbps in downstream). Third DSL generation, very high

---

[1] ISDN can also deliver bit-rates of 144 kbps when additional signalling channel is used for data transmission.

speed DSL (VDSL), was standardized in 2004 with the maximum used frequency going up to 12 MHz for the first VDSL flavour (VDSL1) [33] and up to 30 MHz for the second VDSL flavour (VDSL2) [22]. VDSL1 promises downstream bit-rates of up to 52 Mbps while VDSL2 achievable bit-rates depend on the chosen spectrum profile. More precisely, VDSL2 has nine spectrum profiles (8a, 8b, 8c, 8d, 12a, 12b, 17a, 30a, and 35b) which differ based on the PSD, carrier spacing (i.e., Δf), and maximum used frequency. The ITU recommendation G.993.5 [34] defines self-FEXT (far-end crosstalk) cancellation in the downstream and upstream directions and therefore enables crosstalk-free bit-rates in both transmission directions. However, the VDSL2 30a carrier spacing (8.625 kHz) is different from the VDSL2 17a carrier spacing (4.3125 kHz) preventing vectoring between 17a and 30a VDSL2 lines. This makes upgrades of the existing 17a deployments to 30a unattractive as it would require a full swap of the installed VDSL2 CPE base. Vplus (i.e., VDSL2 35b) overcomes this limitation by using the same tone spacing as 17a. This allows vectoring across Vplus and 17a lines, and thus mixed deployments and a smooth introduction of Vplus which delivers downstream speeds exceeding 300 Mbps.

DSL access networks are slowly evolving to exclusively high-speed fiber networks such as FTTH. However, given the extensive volume of copper lines already in place, and the lower cost of DSL systems, it may take several years before incumbent copper lines are replaced with fibre [4–6]. Hybrid fiber-copper solutions represent an attractive solution for network providers, allowing for a gradual introduction of fiber. More precisely, fiber is deployed step by step closer to the final user while in the residual part of the access network copper lines are used. Consequently, each new DSL standard was further extending the used spectrum and was tailored for shorter loop lengths in order to provide higher bit-rate service. The latest (i.e., fourth) DSL generation, G.fast [7], was standardized in 2014 and is targeting aggregate (upstream and downstream) bit-rates of up to 1 Gbps over a maximum loop length of 250 m. The first version of G.fast specifies a 106 MHz profiles, with another 212 MHz profile planned for the future. Due to the propagation characteristics, higher frequencies as used by G.fast necessitate the deployment from a distribution point (Dp), i.e., FTTDp. However, in the future the fiber will further penetrate into the existing access network and consequently shorter the copper lines allowing for an even higher frequency span then is currently used by G.fast. XG-Fast [35] is the (upcoming) fifth DSL generation which will potentially extend the frequency spectrum above 500 MHz. It will target FTTB deployment scenarios and bit-rates up to 10 Gbps over very short (<50 m) copper lines. Therefore, XG-Fast would complement fiber and next-generation 5G wireless networks and would be a further evolution of the G.fast standard. Figure 1.2 illustrates graphically the evolution of DSL access network.

G.fast can be seen as a logical evolution of VDSL2 but there are some implementation
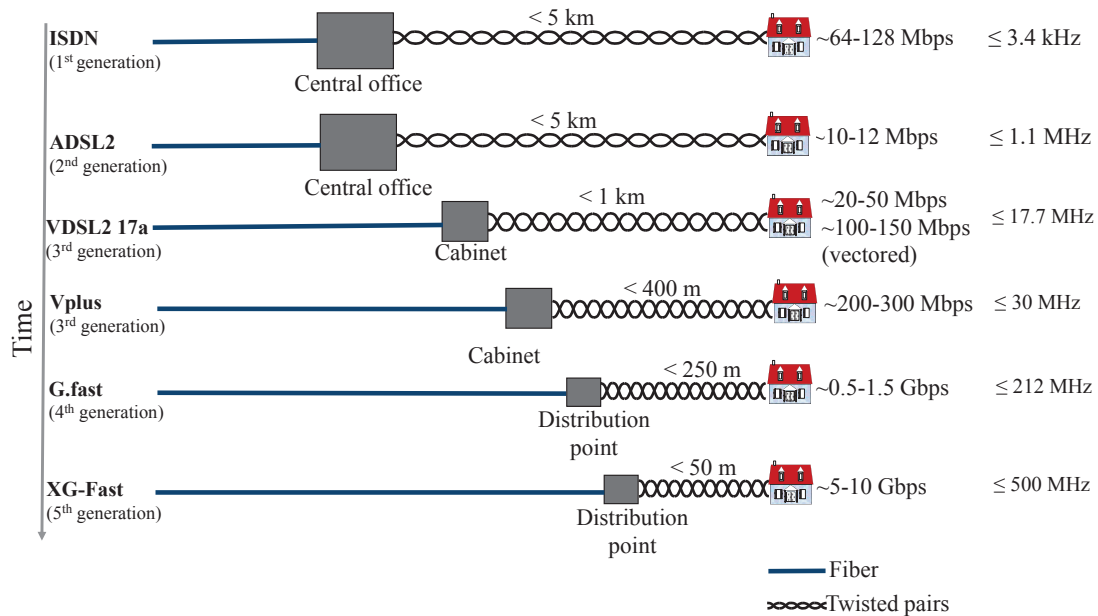
Figure 1.2: DSL access network evolution.

differences. Besides the wider 106 MHz spectrum, G.fast has different parameters such as duplexing scheme, carrier spacing, and potentially sampling rate. These modulation differences are the main limitation for joint VDSL2 and G.fast vectoring (for more details see Chapter 4). Furthermore, G.fast vectoring plays a key role in enabling network providers to get the full benefit of G.fast. The high frequencies used by G.fast create strong crosstalk between active neighboring copper pairs; significantly stronger than created by VDSL2 technology. This crosstalk takes away much of the capacity boost offered by G.fast. Therefore, network providers must use vectoring to cancel this crosstalk and allow each line to perform to its potential.

In this thesis I focus on G.fast and analyze G.fast deployment issues regarding the G.fast/legacy DSL joint deployment and G.fast vectoring. More thorough motivation regarding the latter topics is discussed in the upcoming Section 1.2.

1.2 State-of-the-Art and Research Motivation

In this Section, I summarize lines of work studying topics/open issues closely related to the scope of this thesis and highlight the main motivation of my work. In Section 1.2.1, I provide references which analyze performance of signal and spectrum coordination under G.fast compliant setup. Note that in the rest of the thesis I use spectrum coordination, spectrum optimization, and spectrum management interchangeably. I discuss which

issues are not covered by given literature and consequently outline motivation for the first part of my thesis. In Section 1.2.2, I present related work on modeling ICSI in multi-user and multi-carrier DSL networks with different modulation parameters. The state-of-the-art is briefly outlined, with an emphasis on a novel ICSI problem which arises in mixed G.fast/legacy DSL deployment scenarios and therefore motivates the second part of my thesis.

1.2.1   Signal and spectrum coordination for G.fast

Up to the beginning of the work on this thesis only little effort has been made on analysis of signal coordination, i.e., crosstalk cancellation in G.fast especially under erroneous CSI. The authors of [25, 36, 37] evaluate the achievable bit-rates of the linear vectoring in G.fast regarding only frequencies up to 100 MHz [36, 37] and 140 MHz [25]. Furthermore, all available work at that time assumed perfect CSI; therefore neglecting the impact of channel variations. In this work I therefore analyze the performance of linear vectoring schemes (zero-forcing equalizer and diagonalizing precoder) under perfect and erroneous CSI for G.fast frequencies up to 212 MHz. Based on my analysis I also give an intuition behind the CSI error definition for linear vectoring in [38]. Furthermore, non-linear vectoring is discussed as an alternative to linear methods for the 212 MHz profile. The ITU contributions in [39, 40] argue that non-linear vectoring is capable of achieving significant bit-rate improvements compared to linear vectoring (e.g., up to 20% [40]), while contributions in [41–46] claim that the achievable bit-rates of linear vectoring marginally differ from one expected from using non-linear vectoring, especially when in addition to linear vectoring DSM schemes are used. Therefore, in this work I also analyze the achievable bit-rates of spectrally optimized linear and spectrally optimized non-linear vectoring schemes in order to confirm one of the statements. Similar work was also carried out in [10, 11, 47–53] where the authors in [52, 53] compare the performance of linear and non-linear vectoring without spectrum optimization, authors in [47–50] consider only power optimization for linear vectoring schemes while the authors in [10, 11, 51] spectrally optimize both linear and non-linear vectoring schemes. Again, most of the available performance analysis and comparison of linear and non-linear vectoring was done based on the perfect CSI assumption. An exception is the work in [54] where the performance of (spectrally optimized) linear and non-linear vectoring under CSI errors is compared. Up to my knowledge a little has been done to systematically analyze vectoring performance under G.fast compliant setup taking in consideration everything what has been partially analyzed in previous work, such as impact of CSI errors and improvement under spectrum optimization for both linear and non-linear vectoring. Therefore, in this work I extend CSI error model for linear vectoring in [38] to non-linear vectoring

and compare the performance of both linear and non-linear vectoring with and without spectrum optimization under perfect as well as erroneous CSI.

For previous DSL systems spectrum coordination schemes, i.e., DSM-L1 and DSM-L2 schemes were used in order to mitigate inter-group crosstalk as analyzed in [19–21]. Authors in [55, 56] also propose interference alignment (IA) as alternative to DSM-L2 but evaluate IA performance only under VDSL2 compliant setup, i.e., for frequencies up to 17 MHz. However, there is a lack of performance analysis regarding the mitigation of inter-group crosstalk for G.fast. In this work, I analyze DSM-L2 and IA in G.fast compliant setup for both frequency profiles (i.e., 106 MHz and 212 MHz) and I also propose simple time division multiple access (TDMA) for coordination of multiple G.fast vectoring groups in partial vectoring scenarios.

1.2.2 ICSI modeling

Network operators will deploy G.fast in the upcoming years, where this technology will coexist with legacy DSL (e.g., VDSL2). Asynchronism and differences in modulation parameters such as sampling rate and carrier width result in ICSI. Models currently available in the literature [47, 57–72] deal with ICSI, but they do not take these sources of ICSI jointly into account. More precisely, the problem of ICSI in asynchronous DSL systems with *identical modulation parameters* has been studied in [57, 58]. A frequency-domain crosstalk cancelation model between *synchronous* VDSL2 systems with different tone spacing has been presented in [59]. The authors in [47] analyze coexistence of G.fast and VDSL2 taking FEXT and NEXT into account, but neglecting the effects of ICSI. The problem of ICSI due to time and frequency offsets has also been well studied in the wireless literature. Exemplary studies modeling and dealing with ICSI originating from wireless channel variations can be found in [60–64] while the authors in [70–72] address ICSI due to carrier frequency offsets. Models for ICSI produced jointly by frequency and time variations have been studied in [65–69]. As mentioned, all these ICSI models do not take differences in modulation parameters such as tone spacings and sampling rates jointly into account and therefore can not be used for characterization of ICSI coefficients in a G.fast/legacy DSL coexistence scenarios. Therefore, in this work I derive an analytical model for the ICSI coefficients that captures the modulation properties of G.fast and legacy DSL systems.

1.3   Research Questions and Objectives

The high-level research questions and goals of my thesis are as follows:

- How are performance of liner and non-linear vectoring influenced by channel variations (i.e., CSI errors) and spectrum optimization?

- How spectrum coordination schemes used for currently deployed DSL systems perform (i.e., mitigate inter-group crosstalk) in G.fast compliant setup? Investigate potential alternatives such as IA.

- Develop novel ICSI model which is suitable for characterizing ICSI coefficients in case of mixed G.fast/legacy DSL deployment scenarios. Apply it to a specific problem of current interest to network operators, that is the selection of the spectral separation between G.fast and VDSL2.

1.4   Outline and Contributions

This thesis is based on work which is partly published in the following peer-reviewed papers:

- S. Drakulić, D. Statovci and M. Wolkerstorfer, "Performance of linear crosstalk cancelation in fourth generation wired broadband access networks," European Signal Processing Conference (EUSIPCO 2013), September 2013.

- S. Drakulić, M. Wolkerstorfer and D. Statovci, "Coexistence analysis of asynchronous digital subscriber lines with different sampling rate and carrier frequency spacing," IEEE Global Communications Conference (GLOBECOM 2014), December 2014.

- S. Drakulić, D. Statovci, M. Wolkerstorfer and T. Zemen, "Comparison of interference mitigation techniques for next generation DSL systems," IEEE International Conference on Communications (ICC 2015), May 2015.

- M. Wolkerstorfer, D. Statovci and S. Drakulić, "Maintaining harmony in the vectoring xDSL family by spectral coordination," Asilomar Conference on Signals, Systems and Computers, December 2015.

- S. Drakulić, M. Wolkerstorfer and D. Statovci, "Coexistence in fourth generation DSL broadband networks: Modeling and simulation results", submitted to IEEE Transactions on Communications, December 2016.

The content of the individual chapters and the main contributions of the thesis are briefly described in the following:

Chapter 2 reviews the fundamental principles of DSL transmission. I introduce the main performance impairments in DSL, i.e., crosstalk and shortly analyze DSL methods for crosstalk mitigation and cancellation (i.e., vectoring) and discuss performance metrics.

Chapter 3 provides performance analysis of linear and non-linear vectoring for G.fast frequencies up to 212 MHz. The results show that while there is a substantial performance gap between linear and non-linear vectoring, in case when in addition spectral optimization is used linear vectoring approaches the performance of non-linear vectoring which confirms the results obtained in [11, 41, 43]. The impact of erroneous CSI is also taken into account through performance models for linear vectoring in [38] and non-linear vectoring proposed in this thesis. An intuition behind the CSI error model in [38] is developed which allows to make a sophisticated guess on the impact of estimation errors on bit-rates. Based on CSI error models I show that both linear and non-linear vectoring are very sensitive to CSI errors while this sensitivity is reduced by using spectral optimization in addition. Results also show that spectrally optimized non-linear vectoring is more sensitive to CSI errors than spectrally optimized linear vectoring. Furthermore, in this Chapter I also analyze different mitigation techniques for uncancelled crosstalk in case of partial vectoring in a G.fast compliant setup. Besides the traditionally used DSM-L2 [19, 20] I propose IA as an alternative method to DSM-L2 for dealing with the uncancelled interference in G.fast and show that IA is superior to DSM-L2 in non-vectoring scenarios. Furthermore, I also propose TDMA for coordination of multiple vectoring groups in partial vectoring scenarios for G.fast.

Chapter 4 describes a novel ICSI model for multi-user and multi-carrier DMT systems which accounts for the per-tone worst-case asynchronous transmission, differences in modulation parameters such as sampling rates and carrier width, and the impact of realistic filtering. The derived model is verified through time domain simulations and it is also shown that in a special case of the identical modulation parameters the derived ICSI model coincides with the ICSI model in [57].

Chapter 5 describes a joint performance model which encompasses the impact of CSI errors, vectoring, and ICSI. In this Chapter I use this joint model in order to determine the required spectral separation between G.fast and VDSL2 and appropriate VDSL2 filtering which ensure negligible interference between the two systems. Results show that starting G.fast immediately after the VDSL2 band causes significant out-of-band leakage especially into the last VDSL downstream band. A G.fast start frequency above 23 MHz ensures a negligible impact of G.fast

on VDSL2 and vice versa (i.e., <-130 dBm/Hz) under the assumption of high or-
der filtering such as a Chebyshev type I filter with order 8. In this Chapter I also
show that neglecting the ICSI can potentially lead to a significant bit-rate overes-
timation for G.fast users (up to 18%) which further motivates the exact modeling
of ICSI impact and the work presented in Chapters 4 and 5.

Chapter 6 contains concluding remarks and a summary of open issues.

2 DSL ENVIRONMENT

This Chapter provides the fundamental principles of digital subscriber line (DSL) transmission and the DSL environment in order to give a better understanding of the problems analyzed in following chapters. This Chapter proceeds as follows. In Section 2.1 the main characteristics of DSL such as discrete multi-tone (DMT) modulation are shown. Furthermore, the strongest performance impairment in DSL networks, i.e., crosstalk is also discussed along with the channel models used in this thesis. Dynamic spectrum management (DSM) with respect to different coordination levels is described in Section 3.4.2.

2.1 Main DSL Properties

One of the principal advantages of DSL technology is the use of already existing physical communication infrastructure, namely, the twisted pair copper network. Traditional phone service was created for voice transmission with other phone users based on analog signal transmission. An input device such as a phone set takes an acoustic signal and converts it into an electrical equivalent in terms of volume (signal amplitude) and pitch (frequency of wave change). DSL is, as its name states, a technology which uses digital signals for transmission. Several modulation types are used by various DSL technologies for converting a stream of bits into equivalent analog signals that are suitable for transmission over twisted wire pairs. I consider the most widely used type of modulation in DSL, i.e., DMT modulation. A similar modulation technique used in wireless transmission systems is called orthogonal frequency division multiplexing (OFDM). The concept of DMT is to transform the DSL channel into K orthogonal (i.e., independent) narrowband sub-channels. Discrete carriers (or tones) are then used in the center of each sub-channel and carry data independently of other carriers. Furthermore, the major performance impairments in DSL networks are channel attenuation and noise which is composed of inherited background noise and crosstalk (i.e., interference) noise. Crosstalk noise is the interference coupled between active DSL lines operating in the same cable bundle and is the only impairment that can be influenced by signal processing. The complicated and unpredictable nature of the individual crosstalk signals steers practical
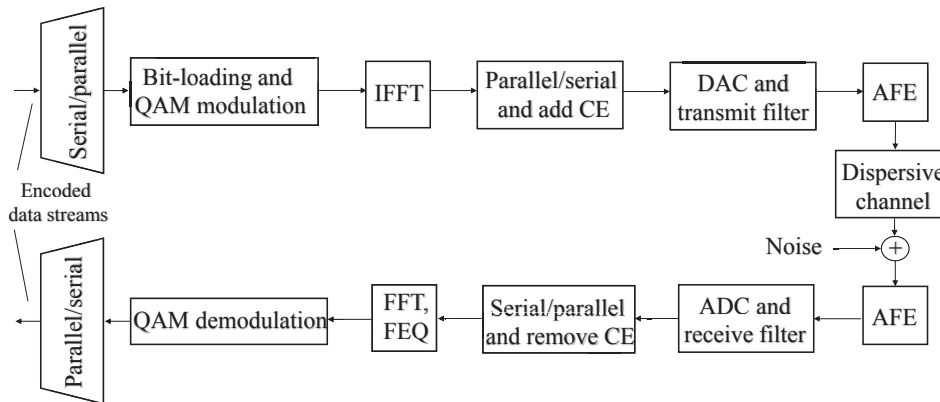
Figure 2.1: Basic DMT transmission scheme highlighting various signal processing blocks such as quadrature amplitude modulation (QAM), the (inverse) discrete Fourier transformation ((I)DFT), add/remove cyclic extension (CE), the digital-to-analog conversion (DAC) and analog-to-digital conversion (ADC), analog front-end (AFE), and the frequency domain equalizer (FEQ).

analysis of DSL performance to simplified models of the trends. In this Chapter, I first describe basic principles of DMT transmission. Then I discuss crosstalk noise in detail and show the most commonly used crosstalk models. I also briefly describe performance metrics used in this thesis.

2.1.1   Discrete Multi-Tone (DMT) Modulation

One of the main characteristics of the twisted wire pair channel is the extreme variation in its transmission function versus frequency within the range of interest. To overcome this variations, DMT effectively splits the channel into K independent (orthogonal) narrowband sub-channels by means of an inverse discrete Fourier transform (IDFT) and DFT pair. Each sub-channel is characterized by its carrier frequency, i.e., tone which is laying in the center of the sub-channel and all tones are equally spaced by Δf Hz. These tones are used to transmit data independently in each sub-channel by means of quadrature amplitude modulation (QAM). Furthermore, DMT systems generally use tones that are reasonably closely spaced (small Δf), which implies that the magnitude response of the channel is almost flat across each sub-channel. Based on the estimated frequency response and noise power spectral density (PSD) on each sub-channel a number of bits is allocated to each tone. The process of mapping an integer number of bits to each tone is referred to as bit-loading. This number of bits determines the QAM constellation size for that particular sub-channel.

Figure 2.1 illustrates a simplified scheme of DMT transmission, showing a transmitter, a receiver, and a channel with non-ideal impulse response. More precisely, the twisted-pair channel introduces amplitude and phase distortion in the transmitted signal which means that the channel does not fulfill the condition for perfect reconstruction [73]. Therefore, successive transmission of DMT symbols over the channel causes inter-symbol interference (ISI) at the receiver and the sub-carriers will also lose the orthogonality resulting in inter-carrier interference (ICI) [74]. ISI refers to the mixing of energy belonging to neighboring, in time, DMT symbols during transmission, whereas ICI refers to a similar process for the sub-channels belonging to the same DMT symbol. If the length of the channel impulse response is less than or equal to ϑ_{CP} samples, adding a guard period of ϑ_{CP} samples at the beginning of the DMT symbol prevents the occurrence of ISI and consequently ICI. In DSL standards this guard period, also known as cyclic prefix (CP), is chosen to be the copy of the last ϑ_{CP} samples of a DMT symbol.[1] While CP is used to combat ISI, a cyclic suffix (CS) is used to enable synchronization between the DMT receiver and transmitter [75]. As its name implies, the CS is copy of some number of samples ϑ_{CS} from the beginning of the symbol, and it is appended to the end of the DMT symbol. In order to ensure synchronization between the DMT receiver and transmitter the duration of the CS, at smallest, needs to exceed the one-way delay of the DSL line. Therefore, DMT symbol is composed of CP, a data portion, and a CS. Often the CP and CS are referred to cyclic extension (CE). After adding the CE, the DMT symbol is digitally filtered, digital-to-analog converted (DAC) and passed through the analog front-end (AFE), which provides analog filtering and power amplifiers, in order to match signal requirements such as a regulatory power spectral mask. The equivalent reverse operations are performed at the receiver side to recover the received, encoded data stream. The only additional element is a single tap frequency domain equalizer (FEQ) which tunes the different tones in phase and amplitude, compensating for dispersion owning to the channel and analog components.

2.1.1.1 DMT Receiver and Transmitter

A more detailed illustration of the DMT transmitter and the DMT receiver are provided in Figures 2.2 and 2.3. The IDFT at the DMT transmitter implements the equation

$$x_n = \sum_{k=0}^{2N-1} X_k e^{-j\frac{2\pi kn}{2N}}, \quad n \in [0, 2N-1] \tag{2.1}$$

---

[1] The CP chosen to be a copy of the last ϑ_{CP} samples converts linear channel convolution in to circular channel convolution which eases the process of detecting the received signal by using a simple single tap equalizer.
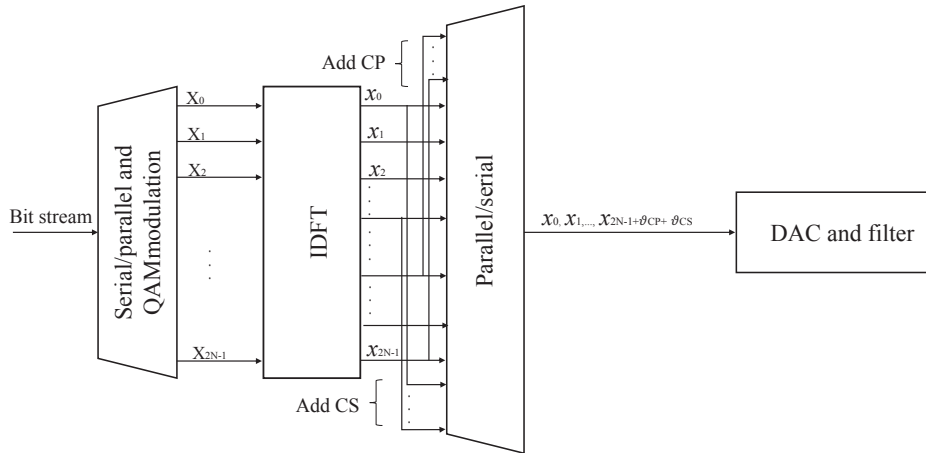
Figure 2.2: DMT transmitter block diagram.
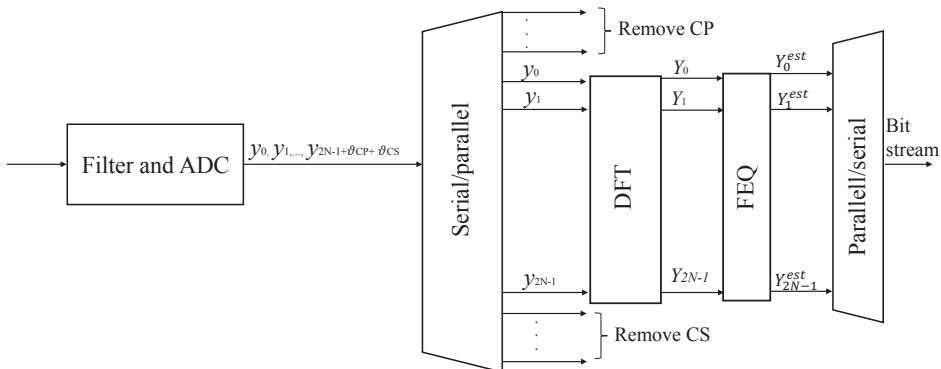
Figure 2.3: DMT receiver block diagram.

where x_n are time domain transmitter outputs, i.e., DFT coefficients. The frequency-domain inputs, i.e., IDFT coefficients X_k are two-dimensional (complex) modulated inputs that are derived from the QAM constellation. The values of the IDFT coefficients must be real valued due to the fact that the twisted-pair channels have baseband transmission characteristics. To assure this constraint the DFT coefficients with indices greater then N (I assume that N is always an even number) must have the Hermitian symmetry property [75], i.e., the $X_k = X_{2N-k}^*$ for $k = N+1, ..., 2N-1$. Furthermore, in practical systems tones indexed by 0 (DC) and N (Nyquist frequency) are usually not

used, in which case $X_0 = X_N = 0$. In general, tones above N are denoted as negative tones/frequencies and are not used for bit-loading in DMT based systems. Furthermore, CE ($\vartheta_{CP} + \vartheta_{CE}$) is appended to x_n to form a cyclically extended DMT symbol x_n^{CE} where $n \in [0, 2N + \vartheta_{CP} + \vartheta_{CE}]$. When the channel impulse response is less than or equal to CE length the transmitted DMT symbol and the channel are circularly convolved:

$$\dot{y}_n = h_n \otimes x_n^{CE} + z_n, \tag{2.2}$$

where the sign $\otimes$ denotes circular convolution and h_n is the channel impulse response while z_n is the noise on the channel. In the rest of the thesis I assume that z_n is spatially white Gaussian noise. If the CE (i.e., CP) is long enough to combat time dispersion introduced by the channel, received DMT symbol will be free of ICI and ISI. Hence, the CE converts a time dispersive DSL channel into $2N$ parallel, narrowband flat sub-channels which can be processed independently of each other. At the DMT receiver the received symbol $\dot{y}_n$ is blocked prior to decoding, discarding the DE. After removing the CE the received discrete symbol at the input of the serial-to-parallel converter at the DMT receiver is given by

$$y_n = h_n \otimes x_n + z_n, \quad n \in [0, 2N - 1]. \tag{2.3}$$

The output of the DFT block produces the following DFT coefficients:

$$Y_k = \frac{1}{2N} \sum_{n=0}^{2N-1} y_n e^{j\frac{2\pi kn}{2N}}, \quad k \in [0, 2N - 1]. \tag{2.4}$$

Knowing that convolution in time domain corresponds to multiplication in frequency domain, (2.3) can also be written as:

$$Y_k = H_k X_k + Z_k, \quad k \in [0, 2N - 1], \tag{2.5}$$

which shows that each received symbol is actually a scaled version of the transmitted symbol plus the Gaussian noise. Therefore, the estimated received DMT symbols can be easily obtained by compensating for the channel frequency response by

$$X_k^{est} = \frac{Y_k}{H_k}, \tag{2.6}$$

where H_k is the channel transfer function (a complex value) of the equivalent discrete time channel h_n. This normalization process is known as frequency-domain equalizer (FEQ). Application of the FEQ requires one complex multiplication per subchannel per DMT symbol, which has a negligible implementation complexity relative to multi-tap
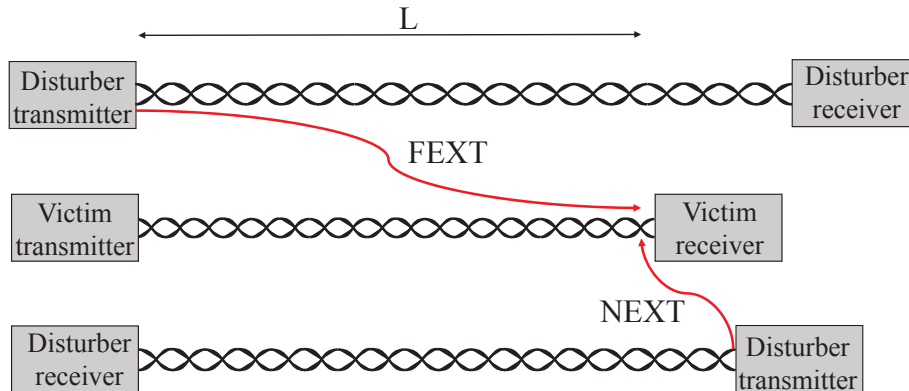
Figure 2.4: Illustration of FEXT and NEXT crosstalk signals.

equalization that might be used if ISI and ICI were not confined to the CE. If the channel is noiseless we see that $X_k^{est} = X_k$. Zero-forcing equalizer (ZFE), which is widely used in DMT systems, performs exactly Equation (2.6) and therefore ignores any impact of the noise (cf. Chapter 3). There are also other FEQ methods such as maximum likelihood (ML) sequence detection, minimum mean square error (MMSE) symbol detection, matched filter etc. For more detalis on the different FEQ methods interested reader is referred to [75].

2.1.2   Channel Model

In a DSL environment, the dominant type of noise is interference coming from other DSL lines. This interference, also known as crosstalk, occurs when electromagnetic radiation that is the consequence of signal transmission on one line creates an undesirable signal on neighbouring lines. Hence, if two lines share the same cable bundle, they can see each other's signals. Significant mitigation of created crosstalk is achieved by three Bell's principles: i) differential signalling, ii) use of shielding, and iii) use of pair twisting [75]. However, although these three principles reduce created crosstalk still for most of the practical DSL implementations spectrum or signal coordination is required to achieve targeted performance. In general, there are two types of crosstalk: near-end crosstalk (NEXT) and far-end crosstalk (FEXT). NEXT refers to interfering signals at the victim receiver originating from disturber transmitters at the same side of the line as the victim receiver. FEXT signals originate from the disturber transmitters at the opposite side of the line from the victim receiver. Both types of crosstalk are illustrated in Figure 2.4. All current FEXT and NEXT models used in DSL are empirically based [75], meaning that these models are based on (several) empirical measurements of different parameters

such as crosstalk transfer functions. Due to the variability and unpredictability of the crosstalk transfer function, crosstalk is usually analyzed using the worst-case crosstalk transfer function. It is common to use 99% worst-case crosstalk models [75]. This means that in no more than 1% of the taken channel measurements the FEXT and the NEXT transfer functions exceed the given model. Therefore, if not stated otherwise, in this thesis for crosstalk calculation I rely on 99% worst-case models. The FEXT transfer coefficients from user j to user u on carrier k are given by

$$|H_k^{u,j}|^2 = K_{\mathsf{FEXT}} \cdot f_c^2 \cdot L \cdot |H_k^{u,u}|^2, \tag{2.7}$$

where K_{FEXT} is the empirically determined FEXT constant with suggested value for Europe of $10^{-4.5}$ [75], f_c is the center carrier frequency in MHz of the kth sub-channel, L is the coupling distance in km, and $|H_k^{u,u}|^2$ is the transfer coefficient of the direct channel at carrier frequency k. Transfer coefficients are commonly calculated by a two-port transmission line model [75], with parameters build for specific cabels (e.g., [76], [77]). In general the signal attenuation over the direct channel is larger at higher frequency.

Similarly, the worst-case NEXT transfer coefficients are given by

$$|H_k^{u,j}|^2 = K_{\mathsf{NEXT}} \cdot f_c^{1.5} \cdot (1 - |H_k^{u,u}|^4), \tag{2.8}$$

where K_{FEXT} is the empirically determined NEXT constant with suggested value for Europe of 10^{-5} [75]. NEXT is usually much stronger than FEXT. This is because in case of NEXT there is close proximity from the transmitter of the interferer to the receiver of the victim. In the case of FEXT, the interferer's signal is attenuated all over the coupling length before it reaches the victim. For more details see [75]. NEXT is mostly avoided in all DSL standards by means of frequency or time division duplexing, i.e., FDD or TDD. In asymmetric digital subscriber line (ADSL) and very high bit-rate digital subscriber line (VDSL) FDD is used to separate upstream and downstream transmission bands, which means that the NEXT signal can be ignored. Differently in G.fast NEXT is eliminated using TDD.

For simulation purposes I also use the following three sets of cable measurement data (up to at least $106\,\mathrm{MHz}$) published in ITU: Swisscom outside plant quad cable of $99\,\mathrm{m}$ length [2], British Telekom (BT) underground cable of $100\,\mathrm{m}$ length [15], and Royal Dutch Telecom (KPN) underground cable of $104\,\mathrm{m}$ length [3] (cf. Figures 2.5-2.7). The direct/crosstalk channel data missing in the Swisscom measurements has been duplicated based on the available data and assumptions on geometrical symmetry. Furthermore, all data is interpolated to the specific tone spacing of the considered technology. For the purpose of loop-length scaling based on the specific measurement, I adopt the FEXT scaling proposed in [78] where it is assumed that the FEXT signal traverses an infinite
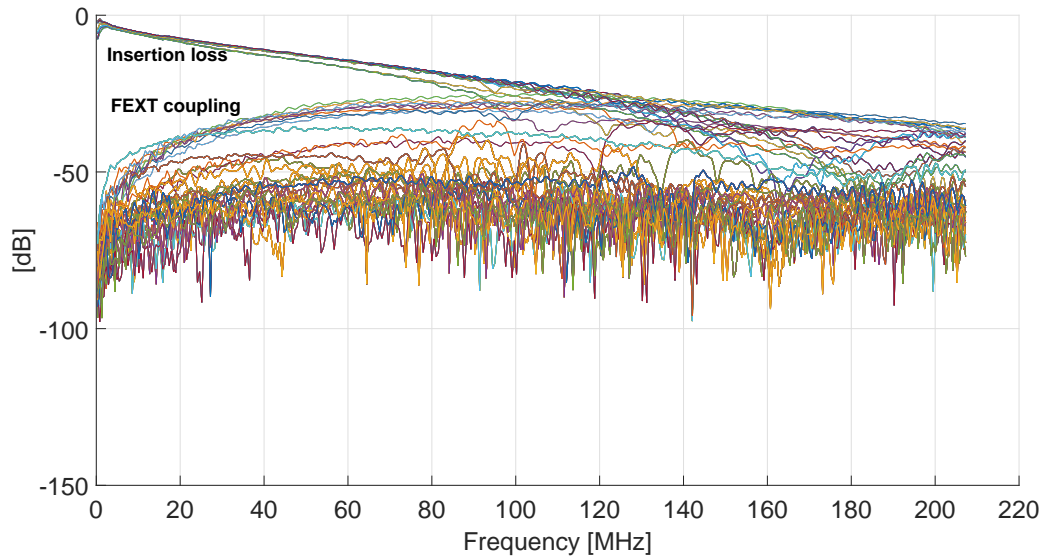
Figure 2.5: Measurement data of a 99 m Swisscom cable [2] up to approximately 212 MHz.
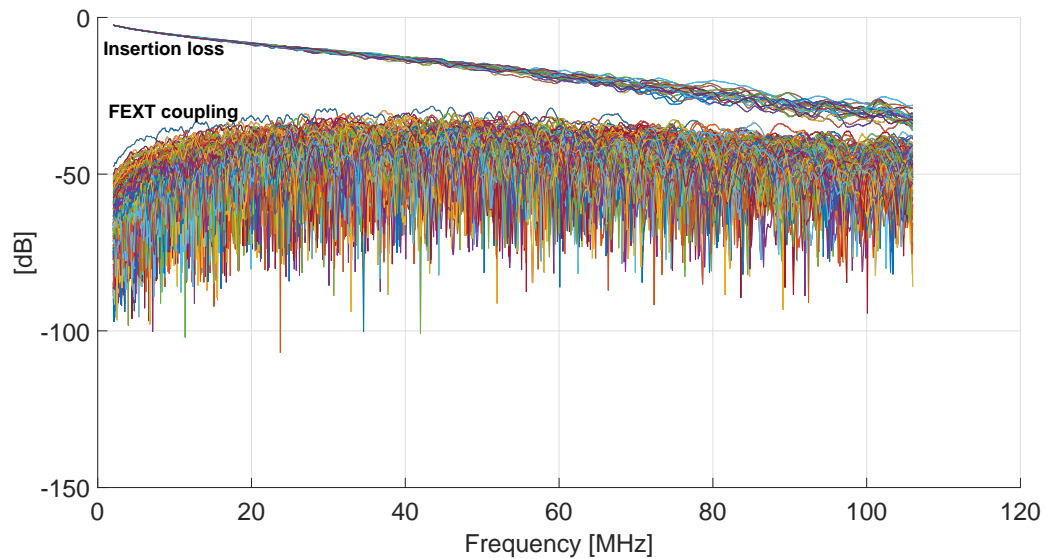
Figure 2.6: Measurement data of a 100 m BT cable [15] up to approximately 106 MHz.

number of sub-signal paths. Each path consists of a certain length where disturber signal is attenuated, then coupled among the pairs, and finally attenuated on the victim line until it reaches the victim receiver. For the following derivation of a length-dependent attenuation factor for the given disturber/victim (i, j) pair, $H(L, i, j)$, I denote the larger and the smaller values of disturber/victim direct channel gains (on a specific tone) as H_1
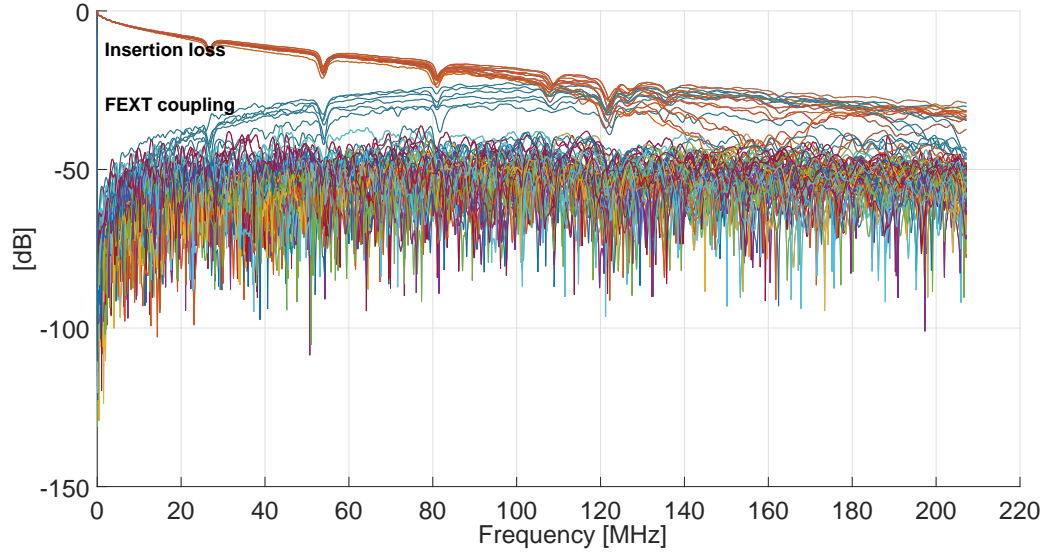
Figure 2.7: Measurement data of a 104 m KPN cable [3] up to approximately 212 MHz. Note that the notches are caused by the presence of so-called "waterplugs" in this type of cable [3].

and H_2, respectively. I define $\tilde{H}_1 = H_1^{\frac{1}{T}}$, $\tilde{H}_2 = H_2^{\frac{1}{T}}$, $\tilde{H}_2 = \tilde{H}_1 \triangle$. Hence, $H_2 = H_1 \triangle^T$ with $\triangle < 1$, for some ("large enough") value T which is the number of discrete line segments by which I replace the actual integral over an infinite number of signal paths. Therefore, the average direct channel attenuation is given by [78]:

$$H(L, i, j) \; = \; \frac{1}{T-1} \sum_{t=1}^{T-1} \tilde{H}_1^t \cdot \tilde{H}_2^{(T-t)} \tag{2.9a}$$

$$= \; \frac{1}{T-1} \sum_{t=1}^{T-1} \tilde{H}_1^t \cdot \tilde{H}_1^{(T-t)} \cdot \Delta^{(T-t)} \tag{2.9b}$$

$$= \; \frac{H_1}{T-1} \sum_{t=1}^{T-1} \Delta^{(T-t)} \tag{2.9c}$$

$$= \; \frac{H_1}{T-1} \cdot \Delta \cdot (1 + \Delta + \ldots + \Delta^{(T-2)}) \tag{2.9d}$$

$$= \; \frac{H_1}{T-1} \cdot \Delta \cdot \frac{1 - \Delta^{(T-1)}}{1 - \Delta}, \tag{2.9e}$$

where $\triangle = (\frac{H_2}{H_1})^{\frac{1}{T}}$. When $\triangle = 1$ (i.e. two direct channels are identical), then $H(L, i, j) = H_1 = H_2$. According to the proposed crosstalk model, the measured/interpolated crosstalk gain between lines i and j is divided by the $H(L, i, j)$ calculated as in (2.7) and by $\sqrt{L}$ to obtain the crosstalk coefficient K, which may be different for different tone. Note that this is the main difference, beside having unequal direct

channels between victim and disturber, to standard $99\,\%$ worst-case FEXT model [75].

2.1.3 Performance Models

In this thesis I consider a DSL network with a set of users indexed by $\mathcal{U} = \{1, \ldots, U\}$ and a set of Δf [Hz] spaced tones indexed by $\mathcal{K} = \{1, \ldots, K\}$. The received DMT symbol for user u on tone k is given as

$$Y_k^u = H_k^{u,u} X_k^u + \sum_{j \in \mathcal{U} \backslash u} H_k^{u,j} X_k^j + Z_k^u, \tag{2.10}$$

where $X_k^u \sim \mathcal{N}(0, p_k^u)$ and $Z_k^u \sim \mathcal{N}(0, \sigma_k^u)$ are transmitted symbol and additive White Gaussian backgorund noise for user u on tone k, respectively, while p_k^u is the power spectral denisty (PSD) of user u on tone k and σ_k^u is noise spectral density of user u on tone k. Distribution $\mathcal{N}(\kappa, \iota^2)$ represents a circular symmetric complex normal distribution with mean κ and variance ι^2. In (2.10) I assume synchronous DMT transmission with all users having the same modulation parameters and ,therefore, I model transmission independently on each tone k. With this assumption I also define the signal-to-interference-plus-noise ratio (SINR) for user u on tone k as

$$\mathrm{SINR}_k^u = \frac{|H_k^{u,u}|^2 p_k^u}{\sum_{j \in \mathcal{U} \backslash u} |H_k^{u,j}|^2 p_k^j + \sigma_k^u}, \tag{2.11}$$

and the number of bits loaded on carrier k for user u as

$$b_k^u = \log_2 \left(1 + \frac{|H_k^{u,u}|^2 p_k^u}{\Gamma (\sum_{m \in \mathcal{U} \backslash u} |H_k^{u,j}|^2 p_k^j + \sigma_k^u)} \right), \tag{2.12a}$$

$$= \log_2 \left(1 + \frac{\mathrm{SINR}_k^u}{\Gamma} \right), \tag{2.12b}$$

where Γ represents the signal-to-noise (SNR)-gap to capacity. The bit-rate for user u is obtained by

$$R^u = f_s \sum_{k=1}^{K} b_k^u, \tag{2.13}$$

where f_s denotes the DMT symbol rate.

Note that in some parts of this thesis I will differentiate between upstream and downstream transmissions where for upstream parameters I will use $'^{\wedge}'$ sign and for downstream parameters I will use $'^{\vee}'$ sign. I use plane parameters when definitions are identical for both transmission directions.

2.2 Dynamic Spectrum Management (DSM)

Dynamic spectrum management (DSM) represents a set of spectrum management algorithms used in DSL to mitigate or completely remove the influence of crosstalk. In general, multi-user DSM algorithms can be divided into two groups based on the implementation of coordination levels, i.e., spectrum and signal coordination. Spectrum coordination (i.e., spectrum balancing) comes down to allocating the transmit power spectral density (PSD) over all frequencies, to the different users such that certain design objectives are achieved. Differently, signal coordination (also known as *vectoring*) assumes advanced signal processing methods which eliminate all crosstalk between the lines. Very often DSM algorithms have even finer granulation where three levels of coordination are defined, i.e.,:

- Level 1: Autonomous (single-user) power allocation aiming at crosstalk avoidance,

- Level 2: Coordinated (multi-user) power allocation aiming at crosstalk avoidance,

- Level 3: Multi-user signal processing aiming at crosstalk cancellation (i.e., vectoring).

Levels 1,and 2 algorithms are part of spectrum coordination while Level 3 algorithms belong to signal coordination. As I will show in this thesis, DSM represents a key feature, especially for future DSL standards such as G.fast, in enabling the targeted speeds.

2.2.1 Spectrum Balancing

Spectrum balancing is deployed in systems that can alter their transmit PSD. DMT based systems (such as DSL) allow that because they can transmit any power level (below PSD mask[2]) in each sub-channel. In general, spectrum balancing algorithms aim to find optimal transmit spectra for a bundle of interfering DSL lines, following a certain optimization objective and subject to a number of constraints. The most common spectrum balancing optimization objectives are: bit-rate maximization, power minimization, and noise margin maximization. An optimal solution has to be then found within the domain set out by the various constraints. In this thesis I focus on spectrum balancing algorithms which perform bit-rate maximization, i.e., I consider the following

---

[2] The PSD mask is an upper bound on the transmit per-tone PSD.

optimization problem:

$$\max_{\mathbf{p}^u, u \in \mathcal{U}} \sum_{u=1}^{U} R^u, \qquad (2.14a)$$

$$\text{s.t.} \sum_{k \in \mathcal{K}} p_k^u \leq P_{tot}^u, \forall u \in \mathcal{U} \qquad (2.14b)$$

$$0 \leq p_k^u \leq p_{k,mask}^u, \forall k \in \mathcal{K}, \forall u \in \mathcal{U} \qquad (2.14c)$$

where p_k^u is the transmit PSD of user u on carrier k, P_{tot}^u is the total transmit power budget for user u, $p_{k,mask}^u$ is the PSD mask for user u on tone k, and $\mathbf{p}^u$ is the vector containing the PSD of user u over all tones. The total power constraint is given in (2.14b). This constraint ensures that each user's total transmit power does not exceed the maximum allowed total transmit power budget. The spectral mask constraint is given in (2.14c) which limits the transmit PSD allocated to each carrier in order to not exceed associated PSD mask. The optimization problem in (2.14) is also referred to as rate-adaptive DSM (RA-DSM).

The RA-DSM problem is known to be an NP-hard, separable non-convex optimization problem, and often difficult to solve efficiently for the global optimum [79, 80]. The iterative waterfilling (IWF) approach [81], which belongs to DSM-L1 algorithms, finds a heuristic solution by splitting this problem into U convex sub-problems, then iterating over these until convergence. Each sub-problem concerns only the powers of one user u, fixing the powers of all the other users $j \neq u$ and treating their contributions as noise. IWF has been shown to converge to a competitive Nash equilibrium [81], and is suitable for practical implementations [82]. A very different approach is made in optimal spectrum balancing (OSB) [83] which attempts to solve the optimization problem in (2.14) directly. The innovation was to formulate the Lagrangian dual problem. It was then possible to iterate over K separate sub-problems for fixed Lagrangian dual variables where each sub-problem is concerning only $p_k^u, \forall u \in \mathcal{U}$ on a tone $k \in \mathcal{K}$. Each sub-problem is solved with a brute-force grid-search having $Q = p_{k,mask}^u / \triangle_P$ quantized power levels where $\triangle_P$ is predetermined power quantization, requiring at least Q^U operations each. Although OSB has exponential complexity in the number of users and linear complexity in number of tones, it has been shown that significant performance gains are possible over IWF but for a limited number of users [84]. Iterative spectrum balancing (ISB) [85] was introduced in order to reduce OSB's exponential complexity through a series of line-searches, avoiding the grid-search "bottleneck". Furthermore, IWF is completely autonomous DSM algorithm, i.e., it does not require any information exchange among users while OSB and ISB are centralized algorithms requiring information exchange among users which is in general handled by a spectrum manegement center. More

detailed discussion on different spectrum balancing algorithms can be found in [84].

2.2.2 Crosstalk Cancellation (Vectoring)

Signal coordination, also known as vectoring, involves multiple-input multiple-output (MIMO) signal processing, either two-sided (at transmitter and receiver) or one-sided (at transmitter or receiver). In this thesis I consider the case with one-sided signal coordination, i.e., with DSL transceivers coordinated at the office/distribution point (CO/Dp) and non-coordinated customer premises equipments (CPEs) since this is the case in the most of the practical implementations of interest. With signal coordination, the requirements on the underlying infrastructure are much higher compared to spectrum coordination. For vectoring, users have to have some physically collocated transmitters or/and receivers and full channel state information (CSI), i.e., both signal amplitude and phase knowledge is required. On the other hand, vectoring is able to deliver substantial performance gains compared to spectrum coordination, eliminating most or all FEXT and therefore substantially increasing the achievable bit-rates.

The effect of FEXT is not uniform across DSL lines; it becomes stronger as the loop lengths become shorter [3], and as higher frequencies are used. Moreover, the degradation experienced by a given line as a result of crosstalk depends on various factors such as whether there are active neighboring DSL lines that are sharing the same cable (or sharing part of the cable), on the relative proximity of these active neighboring lines to the given line, and on the transmission power levels used by these neighboring lines.

In general, vectoring schemes can be divided into two groups: linear and non-linear. While non-linear schemes lead potentially to larger performance gains (in terms of achievable bit-rates) they unfortunately result in a higher computational complexity. Tomlinson-Harashima precoder (THP) [86] and decision feedback equalizer (DFE) [87], represent the most popular non-linear DSL vectoring schemes. It has been shown that simple linear vectoring schemes such as zero forcing equalizer (ZFE) [88] and diagonalizing precoder (DP) [89] achieve near optimal performance under the assumption of the diagonal dominant nature of the DSL channel matrix [88, 89]. In this thesis I analyze both linear and non-linear vectoring schemes and analyze their performance in G.fast compliant setup. Furthermore, vectoring requires joint signal processing of all signals of the interest in order to successfully cancel crosstalk. Sometimes users are divided into separate vectoring groups where signal coordination can be applied only in each group. For these scenarios usually spectrum coordination is used for crosstalk mitigation among different vectoring groups. In this thesis I investigate joint vectoring and DSM-L2

---

[3] To be exact, FEXT in very short loops is low because there is not enough coupling. For details see [75, Ch.3].

algorithms in G.fast compliant setup and also propose wireless interference mitigation techniques as alternative to DSM-L2 (cf. Section 3). Furthermore, both linear and non-linear vectoring schemes require accurate CSI. Even small CSI errors can potentially cause a severe bit-rate drop especially on higher frequencies as used by G.fast. Therefore, in the Section 3 I also investigate the impact of the CSI errors on linear and non-linear vectoring schemes in a G.fast compliant setup and under different deployment scenarios.

3. CROSSTALK MITIGATION AND CANCELLATION FOR G.FAST

Two types of crosstalk noise arise in DSL networks: near-end crosstalk (NEXT) and far-end crosstalk (FEXT). NEXT is the interference received by neighbouring lines at the transmitting end and FEXT is the interference received by neighbouring lines at the receiving end (recall Figure 2.4). In G.fast NEXT is avoided by separating the upstream and downstream transmission into non-overlapping time slots, i.e., by time division duplexing (TDD). To cancel FEXT, crosstalk cancellation, also known as *vectoring*, is a mandatory feature for G.fast [90]. The first version of G.fast occupies frequencies up to 106 MHz and uses linear vectoring schemes. However, there is still an ongoing discussion within International Telecommunication Union (ITU) Study Group 15, which is in charge for G.fast recommendations, whether linear vectoring will be also used for 212 MHz profile or more advanced non-linear schemes should be used. While results from ITU contributions in [39, 40] argue that non-linear vectoring is capable of achieving significant bit-rate improvement compared to linear vectoring (e.g. up to 20% [40]), results from contributions in [41–46] claim that achievable bit-rates of linear vectoring marginally differs from one expected by using non-linear vectoring, especially when in addition to linear vectoring dynamic spectrum management level 2 (DSM-L2) is used. Furthermore, although non-linear schemes potentially can attain higher bit-rates, linear schemes have certain advantages such as: a) lower complexity leading to more energy efficient hardware, b) better dynamic adaptability leading to better flexibility with respect to re-entry from/to low power modes, and a faster initialization time, and c) non-linear schemes require replacement of the receiver at the customer-premises equipment (CPE) (issue with legacy CPEs) [43]. Furthermore, vectoring performance (bit-rates) heavily depends on accurate channel state information (CSI), the estimation of which can be challenging especially on high frequencies (>100 MHz). This Chapter therefore focuses on analysis of both linear and non-linear vectoring performance under perfect and erroneous CSI and with regard to various network topologies, start frequencies, and quality of the underlying cabling [91]. Vectoring also requires joint signal processing among the users the receiver and the transmitter side for upstream and downstream transmissions,

respectively. However, there are scenarios where joint signal processing is only possible among different groups of users, referred to as partial vectoring. Since vectoring cancels only crosstalk originating within each group, for previous DSL systems dynamic spectrum management level 1 and level 2 (DSM-L1 and DSM-L2, respectively) have been proposed to mitigate crosstalk originating among different groups [19, 20]. Hence, in this Chapter an analysis of partial vectoring in a G.fast compliant setup will be carried out. Besides DSM-L2 algorithms, interference alignment (IA) and time division multiple access (TDMA) will be proposed as a new approaches to mitigate the impact of uncanceled crosstalk in G.fast [92].

This Chapter proceeds as follows. Sections 3.1 and 3.2 describe linear and non-linear vectoring schemes, respectively. Performance models under perfect and erroneous CSI are analyzed in Section 3.3. Section 3.4 introduces the system model for partial vectoring with DSM-L2 algorithms and the newly proposed IA algorithm. Furthermore, performance evaluation of schemes and models described in Section 3.1, Section 3.2, and Section 3.4 are shown in Section 3.5.

3.1 Linear Vectoring Schemes

In this Section I provide a short overview of the analyzed linear vectoring schemes.

3.1.1 Zero-forcing Equalizer

The zero-forcing equalizer (ZFE) [88] applies crosstalk cancellation matrix $\mathbf{R}_k$ on to the upstream received signal:

$$\hat{\mathbf{X}}_{k,\text{est}} = \hat{\mathbf{R}}_k \hat{\mathbf{Y}}_k, \tag{3.1a}$$

$$= \hat{\mathbf{R}}_k \hat{\mathbf{H}}_k \hat{\mathbf{X}}_k + \hat{\mathbf{R}}_k \hat{\mathbf{Z}}_k, \tag{3.1b}$$

$$= \hat{\mathbf{X}}_k + \hat{\mathbf{R}}_k \hat{\mathbf{Z}}_k, \tag{3.1c}$$

where $\hat{\mathbf{R}}_k = \hat{\mathbf{H}}_k^{-1}$, i.e., ZFE applies the inverse of the upstream channel matrix on to the upstream received signal to restore the signal after the channel. All parameters are defined on a per-tone basis where $\hat{\mathbf{H}}_k$ is the upstream channel matrix, $\hat{\mathbf{Z}}_k$ is the upstream white Gaussian background noise while $\hat{\mathbf{X}}_{k,\text{est}}$, $\hat{\mathbf{X}}_k$, and $\hat{\mathbf{Y}}_k$ are estimated transmitted upstream symbol, transmitted upstream symbol, and received upstream symbol. Equation (3.1c) implies that each user experiences a crosstalk-free channel, under the assumption of the perfect CSI, affected only by the filtered background noise.

3.1.2   Diagonalizing Precoder

For the downstream transmission, vectoring is based on re-shaping the signal prior to the transmission. In other words, downstream signal is precoded with a precoding matrix $\check{\mathbf{S}}_k$ prior to transmission. The working principle of the diagonalizing precoder (DP) [89] is based on constructing $\check{\mathbf{S}}_k$ as a diagonalizing downstream channel matrix $\check{\mathbf{H}}_k$:

$$\check{\mathbf{X}}_{k,\text{est}} = \check{\mathbf{H}}_k \check{\mathbf{S}}_k \check{\mathbf{X}}_k + \check{\mathbf{Z}}_k, \tag{3.2a}$$

$$= \zeta_k^{-1} \check{\mathbf{D}}_k \check{\mathbf{X}}_k + \check{\mathbf{Z}}_k, \tag{3.2b}$$

where again all parameters are defined on a per-tone basis. Precoding matrix $\check{\mathbf{S}}_k = \zeta_k^{-1} \check{\mathbf{H}}_k^{-1} \check{\mathbf{D}}_k = \zeta_k^{-1} \check{\mathbf{R}}_k \check{\mathbf{D}}_k$ and $\check{\mathbf{D}}_k = \text{diag}\{\check{H}_k^{1,1}, \check{H}_k^{2,2}, ... \check{H}_k^{U,U}\}$, where $\text{diag}\{...\}$ denotes a matrix with elements on its main diagonal, while $\check{\mathbf{X}}_{k,\text{est}}$, $\check{\mathbf{X}}_k$, and $\check{\mathbf{Y}}_k$ are estimated transmitted downstream symbol, transmitted downstream symbol, and received downstream symbol. The scaling factor $\zeta_k = \max_u \|[(\check{\mathbf{H}}_k)^{-1} \text{diag}\{\check{\mathbf{H}}_k\}]_{\text{row } u}\|$ is a parameter selected to ensure compliance with the spectral mask constraints after precoding [89]. Therefore, under perfect CSI each user experiences its direct channel scaled by ζ_k and completely free from crosstalk noise.

3.2   Non-linear Vectoring Schemes

In this Section I provide a short overview of the analyzed non-linear vectoring schemes.

3.2.1   Decision Feedback Equalizer

The structure of the decision feedback equalizer (DFE) [87] considers the QR decomposition of the crosstalk channel matrix

$$\hat{\mathbf{H}}_k \stackrel{\text{qr}}{=} \hat{\mathbf{\Lambda}}_k \hat{\mathbf{\Upsilon}}_k, \tag{3.3}$$

where $\hat{\mathbf{\Lambda}}_k$ is a unitary matrix and $\hat{\mathbf{\Upsilon}}_k$ is upper triangular matrix. The DFE applies the linear feed-forward filter $\hat{\mathbf{\Lambda}}_k^\dagger$ to the received vector and yields

$$\tilde{\hat{\mathbf{Y}}}_k = \hat{\mathbf{\Lambda}}_k^\dagger \hat{\mathbf{Y}}_k, \tag{3.4a}$$

$$= \hat{\mathbf{\Upsilon}}_k \hat{\mathbf{X}}_k + \tilde{\hat{\mathbf{Z}}}_k, \tag{3.4b}$$

where the filtered noise $\tilde{\hat{\mathbf{Z}}}_k = \hat{\mathbf{\Lambda}}_k^\dagger \hat{\mathbf{Z}}_k$ and $(\cdot)^\dagger$ is used to denote a Hermitian transpose. If the noise is spatially white, as stated in Section 2.1.3, then a filtering with a uni-

tary matrix $\hat{\mathbf{\Lambda}}_k^\dagger$ does not alter the noise statistics. In case of spatially coloured noise pre-whitenig must be applied prior to the DFE, which leads to a more complex receiver sturcture [93]. From (3.4b) it is clear that $\hat{\mathbf{\Lambda}}^\dagger$ is used to reflect or to rotate the equivalent channel so that zero elements are produced in the lower triangle. Therefore, the equivalent channel matrix is iteratively transformed to an upper triangular one where the user U experiences no crosstalk, user U-1 experiences crosstalk only from user U, user U-2 experiences crosstalk from user U and U-1 etc. Hence, the signal of user U can be detected, and the crosstalk it causes to the other components of $\hat{\mathbf{Y}}_k$ can be removed. At this point user U-1 can be detected free from crosstalk, and the crosstalk it causes to the remaining users can be removed. The estimate for user u is calculated as [87]

$$\hat{X}_{k,\text{est}}^u = \text{dec}\left[\frac{1}{\hat{\Upsilon}_k^{u,u}}(\hat{Y}_k^u - \sum_{j=u+1}^U \hat{\Upsilon}_k^{u,j}\hat{X}_{k,\text{est}}^j)\right] \tag{3.5}$$

where $\text{dec}[\cdot]$ denotes the decision operator, $\hat{\Upsilon}_k^{u,j} = [\hat{\mathbf{\Upsilon}}_k]_{u,j}$, and $\hat{X}_{k,\text{est}}^u = [\hat{X}_{k,\text{est}}]_{u,u}$. In this thesis I assume error-free decisions, i.e., $\hat{X}_{k,\text{est}} = \hat{X}_k$ which requires perfect channel code. In practice imperfect channel codes are used, which leads to decision errors and consequently error propagation which decreases DFE achievable bit-rates.

3.2.2   Tomlinson-Harashima Precoder

The structure of the Tomlinson-Harashima precoder (THP) [94], similarly as in Section 3.2.1, considers the QR decomposition of the crosstalk channel matrix

$$\check{\mathbf{H}}_k \overset{\text{qr}}{=} \check{\mathbf{\Upsilon}}_k^\dagger \check{\mathbf{\Lambda}}_k^\dagger. \tag{3.6}$$

Prior to transmission, the signal is pre-multiplied by $\check{\mathbf{\Lambda}}_k$ and the received vector is given by

$$\check{\mathbf{Y}}_k = \check{\mathbf{H}}_k \check{\mathbf{\Lambda}}_k \check{\tilde{\mathbf{X}}}_k + \check{\mathbf{Z}}_k, \tag{3.7a}$$
$$= \check{\mathbf{\Upsilon}}_k^\dagger \check{\tilde{\mathbf{X}}}_k + \check{\mathbf{Z}}_k. \tag{3.7b}$$

Since $\check{\mathbf{\Lambda}}_k$ is unitary, compliance with the spectral masks (2.14c) is maintained after the precoding operation. From (3.7b) it follows that the transmission channel has been transformed into a lower triangular channel where user 1 experiences no crosstalk, user 2 experiences crosstalk only from user 1, user 3 experiences crosstalk from users 1 and 2 etc. This structure allows that each user precompensates for the effects of crosstalk

where the signal of user 1 is transmitted directly, i.e.,

$$\check{X}^1_k = \check{X}^1_k \tag{3.8}$$

where $\check{X}^u_k$ denotes the true symbol intended for user u on tone k. At this point the signal transmitted by user 1 is known which allows for the user 2 to predistort its signal, and cancles the crosstalk introduced by user 1. User 2 then operates crosstalk free. This procedure iterates until all users have predistored their signals to annihilate all crosstalk intorduced in the channel. However, this predistortion may lead to a significant energy increase of $\check{\check{X}}^1_k$ (and subsequently of $\check{X}^1_k$). In that case, the solution is to employ modulo operation to bound the power of the transmitted signals to not exceed PSD mask. However, in this thesis I assume that there is no power increase due to the predistortion and consequently the transmitted signals obey PSD masks (i.e., constraint (2.14c)). Under given assumption, at the receiver estimated transmitted symbols is given by

$$\check{X}^u_{k,\text{est}} = \check{X}^u_k + \frac{\check{Z}^u_k}{\Upsilon^{u,u}_k}. \tag{3.9}$$

3.3   Channel State Information (CSI) Error Model

Although channel gains in copper access systems are more stable over the time than in wireless systems, they do exhibit dynamic behaviour, i.e., they are quasi-stationary. Sources of channel dynamics include slow changes in ambient conditions [16] or sudden termination changes on coupled loops [17, 18]. Other sources of imperfect CSI include for example limited error feedback and analog front end design limitations. Therefore, in this Section I present the formulas used for computing the SINR and the achievable bit-rates for linear and non-linear vectoring schemes discussed in Sections 3.1 and 3.2 under erroneous CSI. I denote upstream and downstream channel matrices as $\hat{\mathbf{H}}_k$ and $\check{\mathbf{H}}_k$, respectively, while their estimates are given by $\hat{\mathbf{H}}_{k,\text{est}}$ and $\check{\mathbf{H}}_{k,\text{est}}$. The resulting upstream estimation error matrix on tone k is defined as $\hat{\mathbf{E}}_k = \hat{\mathbf{H}}_k - \hat{\mathbf{H}}_{k,\text{est}}$ while the real channel can thus be written as $\hat{\mathbf{H}}_k = \hat{\mathbf{H}}_{k,\text{est}} + \hat{\mathbf{E}}_k$. I assume that direct channels are always perfectly estimated, i.e., $\hat{H}^{u,u}_{k,\text{est}} = \hat{H}^{u,u}_k$. Equivalent definitions also hold for the dowsntream channel. Assuming that the estimation error matrix $\hat{\mathbf{E}}_k$, the vector of upstream transmitted and received symbols $\hat{\mathbf{X}}_k$ and $\hat{\mathbf{Y}}_k$, and the upstream noise vector $\hat{\mathbf{Z}}_k$ are statistically independent and zero mean, the upstream received PSD for user u

after ZFE is given by [38]

$$\frac{\mathbb{E}\{|\hat{X}^u_{k,\text{est}}|^2\}}{\Delta f} = \frac{\mathbb{E}\left\{\left|\sum_{i,j\in U}\hat{R}^{u,i}_k\hat{H}^{i,j}_k\hat{X}^j_k + \sum_{i\in U}\hat{R}^{u,i}_k\hat{Z}^u_k\right|^2\right\}}{\Delta f}, \tag{3.10a}$$

$$= \frac{\mathbb{E}\left\{\left|\sum_{i,j\in U}\hat{R}^{u,i}_k(\hat{H}^{i,j}_{k,\text{est}} + \hat{E}^{i,j}_k)\hat{X}^j_k + \sum_{i\in U}\hat{R}^{u,i}_k\hat{Z}^u_k\right|^2\right\}}{\Delta f}, \tag{3.10b}$$

$$= \hat{p}^u_k + \sum_{i,j\in U}|\hat{R}^{u,i}_k|^2\hat{\delta}^{i,j}_k\hat{p}^j_k + \sum_{i\in U}|\hat{R}^{u,i}_k|^2\hat{\sigma}^u_k, \tag{3.10c}$$

where $\hat{p}^u_k = \frac{\mathbb{E}\{|\hat{X}^u_k|^2\}}{\Delta f}$ is the upstresm transmitted PSD, $\hat{\delta}^{i,j}_k = \mathbb{E}\{|\hat{E}^{i,j}_k|^2\}$ is the estimation error variance, and $\hat{\sigma}^u_k = \frac{\mathbb{E}\{|\hat{Z}^u_k|^2\}}{\Delta f}$ is the upstream power noise density where $\mathbb{E}\{\cdot\}$ denotes the expectation operator. Note that the term $\sum_{i,j\in U}|\hat{R}^{u,i}_k|^2\hat{\delta}^{i,j}_k\hat{p}^j_k$ represents upstream residual crosstalk due to the CSI error, i.e. intra-group crosstalk while $\sum_{i\in U}|\hat{R}^{u,i}_k|^2\hat{\sigma}^u_k$ is enhanced noise caused by ZFE as discussed in [88].

Under the same assumptions on statistical independence the downstream received PSD for user u after DP is given by [38]

$$\frac{\mathbb{E}\{|\check{X}^u_{k,\text{est}}|^2\}}{\Delta f} = \frac{\mathbb{E}\left\{\left|\sum_{i,j\in U}\check{H}^{u,i}_k\check{S}^{i,j}_k\check{X}^j_k + \check{Z}^u_k\right|^2\right\}}{\Delta f}, \tag{3.11a}$$

$$= \frac{\mathbb{E}\left\{\left|\sum_{i,j\in U}(\check{H}^{u,i}_{k,\text{est}} + \check{E}^{u,i}_k)(\zeta^{-1}_k\check{R}^{i,j}_k\check{D}^{j,j}_{k,})\check{X}^j_k + \check{Z}^u_k\right|^2\right\}}{\Delta f}, \tag{3.11b}$$

$$= \zeta^{-1}_k|\check{H}^{u,u}_{k,\text{est}}|^2\check{p}^u_k + \sum_{i,j\in U}\check{\delta}^{u,i}_k|\zeta^{-1}_k\check{R}^{i,j}_k\check{H}^{j,j}_k|^2\check{p}^j_k + \check{\sigma}^u_k, \tag{3.11c}$$

where $\zeta^{-1}_k|\check{H}^{u,u}_{k,\text{est}}|^2\check{p}^u_k$ is scaled direct channel as discussed in [89] while $\sum_{i,j\in U}\check{\delta}^{u,i}_k|\zeta^{-1}_k\check{R}^{i,j}_k\check{H}^{j,j}_k|^2\check{p}^j_k$ represents the downstream residual crosstalk due to the CSI error. I model the error in crosstalk CSI estimation by the frequency-flat and user independet normalized expression, i.e., $\hat{\xi} = \frac{\hat{\delta}^{i,j}_k}{|\hat{H}^{i,j}_{k,\text{est}}|^2}[\%]$ and assume that $\hat{\xi} = \check{\xi}$. Analogously as in (3.10) the upstream

received PSD for user u after DFE is given by

$$\frac{\mathbb{E}\{|\hat{X}_{k,\text{est}}^u|^2\}}{\Delta f} = \frac{\mathbb{E}\left\{\left|\sum_{i,j\in U}\hat{\Lambda}^{\dagger}{}_k^{u,i}\hat{H}_k^{i,j}\hat{X}_k^j + \sum_{i\in U}\hat{\Lambda}^{\dagger}{}_k^{u,i}\hat{Z}_k^u\right|^2\right\}}{\Delta f}, \tag{3.12a}$$

$$= \frac{\mathbb{E}\left\{\left|\sum_{i,j\in U}\hat{\Lambda}^{\dagger}{}_k^{u,i}(\hat{H}_{k,\text{est}}^{i,j} + \hat{E}_k^{i,j})\hat{X}_k^j + \sum_{i\in U}\hat{\Lambda}^{\dagger}{}_k^{u,i}\hat{Z}_k^u\right|^2\right\}}{\Delta f}, \tag{3.12b}$$

$$= |\hat{\Upsilon}_k^{u,u}|^2\hat{p}_k^u + \sum_{i,j\in U}|\hat{\Lambda}^{\dagger}{}_k^{u,i}|^2\hat{\delta}_k^{i,j}\hat{p}_k^j + \sum_{i\in U}|\hat{\Lambda}^{\dagger}{}_k^{u,i}|^2\hat{\sigma}_k^u, \tag{3.12c}$$

where the multiplication by the unitary matrix $\mathbf{\Lambda}_k$ does not alter the noise statistics, as discussed in Section 3.2.1. The downstream received PSD for user u after THP is given analougsly as in (3.11) by

$$\frac{\mathbb{E}\{|\check{X}_{k,\text{est}}^u|^2\}}{\Delta f} = \frac{\mathbb{E}\left\{\left|\sum_{i,j\in U}\check{H}_k^{u,i}\check{\Lambda}_k^{i,j}\check{X}_k^j + \check{Z}_k^u\right|^2\right\}}{\Delta f}, \tag{3.13a}$$

$$= \frac{\mathbb{E}\left\{\left|\sum_{i,j\in U}(\check{H}_{k,\text{est}}^{u,i} + \check{E}_k^{u,i})\check{\Lambda}_k^{u,i}\check{X}_k^j + \check{Z}_k^u\right|^2\right\}}{\Delta f}, \tag{3.13b}$$

$$= |\check{\Upsilon}^{\dagger}{}_k^{u,u}|^2\check{p}_k^u + \sum_{i,j\in U}\check{\delta}_k^{u,i}|\check{\Lambda}_k^{i,j}|^2\check{p}_k^j + \check{\sigma}_k^u. \tag{3.13c}$$

3.3.1 SINR Calculation

The SINR of an ideal vectoring system (i.e., perfect CSI) is only limited by the background noise and given as [75]

$$\text{SINR}_{k,ideal}^u = \frac{|H_k^{u,u}|^2 p_k^u}{\sigma_k^u}. \tag{3.14}$$

where plane parameters $H_k^{u,u}$, p_k^u, and σ_k^u are used when equivalent definintion holds for both upstream and downstream transmission (cf. Section 2.1.3).

The SINR achieved after ZFE under imperfect CSI is obtained as

$$\text{SINR}_{k,ZFE}^u = \frac{\hat{p}_k^u}{\eta_{k,ZFE}^u + \sum_{i\in U}|\hat{R}_k^{u,i}|^2\hat{\sigma}_k^u}, \tag{3.15}$$

where $\eta^u_{k,ZFE} = \sum_{i,j \in U} |\hat{R}^{u,i}_k|^2 \hat{\delta}^{i,j}_k \hat{p}^j_k$.

The SINR in the case of the DP and imperfect CSI is obtained as

$$\text{SINR}^u_{k,DP} = \frac{\zeta_k^{-2} |\check{H}^{u,u}_k|^2 \check{p}^u_k}{\eta^u_{k,DP} + \check{\sigma}^u_k}, \tag{3.16}$$

where $\eta^u_{k,DP} = \sum_{i,j \in U} \check{\delta}^{u,i}_k |\zeta_k^{-1} \check{R}^{i,j}_k \check{H}^{j,j}_k|^2 \check{p}^j_k$. In case of perfect CSI both $\eta^u_{k,ZFE}$ and $\eta^u_{k,DP}$ would disappear and $\text{SINR}^u_{k,ZFE}$ and $\text{SINR}^u_{k,DP}$ would be only limited with enhanced background noise and power scaling factor ζ, respectively.

SINR equations for non-linear vectoring and imperfect CSI are given as

$$\text{SINR}^u_{k,DFE} = \frac{\hat{p}^u_k |\hat{\Upsilon}^{u,u}_k|^2}{\eta^u_{k,DFE} + \hat{\sigma}^u_k}, \tag{3.17}$$

and

$$\text{SINR}^u_{k,THP} = \frac{\check{p}^u_k |\check{\Upsilon}^{\dagger\,u,u}_k|^2}{\eta^u_{k,THP} + \check{\sigma}^u_k}, \tag{3.18}$$

where $\eta^u_{k,DFE} = \sum_{i,j \in U} |\hat{\Lambda}^{\dagger\,u,i}_k|^2 \hat{\delta}^{i,j}_k \hat{p}^j_k$ and $\eta^u_{k,THP} = \sum_{i,j \in U} \check{\delta}^{u,i}_k |\check{\Lambda}^{i,j}_k|^2 \check{p}^j_k$.

3.3.2   Linear Vectoring Efficiency

Vectoring efficiency is commonly defined as by how much vectoring (in dB) reduces the crosstalk noise compared to the non-vectored case. According to the expression in (3.11c), the residual downstream crosstalk for user u on tone k under DP is given as

$$\sum_{i,j \in U} \check{\delta}^{u,i}_k |\zeta_k^{-1} \check{R}^{i,j}_k \check{H}^{j,j}_k|^2 \check{p}^j_k = \sum_{i,j \in U} \check{\xi} |\check{H}^{u,i}_{k,\text{est}} - \text{diag}\{\check{H}^{1,1}_k, \check{H}^{2,2}_k, ..., \check{H}^{U,U}_k\}|^2 |\zeta_k^{-1} \check{R}_k i, j \check{H}^{j,j}_k|^2 \check{p}^j_k, \tag{3.19}$$

where $\check{\delta}^{u,i}_k = \check{\xi} |\check{H}^{u,i}_{k,\text{est}} - \text{diag}\{\check{H}^{1,1}_k, \check{H}^{2,2}_k, ..., \check{H}^{U,U}_k\}|^2$. For diagonally dominant estimated channel matrices $\check{\mathbf{H}}_{k,\text{est}}$ (i.e., $\check{H}^{u,u}_k \gg \check{H}^{u,j}_k$) it holds that $\check{S}_k = \zeta_k^{-1} \check{\mathbf{R}}_k \check{\mathbf{D}}_k \approx \mathbf{I}_k$ [89] where $\mathbf{I}_k$ is an indentity matrix. Therefore, the downstream residual crosstalk approximately equals to $\sum_{j \in U} \check{\xi} \cdot |\check{H}^{u,j}_{k,\text{est}} - \check{D}^{u,j}_k|^2 \cdot \check{p}^j_k$. In other words, for diagonally dominant $\check{\mathbf{H}}_{k,\text{est}}$ the downstream residual crosstalk approximately equals to $\check{\xi}$ percent of the noise received without vectoring. This is what I also empirically observe in simulations, cf. Figure 3.1. Note that for 100% CSI error the downstream residual crosstalk on low frequencies (where diagonal dominance holds) nearly overlaps with the noise obtained for the case when no vectoring is applied in the downstream. However, on higher G.fast tones the channel matrix is not diagonally dominant and therefore the difference between the crosstalk under 100% CSI error and no vectoring starts to increase.
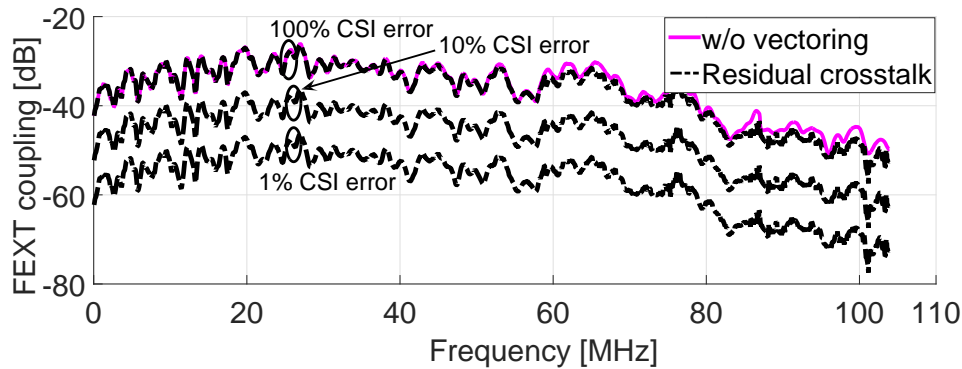
Figure 3.1: Linear reduction of residual downstream FEXT coupling with smaller CSI errors.

3.4 Crosstalk Mitigation Schemes for Partial Vectoring

As mentioned earlier there are network scenarios where signal coordination is possible only among groups of lines (partial vectoring), i.e., each user has signal level coordination with other users in its group, but not with users in other groups. Examples of this include scenario *a)* where two (or more) groups of lines are connected to line terminals that reside on different locations; scenario *b)* where line terminals reside on the same location but are operated by different service providers (sub-loop unbundling); or scenario *c)* where users are partitioned into separate vectoring groups in order to decrease overall vectoring complexity or system level power consumption. For these scenarios, DSM-L1 or L2 have been proposed to mitigate crosstalk between vectoring groups [19–21]. Application scenarios such as scenario *a)* are not expected to occur for FTTDp/FTTB deployments since (G.fast) DSL access multiplexers will be always deployed from the same point (e.g. building basement). However, scenarios like *b)* or *c)* might still arise. An additional scenario which arises for FTTDp/FTTB deployments is where vectoring possibly will not be feasible over all users arises due to one novel aspect of G.fast called reverse power feeding. That is, end user terminals supply power to G.fast devices over the copper line. Furthermore, at the operator's side all equipment will need to draw sufficient power and operate efficiently regardless of how many users are connected to them or how much load is placed on them. Thus, in scenarios with a high number of users it make sense to separate users into different groups in order to reduce system level power consumption. Furthermore, in G.fast setup, i.e., at high frequencies ($\geq 100\,\mathrm{MHz}$) and short loop lengths ($\leq 250\,\mathrm{m}$), crosstalk channel gains become of comparable strength as the direct channel gains or even stronger [3,12]. This resembles the wireless environment characterized with the very strong interference coming from other users. Therefore, in this thesis I also consider interference alignment (IA) [95], a promising wireless mitigation

technique which potentially benefits from strong interference, as an alternative approach to DSM-L2 to mitigate residual crosstalk in partial vectoring.

3.4.1 System and Performance Model for Partial Vectoring

In the following I assume that users are divided into groups indexed by $\mathcal{G} = \{1, \ldots, G\}$, each with N_g members where $\sum_{g=1}^{G} N_g = U$ and $\mathcal{N}_g = \{1, \ldots, N_g\}$. Furthermore, I assume that interference inside each group and among different groups is managed at the signal and transmit power level, respectively. I also assume synchronous DMT among all users having the same modulation parameters. Therefore, transmission can be modeled independently on each tone k as

$$\mathbf{y}_k = \mathbf{H}_k \mathbf{x}_k + \mathbf{z}_k, \tag{3.20}$$

where $\mathbf{H}_k$ is the channel transfer matrix, $\mathbf{X}_k \triangleq \left[(\mathbf{X}_k^1)^\top, (\mathbf{X}_k^2)^\top, ..., (\mathbf{X}_k^G)^\top \right]^\top$, $\mathbf{Y}_k \triangleq \left[(\mathbf{Y}_k^1)^\top, (\mathbf{Y}_k^2)^\top, ..., (\mathbf{Y}_k^G)^\top \right]^\top$, and $\mathbf{Z}_k \triangleq \left[(\mathbf{Z}_k^1)^\top, (\mathbf{Z}_k^2)^\top, ..., (\mathbf{Z}_k^G)^\top \right]^\top$ are the transmitted signal, received signal and background noise vectors, respectively, all on tone k. Sub-vectors $\mathbf{X}_k^g$, $\mathbf{Y}_k^g$, and $\mathbf{Z}_k^g$ are the transmitted signal, received signal and background noise vectors of group g. Thus, (3.20) can also be written as follows

$$\begin{bmatrix} \mathbf{Y}_k^1 \\ \vdots \\ \mathbf{Y}_k^G \end{bmatrix} = \begin{bmatrix} \mathbf{H}_k^{1,1} & \cdots & \mathbf{H}_k^{1,G} \\ \vdots & \ddots & \vdots \\ \mathbf{H}_k^{G,1} & \cdots & \mathbf{H}_k^{G,G} \end{bmatrix} \begin{bmatrix} \mathbf{X}_k^1 \\ \vdots \\ \mathbf{X}_k^G \end{bmatrix} + \begin{bmatrix} \mathbf{Z}_k^1 \\ \vdots \\ \mathbf{Z}_k^G \end{bmatrix} \tag{3.21}$$

where $\mathbf{H}_k^{g,g'}$, $g \neq g'$ contains crosstalk channel gains from group g' to group g while $\mathbf{H}_k^{g,g}$ contains direct channel gains (diagonal elements) and crosstalk channel gains within group g. Furthermore, I denote the u-th user in the group g by (g, u). The transmitted power spectral density (PSD) of user (g, u) on tone k is defined as $p_k^{(g,u)} \triangleq \mathbb{E}\{|X_k^{(g,u)}|^2\}/\Delta f$ while the noise power density of user (g, u) on tone k is defined as $\sigma_k^{(g,u)} \triangleq \mathbb{E}\{|Z_k^{(g,u)}|^2\}/\Delta f$. I assume that the channel matrix $\mathbf{H}_k^{g,g}$ is perfectly known and can be used for the calculation of the per-group crosstalk cancelation matrices. I consider DP and ZFE as downstream and upstream crosstalk cancellation schemes, respectively. Downstream received symbol vector of group g on tone k is given by

$$\check{\mathbf{Y}}_k^g = \check{\mathbf{H}}_k^{g,g} \check{\mathbf{S}}_k^g \mathbf{X}_k^g + \sum_{g' \neq g} \check{\mathbf{H}}_k^{g,g'} \check{\mathbf{S}}_k^{g'} \check{\mathbf{X}}_k^{g'} + \check{\mathbf{Z}}_k^g, \tag{3.22}$$

where $\check{\mathbf{S}}_k^g = (\zeta_k^g)^{-1}(\check{\mathbf{H}}_k^{g,g})^{-1}\operatorname{diag}\{\check{\mathbf{H}}_k^{g,g}\}$ and $\zeta_k^g = \max\limits_{u \in \mathcal{N}_g}\|[(\check{\mathbf{H}}_k^{g,g})^{-1}\operatorname{diag}\{\check{\mathbf{H}}_k^{g,g}\}]_{\operatorname{row} u}\|$.
upstream received symbol vector of group g on tone k is given by

$$\hat{\mathbf{Y}}_k^g = \hat{\mathbf{X}}_k^g + \sum_{g' \neq g} \hat{\mathbf{R}}_k^{g'}\hat{\mathbf{H}}_k^{g,g'}\hat{\mathbf{X}}_k^{g'} + \hat{\mathbf{R}}_k^g\hat{\mathbf{Z}}_k^g. \tag{3.23}$$

where $\hat{\mathbf{R}}_k^{g'} = (\hat{\mathbf{H}}_k^{g',g'})^{-1}$. The SINR of user (g, u) on tone k for ZFE is given by

$$\operatorname{SINR}_{k,ZFE}^{(g,u)} = \frac{p_k^{(g,u)}}{\left(\sum_{g'=1;g'\neq g}^{G}\sum_{u'=1}^{N_{g'}}|\hat{R}_k^{(g,u)}|^2|\hat{H}_k^{(g,u),(g',u')}|^2 p_k^{(g',u')} + |\hat{R}_k^{(g,u)}|^2\hat{\sigma}_k^{(g,u)}\right)}, \tag{3.24}$$

where $\hat{R}_k^{(g,u)} = \hat{R}_k^u$ for $u \in \mathcal{N}_g$ and $\hat{H}_k^{(g,u),(g',u')}$ denotes upstream crosstalk channel gain from user u' in group g' to user u in group g on tone k. The SINR of user (g, u) on tone k under DP is given by

$$\operatorname{SINR}_{k,DP}^{(g,u)} = \frac{p_k^{(g,u)}|\check{H}_k^{(g,u),(g,u)}|^2}{\left(\sum_{g'=1;g'\neq g}^{G}\sum_{u'=1}^{N_{g'}}|\check{H}_k^{(g,u),(g',u')}|^2|\check{S}_k^{(g',u)}|^2 p_k^{(g',u')} + \check{\sigma}_k^{(g,u)}\right)}, \tag{3.25}$$

where $\check{H}_k^{(g,u),(g',u')}$ denotes the downstream crosstalk channel gain from user u' in group g' to user u in group g on tone k. Note that analogously to (3.24) and (3.25) SINR for DFE and THP under partial vectoring can be defined. Furthermore, note that the first summation in (3.24) and (3.25) corresponds to the intra-group crosstalk due to the erroneous CSI while the second summation corresponds to the crosstalk noise generated among different vectoring groups and is avoided by means of DSM-L2 or IA, as I will discuss in the following Section. The number of bits that can be reliably transmitted in upstream and downstream under ZFE and DP on a particular tone k for user (g, u) are determined by [75]

$$\hat{b}_k^{(g,u)} = \log_2\left(1 + \frac{\operatorname{SINR}_{k,ZFE}^{(g,u)}}{\Gamma}\right), \tag{3.26}$$

$$\check{b}_k^{(g,u)} = \log_2\left(1 + \frac{\operatorname{SINR}_{k,DP}^{(g,u)}}{\Gamma}\right), \tag{3.27}$$

while the corresponding achievable bit-rates for user (g, u) are obtained as

$$\hat{R}_k^{(g,u)} = f_s \sum_{k=1}^{K} \hat{b}_k^{(g,u)}, \tag{3.28}$$

$$\check{R}_k^{(g,u)} = f_s \sum_{k=1}^{K} \check{b}_k^{(g,u)}. \tag{3.29}$$

Metrics (3.24)-(3.29) can analogously be derived also for DFE and THP.

3.4.2   Joint Vectoring and DSM-L2

A typical rate-adaptive DSM (RA-DSM) design problem in (2.14) modified for the partial vectoring case is formulated as follows:

$$\max_{\{\mathbf{p}^{(g,u)}, \forall u \in \mathcal{N}_g, g \in \mathcal{G}\}} \sum_{g=1}^{G} \sum_{u=1}^{N_g} R^{(g,u)}, \tag{3.30a}$$

$$\text{s.t.} \sum_{k \in \mathcal{K}} p_k^{(g,u)} \leq P_{tot}^{(g,u)}, \forall u \in \mathcal{N}_g, g \in \mathcal{G} \tag{3.30b}$$

$$0 \leq p_k^{(g,u)} \leq p_{k,mask}^{(g,u)}, \forall u \in \mathcal{N}_g, g \in \mathcal{G}, k \in \mathcal{K}, \tag{3.30c}$$

where $p_k^{(g,u)}$ is a transmit PSD of user (g,u) on tone k, $P_{tot}^{(g,u)}$ is the total transmit power budget for user (g,u), $p_{k,mask}^{(g,u)}$ is the PSD mask for user (g,u) on tone k, and $\mathbf{p}^{(g,u)}$ is the vector containing the PSD of user u in group g on all tones. In this work I apply iterative spectrum balancing (ISB) [85] to the problem in (3.30). The ISB is a fully centralized algorithm, which relies on a centralized network management center to optimize PSDs for all users. The ISB algorithm aims to find a heuristic solution to the problem in (3.30) by sequential (Gauss-Seidel type) optimization of $\mathbf{p}^{(g,u)}$ over all users u and over all vectoring groups g.

3.4.3   Joint Vectoring and IA

Contrary to vectoring, interference alignment does not require all line termination units to be co-located and, therefore, is considered as alternative technique for partial vectoring scenarios. IA is a novel approach for dealing with interference in wireless communications where users experience strong interference and low SINR. Similarly, the strength of crosstalk channels in G.fast becomes comparable with the direct channel or even stronger. Thus, G.fast interference channels resemble wireless interference channels in this respect and this motivates us to investigate application of IA in G.fast. IA cooperatively aligns interfering signals over time, space, or frequency dimensions which are seen as degrees of freedom (DoF). The IA problem is to design the decoders and precoders in such a way that the interfering signals at each receiver fall into a reduced-dimensional subspace. The receivers can then extract the projection of the desired signal that lies in the interference-free subspace. When applied in a partial vectoring scenario, the aim of IA is to align the

interference generated between groups. Thus, the original IA problem for user $u \in \mathcal{N}_g$ and upstream (vectored) transmission for ZFE can be summarized as follows [95]

$$(\hat{\mathbf{U}}^{(g,u)})^{\dagger}\hat{\mathbf{R}}^{(g,u)}\hat{\mathbf{H}}^{(g,u),(g',u')}\hat{\mathbf{V}}^{(g',u')} = \mathbf{0}_{d_{(g,u)} \times d_{(g,u)}}, \forall g' \neq g, \tag{3.31}$$

$$\text{rank}((\hat{\mathbf{U}}^{(g,u)})^{\dagger}\hat{\mathbf{R}}^{(g,u)}\hat{\mathbf{H}}^{(g,u),(g,u)}\hat{\mathbf{V}}^{(g,u)}) = d^{(g,u)}, \tag{3.32}$$

where $\hat{\mathbf{V}}^{(g,u)}$ and $\hat{\mathbf{U}}^{(g,u)}$ are $K \times d^{(g,u)}$ US precoder and decoder matrices for user (g,u), respectivley, $d^{(g,u)}$ denotes the desired number of DoF for user (g,u), and $\hat{\mathbf{H}}^{(g,u),(g,u)}$ and $\hat{\mathbf{R}}^{(g,u)}$ are $K \times K$ US channel matrix and ZFE cancellation matrix for user (g,u), respectivley. For user $u \in \mathcal{N}_g$ and downstream (vectored) transmission for DP the IA problem is:

$$(\check{\mathbf{U}}^{(g,u)})^{\dagger}\check{\mathbf{H}}^{(g,u),(g',u')}\check{\mathbf{S}}^{(g',u')}\check{\mathbf{V}}^{(g',u')} = \mathbf{0}_{d_{(g,u)} \times d_{(g,u)}}, \forall g' \neq g, \tag{3.33}$$

$$\text{rank}((\check{\mathbf{U}}^{(g,u)})^{\dagger}\check{\mathbf{H}}^{(g,u),(g,u)}\check{\mathbf{S}}^{(g',u')}\check{\mathbf{V}}^{(g,u)}) = d^{(g,u)}, \tag{3.34}$$

where $\check{\mathbf{V}}^{(g,u)}$ and $\check{\mathbf{U}}^{(g,u)}$ are $K \times d^{(g,u)}$ downstream precoder and decoder matrices for user (g,u), respectivley, while $\check{\mathbf{H}}^{(g,u),(g,u)}$ and $\check{\mathbf{S}}^{(g,u)}$ are $K \times K$ downstream channel matrix and DP precoding matrix for user (g,u), respectivley. Furthermore, the upstream received signal of user (g,u) after interference alignment is given by:

$$\widetilde{\hat{\mathbf{Y}}}^{(g,u)} = (\hat{\mathbf{U}}^{(g,u)})^{\dagger}\hat{\mathbf{Y}}^{(g,u)} \tag{3.35a}$$

$$= (\hat{\mathbf{U}}^{(g,u)})^{\dagger}\hat{\mathbf{R}}^{(g,u)}\hat{\mathbf{H}}^{(g,u),(g,u)}\hat{\mathbf{V}}^{(g,u)}\hat{\mathbf{X}}^{(g,u)} +$$

$$\sum_{g'=1;g'\neq g}^{G}\sum_{u'=1}^{N_{g'}}(\hat{\mathbf{U}}^{(g,u)})^{\dagger}\hat{\mathbf{R}}^{(g,u)}\hat{\mathbf{H}}^{(g,u),(g',u')}\hat{\mathbf{V}}^{(g',u')}\hat{\mathbf{X}}^{(g',u')} + (\hat{\mathbf{U}}^{(g,u)})^{\dagger}\hat{\mathbf{R}}^{(g,u)}\hat{\mathbf{Z}}^{(g,u)}. \tag{3.35b}$$

Similarly, the downstream received signal of user (g,u) after interference alignment is given by:

$$\widetilde{\check{\mathbf{Y}}}^{(g,u)} = (\check{\mathbf{U}}^{(g,u)})^{\dagger}\check{\mathbf{y}}^{(g,u)} \tag{3.36a}$$

$$= (\check{\mathbf{U}}^{(g,u)})^{\dagger}\check{\mathbf{H}}^{(g,u),(g,u)}\check{\mathbf{S}}^{(g,u)}\check{\mathbf{V}}^{(g,u)}\check{\mathbf{X}}^{(g,u)} +$$

$$\sum_{g'=1;g'\neq g}^{G}\sum_{u'=1}^{N_{g'}}(\check{\mathbf{U}}^{(g,u)})^{\dagger}\check{\mathbf{H}}^{(g,u),(g',u')}\check{\mathbf{S}}^{(g',u')}\check{\mathbf{V}}^{(g',u')}\check{\mathbf{X}}^{(g',u')} + (\check{\mathbf{U}}^{(g,u)})^{\dagger}\check{\mathbf{Z}}^{(g,u)}. \tag{3.36b}$$

In this thesis I assume that users are connected with only one twisted-pair to the network premises. Under this assumption, the DoF lie in the frequency dimension due to the frequency selectivity of the DSL channel. Note that if DSL users were connected with more than one twisted pair to the network premises we could also consider interference alignment in the space dimension, i.e., over multiple-input multiple-output (MIMO) channels. However, in this work I consider the problem of interference alignment over single-input single-output (SISO) frequency selective channels. When IA is done in the frequency dimension, the complexity of IA grows linearly with the number of users and quadratically with the number of tones, i.e., $\mathcal{O}(UK^2)$. However, the scalability of interference alignment can significantly reduce this complexity as I will discuss later.

There are many algorithms in the literature for finding IA precoding and decoding matrices. In general, IA algorithms can be divided into two groups: *a)* algorithms which seek perfect interference alignment (constraints (3.31) are fulfilled) and *b)* algorithms which allow some amount of interference in the signal subspace but tend to maximize some other metrics (e.g., SINR or sum rate). It has been shown that for low to moderate SINR the latter ones yield higher bit-rates [96, 97]. Therefore, in this work I use the Max-SINR algorithm (Algorithm 2 in [96]). Note that authors in [55], who simulate IA for VDSL2 frequencies, use the IA algorithm from the first group of IA algorithms (Algorithm 1 from [96]) in their evaluation and potentially do not gain full benefits from IA for moderate and low SINR scenarios. The Max-SINR algorithm iterates over users and updates precoding and decoding matrices to maximize the SINR. The objective functions of each user (g, u) under ZFE and DP are given by

$$SINR_{ZFE}^{(g,u)} = \frac{\bar{\hat{H}}^{(g,u),(g,u)}\hat{\mathbf{P}}^{(g,u)}(\bar{\hat{H}}^{(g,u),(g,u)})^{\dagger}}{\hat{\mathbf{Q}}^{(g,u)} + \hat{\mathbf{C}}^{(g,u),}} \tag{3.37}$$

$$SINR_{DP}^{(g,u)} = \frac{\bar{\check{H}}^{(g,u),(g,u)}\check{\mathbf{P}}^{(g,u)}(\bar{\check{H}}^{(g,u),(g,u)})^{\dagger}}{\check{\mathbf{Q}}^{(g,u)} + \check{\mathbf{C}}^{(g,u),}} \tag{3.38}$$

where

$$\bar{\hat{H}}^{(g,u),(g,u)} = (\hat{\mathbf{U}}^{(g,u)})^{\dagger}\hat{\mathbf{R}}^{(g,u)}\hat{\mathbf{H}}^{(g,u),(g,u)}\hat{\mathbf{V}}^{(g,u)}, \tag{3.39}$$

and

$$\bar{\check{H}}^{(g,u),(g,u)} = (\check{\mathbf{U}}^{(g,u)})^{\dagger}\check{\mathbf{H}}^{(g,u),(g,u)}\check{\mathbf{S}}^{(g',u')}\check{\mathbf{V}}^{(g,u)}. \tag{3.40}$$

$\hat{\mathbf{C}}^{(g,u)} = \sum_{g'=1;g'\neq g}^{G}\sum_{u'=1}^{N_{g'}}\bar{\hat{H}}^{(g,u),(g',u')}\hat{\mathbf{P}}^{(g',u')}(\bar{\hat{H}}^{(g,u),(g',u')})^{\dagger}$ and
$\check{\mathbf{C}}^{(g,u)} = \sum_{g'=1;g'\neq g}^{G}\sum_{u'=1}^{N_{g'}}\bar{\check{H}}^{(g,u),(g',u')}\check{\mathbf{P}}^{(g',u')}(\bar{\check{H}}^{(g,u),(g',u')})^{\dagger}$ are the upstream and downstream interference covariance matrices while $\hat{\mathbf{Q}}^{(g,u)} = \hat{\sigma}^{(g,u)}\hat{\mathbf{R}}^{(g,u)}(\hat{\mathbf{U}}^{(g,u)})^{\dagger}(\hat{\mathbf{U}}^{(g,u)})$ and $\check{\mathbf{Q}}^{(g,u)} = \check{\sigma}^{(g,u)}(\check{\mathbf{U}}^{(g,u)})^{\dagger}(\check{\mathbf{U}}^{(g,u)})$ are the upstream and downstream noise covariance

matrice of user (g,u). Matrices $\hat{\mathbf{P}}^{(g,u)} = \mathrm{diag}\{\hat{p}_1^{(g,u)}, \hat{p}_2^{(g,u)}, ..., \hat{p}_K^{(g,u)}\}$ and $\check{\mathbf{P}}^{(g,u)} = \mathrm{diag}\{\check{p}_1^{(g,u)}, \check{p}_2^{(g,u)}, ..., \check{p}_K^{(g,u)}\}$ contain the upstream and downstream PSD of user (g,u) over all K tones. I assume that all U users are perfectly synchronized, i.e., $\hat{\mathbf{H}}^{(g,u),(g,u)} = \mathrm{diag}\{\hat{H}_1^{(g,u),(g,u)}, ..., \hat{H}_K^{(g,u),(g,u)}\}$ and $\check{\mathbf{H}}^{(g,u),(g,u)} = \mathrm{diag}\{\check{H}_1^{(g,u),(g,u)}, ..., \check{H}_K^{(g,u),(g,u)}\}$. In a similar way I also define SINR under non-linear vectoring, i.e., DFE and THP where $\bar{\hat{H}}^{(g,u),(g,u)} = (\hat{\mathbf{U}}^{(g,u)})^\dagger (\hat{\mathbf{\Lambda}}^{(g,u)})^\dagger \hat{\mathbf{H}}^{(g,u),(g,u)} \hat{\mathbf{V}}^{(g,u)}$, $\bar{\check{H}}^{(g,u),(g,u)} = (\check{\mathbf{U}}^{(g,u)})^\dagger \check{\mathbf{H}}^{(g,u),(g,u)} \check{\mathbf{\Lambda}}^{(g,u)} \check{\mathbf{V}}^{(g,u)}$, and $\hat{\mathbf{Q}}^{(g,u)} = \hat{\sigma}^{(g,u)} (\hat{\mathbf{\Lambda}}^{(g,u)})^\dagger (\hat{\mathbf{U}}^{(g,u)})^\dagger (\hat{\mathbf{U}}^{(g,u)})$.

Each user (g,u) solves the optimization problem for upstream transmission under ZFE as

$$\max_{\{\hat{\mathbf{V}}^{(g,u)}, \hat{\mathbf{U}}^{(g,u)}, \forall g \in \mathcal{G}, u \in \mathcal{N}_g\}} SINR_{ZFE}^{(g,u)} \tag{3.41a}$$

$$\text{s.t.} \|\hat{V}^{(g,u)}\|_2^2 = 1, \ \forall u \in \mathcal{N}_g, \ g \in \mathcal{G} \tag{3.41b}$$

$$\|\hat{U}^{(g,u)}\|_2^2 = 1, \ \forall u \in \mathcal{N}_g, \ g \in \mathcal{G} \tag{3.41c}$$

where (3.41b) and (3.41c) represent transmit power constraints and $\|.\|_2^2$ denotes the squared L_2 norm. Note that analogous definitions hold for downstream transmission for DP and for upstream and downstream transmissions for DFE and THP, respectively.

3.4.4   Interference Alignment Implementation Issues

Taking into consideration that G.fast systems use 2048 tones for $106\,\mathrm{MHz}$ profile or 4096 tones for $212\,\mathrm{MHz}$ profile, we see how this imposes high computational complexity on IA algorithms. The scalability of interference alignment can significantly reduce this complexity as proposed in [55]. The main idea is to divide the whole available spectrum into K_s sub-bands with $\triangle K_s$ tones per sub-band where the interference alignment is done per each sub-band instead over all tones. Hence, the complexity of IA depends on $\triangle K_s$ instead of K, i.e., $\mathcal{O}(U K_s \triangle K_s^2)$.

Another important factor with respect to the implementation of IA is the diversity of the DSL channel. For SISO channels, diversity both in space and frequency dimensions plays an important role in making IA feasible. Under space diversity I assume different crosstalk channels between different users while frequency diversity is essentially the frequency selectivity of the channel. Based on measurement results [3, 12] it is obvious that DSL exhibits a frequency-selective crosstalk with variations in crosstalk power from one twisted pair to another. Thus, both frequency and spatial diversity requirements are fulfilled. However, the frequently used 99% worst-case FEXT model [75] does not capture entirely the natural diversity of DSL channels. Note that authors in [55] use the 99% worst-case FEXT model and thus potentially obtain lower bit-rates due to the

Table 3.1: Simulation parameters.

Number of users	20 and 12 collocated users
Cable type	Cable model in [1] and measurements in [2] and [3]
Transmit PSD	as defined in [8]
Start (min) frequency	2.2 MHz
End (max) frequency	200 MHz
SNR Gap	10.75 dB
Time asymmetry (US/DS)	1:4
Tone width	$12 * 4.3125$ kHz
Min/max bits per tone	1 bit/12 bits
Background noise	-140 dBm/Hz
Symbol frequency	48000 symbols/s
Sum power	8 dBm
Total loop lengths	10 m, 50 m, 100 m, 150 m, 200 m, 250 m

"poor" diversity of simulated crosstalk channels. In this thesis I consider crosstalk model proposed in [98] where crosstalk dispersion feature is added in order to overcome the limitations of the 99% worst-case FEXT model. The crosstalk model is defined as [98]

$$H_{\text{Ex}-\text{FEXT}}(f) = |H_{\text{FEXT}}(f,d)|e^{j\varphi(f)}10^{-0.05X(f)}, \tag{3.42}$$

where $|H_{\text{FEXT}}(f,d)|$ is the crosstalk amplitude obtained with the 99% worst-case FEXT model, and $\varphi(f)$ and $X(f)$ are random variables modeling the channel phase and amplitude dispersion, respectively.

3.5   Simulation results

3.5.1   Comparison on Linear and Non-linear Vectoring

3.5.1.1   Simulation setup

To encompass the wide range of bit-rates achievable in practical scenarios by the vectoring schemes discussed in Sections 3.1 and 3.2, the following performance evaluation is based on varying loop lengths and different FEXT levels based on offsets of 0 dB and -10 dB. The same simulation conditions listed in Table 3.5.1.1 are used for both linear and non-linear vectoring where for non-linear vectoring I assume sequential line ordering. Furthermore, in the following analysis I compare the achievable bit-rates under linear and non-linear vectoring with and without DSM-L2, where vectoring with DSM-L2 on top is denoted as optimized vectoring. In this thesis I use the DSM-L2 scheme from [99]

(for more details see Section 5.1.1) while when no DSM-L2 is used a simplified power allocation approach is applied, which allows to satisfy the sum-power constraint (2.14b) and PSD mask constraint (2.14c) in the following way

$$p_k^u = \min(p_{k,mask}^u, \mu_{sum})$$ (3.43)

where μ_{sum} is selected to satisfy the sum-power constraint.

3.5.1.2 Results

Figures 3.2 and 3.3 show G.fast average bit-rates under linear and non-linear vectoring, with and without spectrum optimization (i.e. DSM-L2), and using the cable model in [1] for 20 pairs. Presented results confirm the conclusions drawn in [11, 41, 43] where the authors state that spectrum optimization significantly improves linear vectoring bit-rates and therefore reduces the performance gap between the linear and non-linear vectoring. For example, non-linear vectoring outperforms linear vectoring by 17% without DSM-L2 while using DSM-L2 decreases this gap to 8% for the considered downstream transmission (cf. Figure 3.2). Simulations results based on the available measurements of a 20-pair underground cable in [2] and 12-pairs underground cable in [3] also confirm the same conclusions (cf. Figures 3.4–3.6). Furthermore, it should be noted that in this performance analysis the limitations of the considered non-linear vectoring schemes, such as power increase for THP and error propagation for DFE, are neglected and therefore the performance gap under a more realistic setup including this limitations would potentially be even smaller.

In the following, I assume a $-10\,\text{dB}$ FEXT offset, i.e., all FEXT coefficients are reduced by $10\,\text{dB}$. Figures 3.8-3.10 show that in case of a less "harsh" FEXT environment, the performance gap between optimized linear and optimized non-linear vectoring almost vanishes while in the case when no spectrum optimization is applied there is still a performance gap reaching up to 10% , 12%, and 4% for the cable model in [1], measurements in [2], and [3], respectively. The same observations were also found for the corresponding upstream transmissions (results omitted).

Figure 3.2: Average G.fast downstream (DS) bit-rates vs. reach under different precoding methods and for the 20-pair cable model in [1].

Figure 3.3: Average G.fast upstream (US) bit-rates vs. reach under different equalization methods and for the 20-pair cable model in [1].
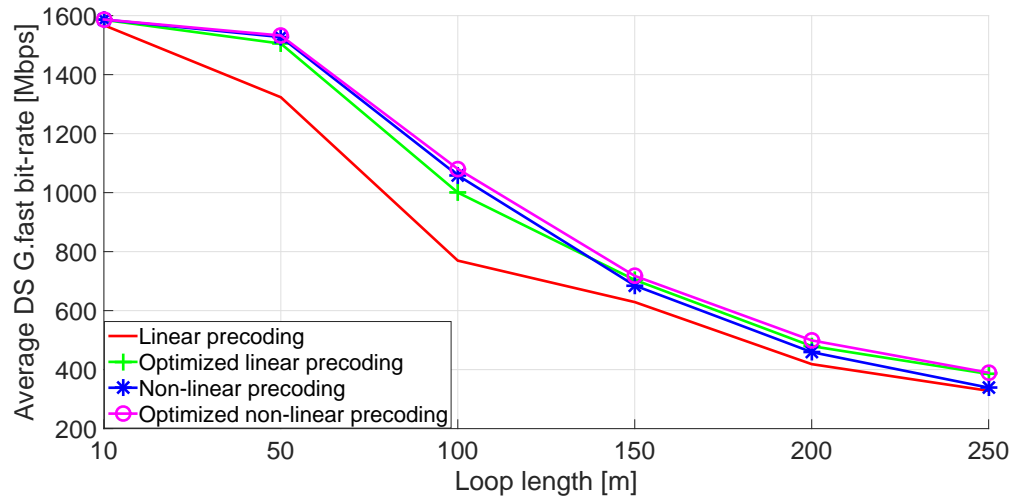
Figure 3.4: Average G.fast downstream (DS) bit-rates vs. reach under different precoding methods and for the 20-pair underground cable in [2].

Figure 3.5: Average G.fast upstream (US) bit-rates vs. reach under different equalization methods and for the 20-pair underground cable in [2].
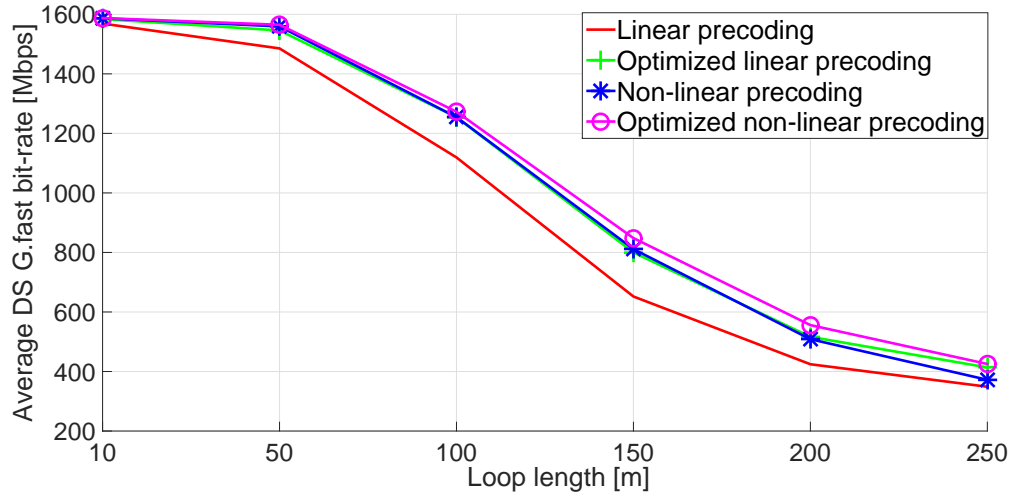
Figure 3.6: Average G.fast downstream (DS) bit-rates vs. reach under different precoding methods and for the 12-pair underground cable in [3].

Figure 3.7: Average G.fast upstream (US) bit-rates vs. reach under different equalization methods and for the 12-pair underground cable in [3].

Figure 3.8: Average G.fast downstream (DS) bit-rates vs. reach under different precoding methods, $-10\,\text{dB}$ FEXT offset and for the 20-pair cable model in [1].

Figure 3.9: Average G.fast downstream (DS) bit-rates vs. reach under different precoding methods, $-10\,\text{dB}$ FEXT offset and for the 20-pair underground cable in [2].

Figure 3.10: Average G.fast downstream (DS) bit-rates vs. reach under different precoding methods, $-10\,\mathrm{dB}$ FEXT offset and for the 12-pair underground cable in [3].

3.5.2 Vectoring with CSI Errors

3.5.2.1 Simulation Setup

In this Section, I will investigate the impact of CSI errors on linear and non-linear vectoring performance. The same simulation setup is used as in Section 3.5.1.1, but additionally assuming CSI errors of 0.1%, 0.5%, and 1%. Since the results in Section 3.5.1.1 provide the same conclusions for both the cable model in [1] and measurements in [2] and [3], in the following I only analyze the results obtained with the model in [1].

3.5.2.2 Results

Figures 3.11-3.13 show the average G.fast downstream bit-rates for different CSI errors and using the 20-pair cable model in [1]. The results indicate that both, optimized linear and optimized non-linear vectoring schemes are very sensitive to a very small variation in CSI (e.g., 0.1%), losing up to 14% and 15% compared to perfect CSI, respectively. However, results also indicate that both, linear and non-linear vectoring benefit from using spectrum optimization where the sensitivity to estimation errors is reduced. For example, linear and non-linear precoding without spectral optimization lose up to 16% and 18% compared to the corresponding bit-rates for perfect CSI scenario, respectively.

In order to compare my results with the results recently published in [44,54] which state that non-linear vectoring is more sensitive to CSI errors than optimized linear vectoring, I also show bit-rate curves for non-linear vectoring without DSM. The results presented in Figures 3.11-3.13 confirm results from [44,54] showing that under CSI errors, optimized linear precoding produces smaller bit-rate losses compared to the perfect CSI scenario than non-optimized non-linear precoding. However, I notice if I also spectrally optimized non-linear vectoring the sensitivity to CSI errors is still higher compared to optimized linear vectoring but the sensitivity is significantly reduced compared to non-optimized non-linear vectoring. Similar observations are also found for upstream transmissions.

Furthermore, similarly as in Section 3.5.1.2 a -10 dB FEXT offset is assumed in order to test the sensitivity of vectoring in a less "harsh" FEXT environment. Figure 3.14 shows the average G.fast downstream bit-rates with 1% CSI error and -10 dB FEXT offset. Comparing the given results with Figure 3.13, the following conclusions are given which also hold for upstream transmission: 1) lower FEXT alleviates the sensitivity of linear and non-linear vectoring on CSI errors and 2.) the performance gap between optimized and non-optimized vectoring (both linear and non-linear) is reduced.
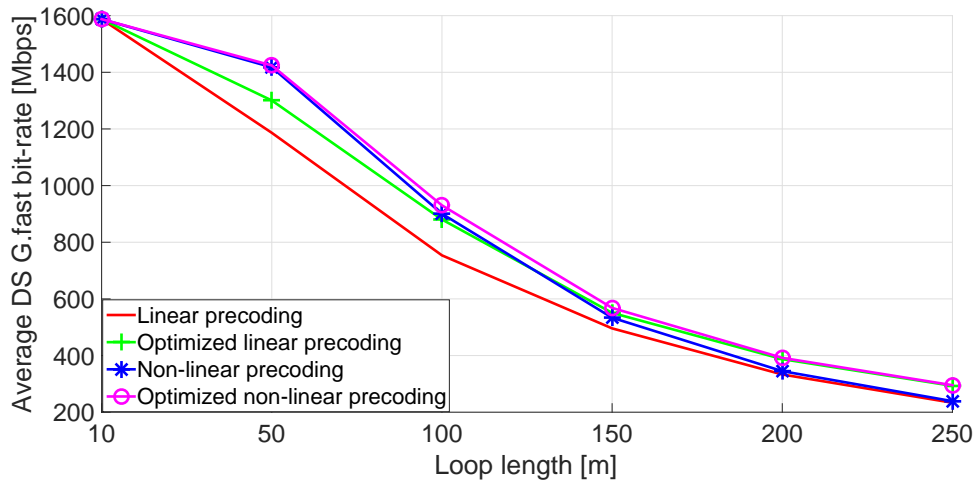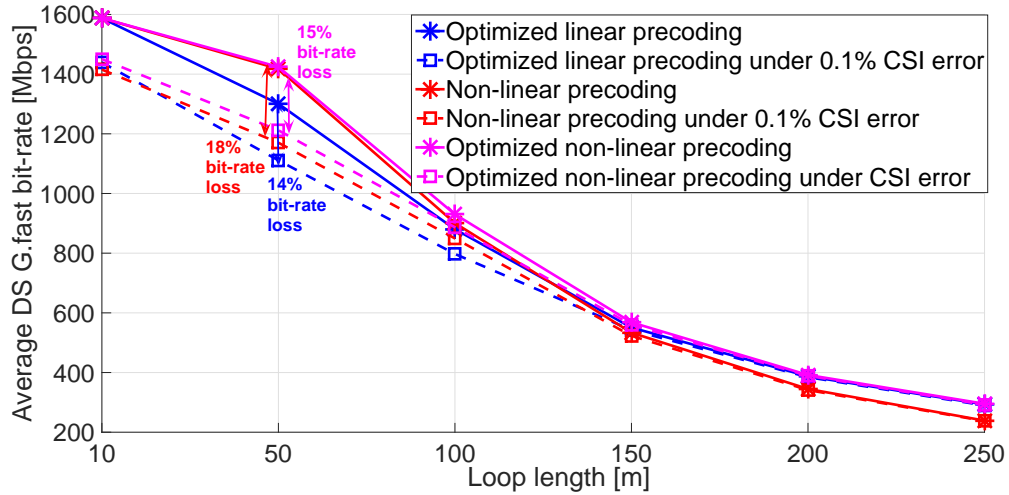
Figure 3.11: Average G.fast downstream (DS) bit-rates vs. reach under different pre-coding methods, 0.1 % CSI error and for the 20-pair cable model in [1].
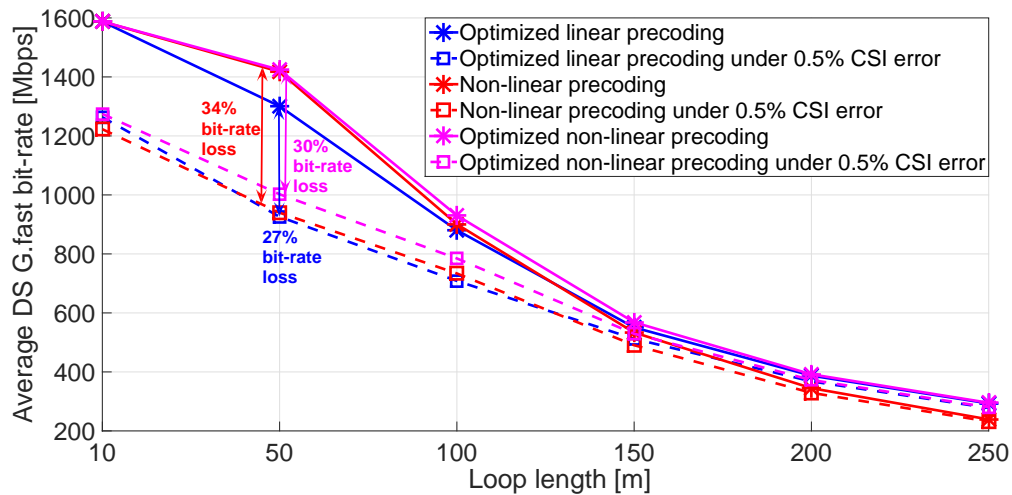
Figure 3.12: Average G.fast downstream (DS) bit-rates vs. reach under different pre-coding methods, 0.5 % CSI error and for the 20-pair cable model in [1].
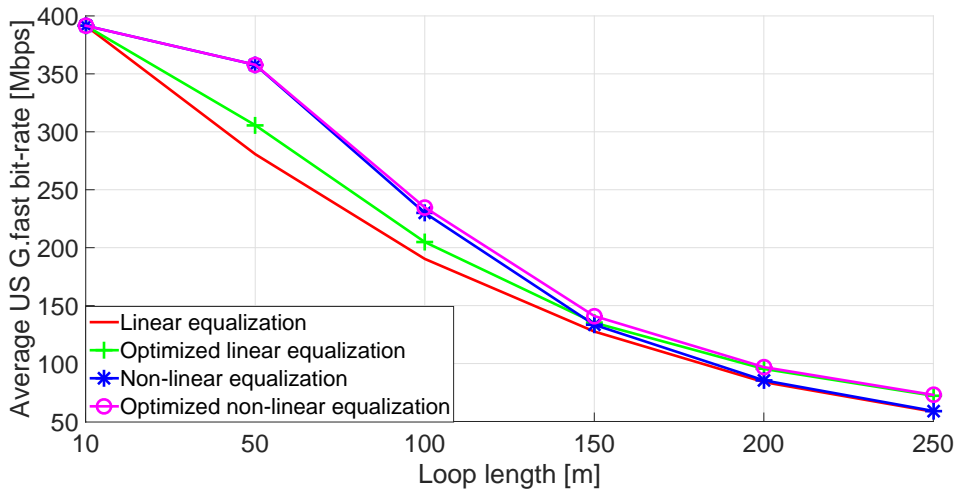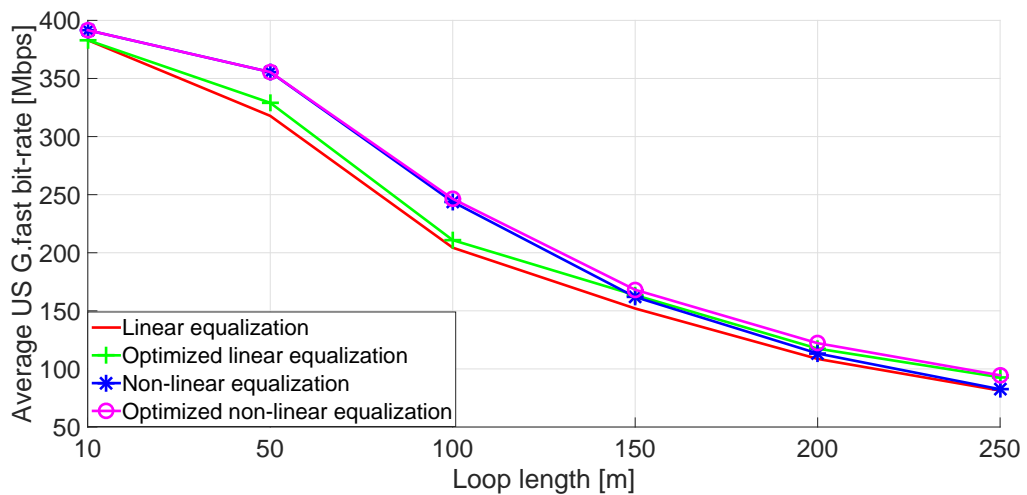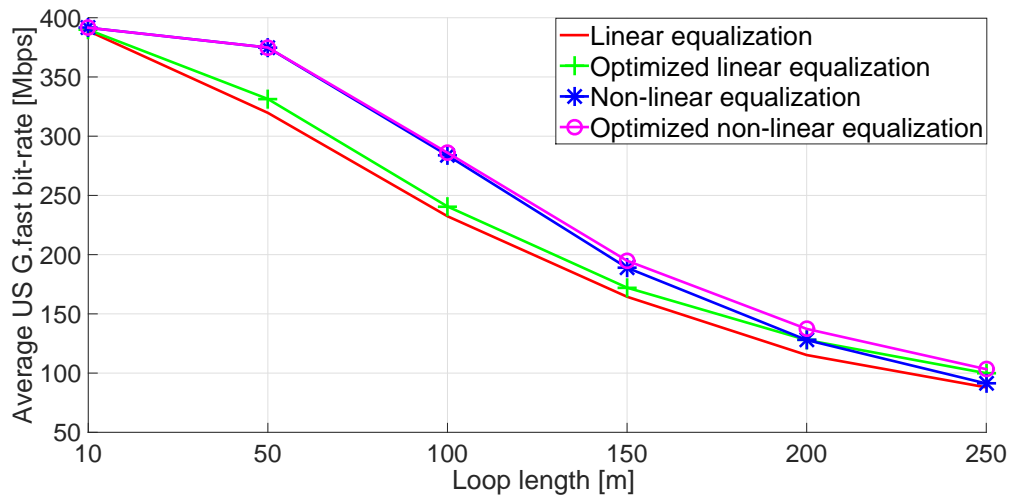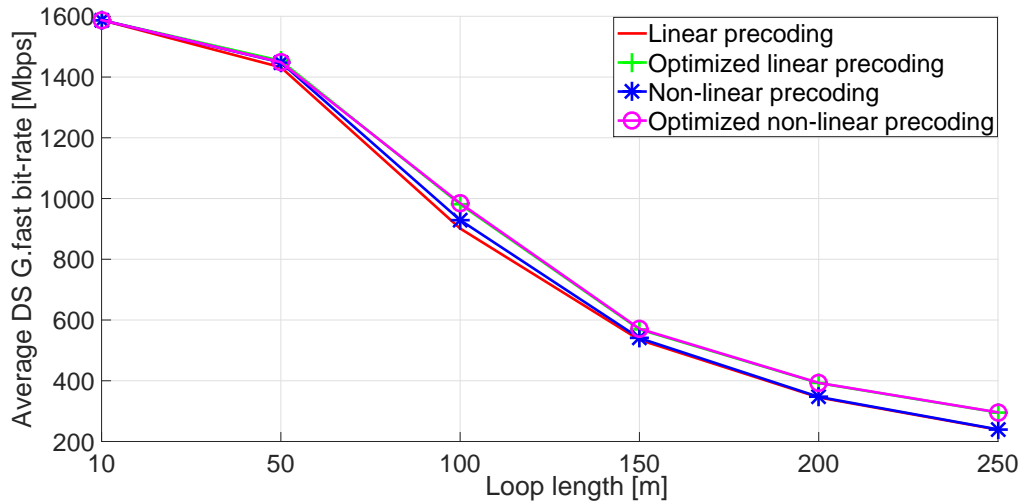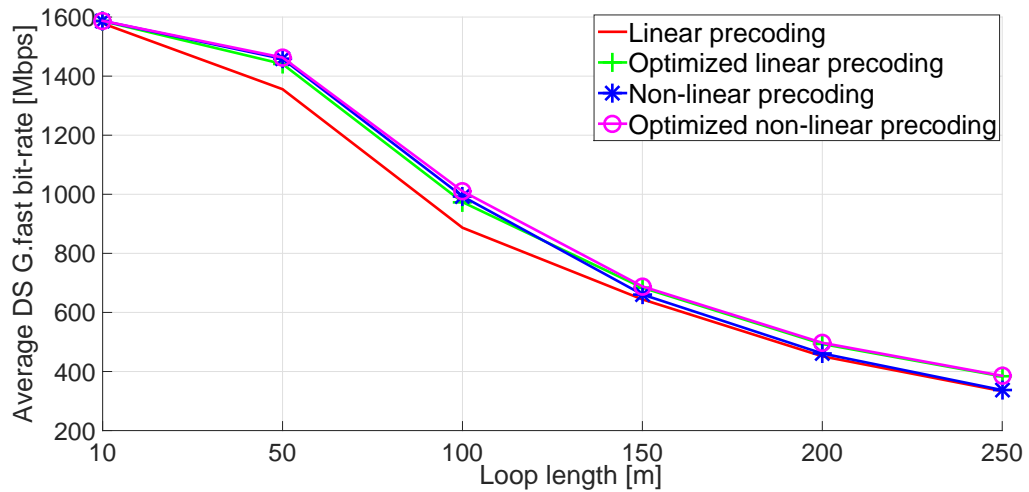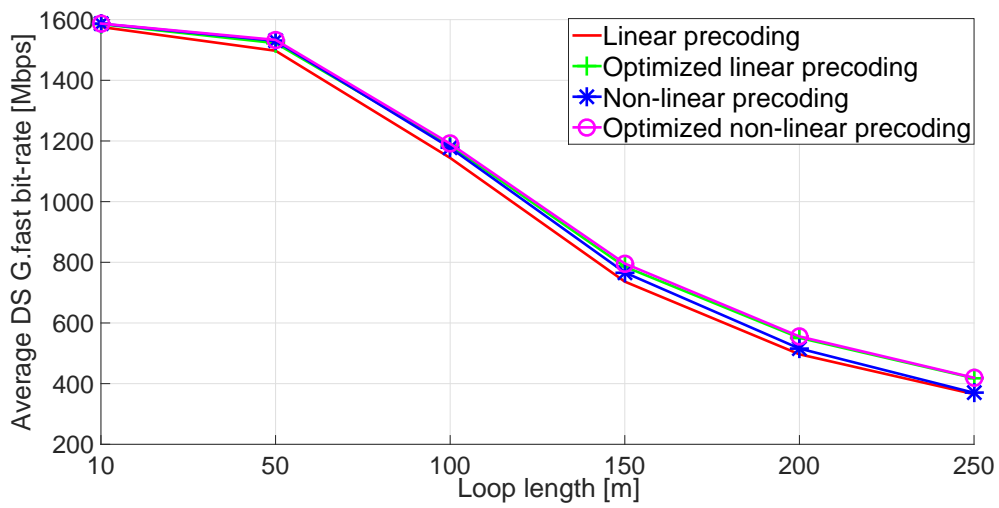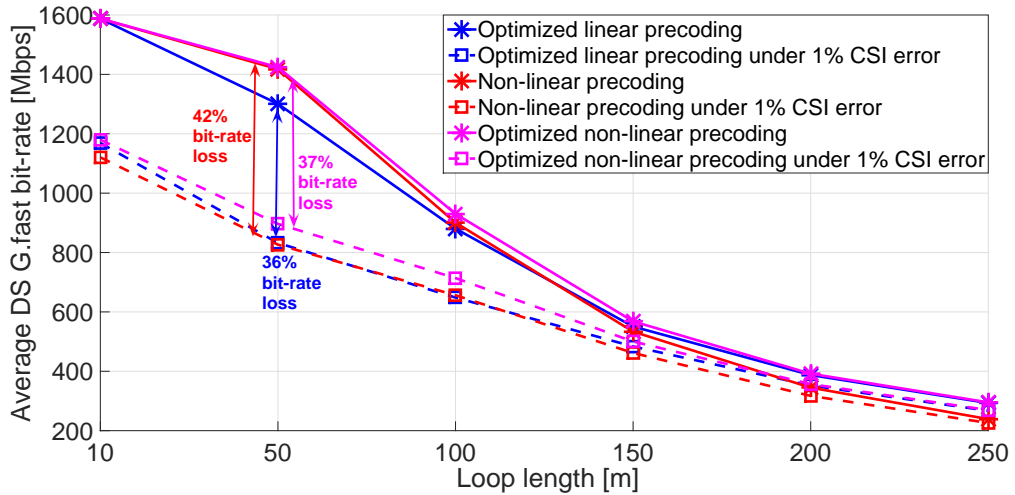
Figure 3.13: Average G.fast downstream (DS) bit-rates vs. reach under different precoding methods, 1% CSI error and for the 20-pair cable model in [1].
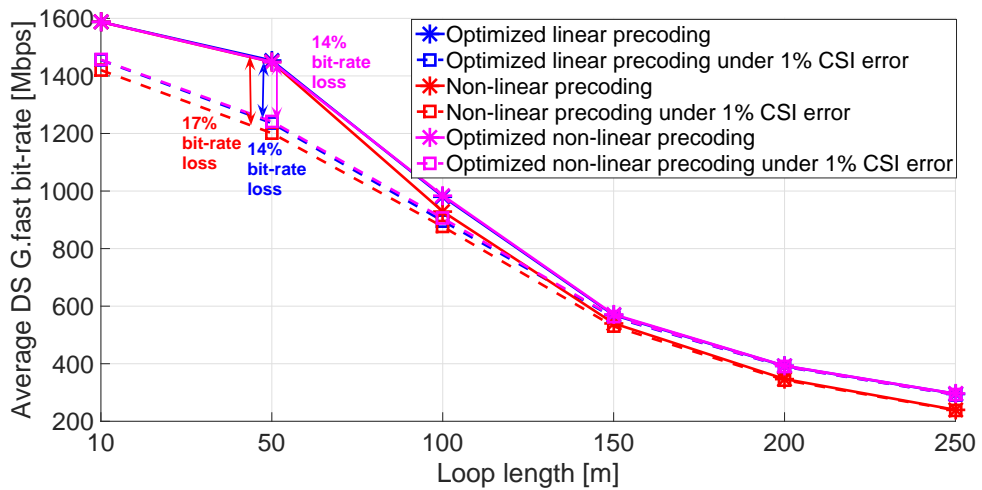
Figure 3.14: Average G.fast downstream (DS) bit-rates vs. reach under different precoding methods, 1% CSI error and for the 20-pair cable model in [1] with $-10\,\mathrm{dB}$ FEXT offset.

3.5.3 Partial Vectoring

3.5.3.1 Simulation Setup

In this Section, I consider two scenarios using the network topology depicted in Figure 3.15:

a) Vectoring is not feasible. Crosstalk noise between users is mitigated with ISB, IA or TDMA.

b) Vectoring is feasible for users within two or three vectoring groups. For two vectoring groups, users $\{1, 2, 3, 7, 8, 9, 13, 14, 15, 19, 20, 21\}$ belong to the first group while all others belong to the second group. For the three groups, users $\{1, 4, 7, 10, 13, 16, 19, 22\}$, $\{2, 5, 8, 11, 14, 17, 20, 23\}$, and $\{3, 6, 9, 12, 15, 18, 21, 24\}$ belong to the first, second, and third group, respectively. Crosstalk noise among groups is mitigated by ISB, IA or TDMA. As a reference I also consider the case where no interference mitigation between groups is applied.
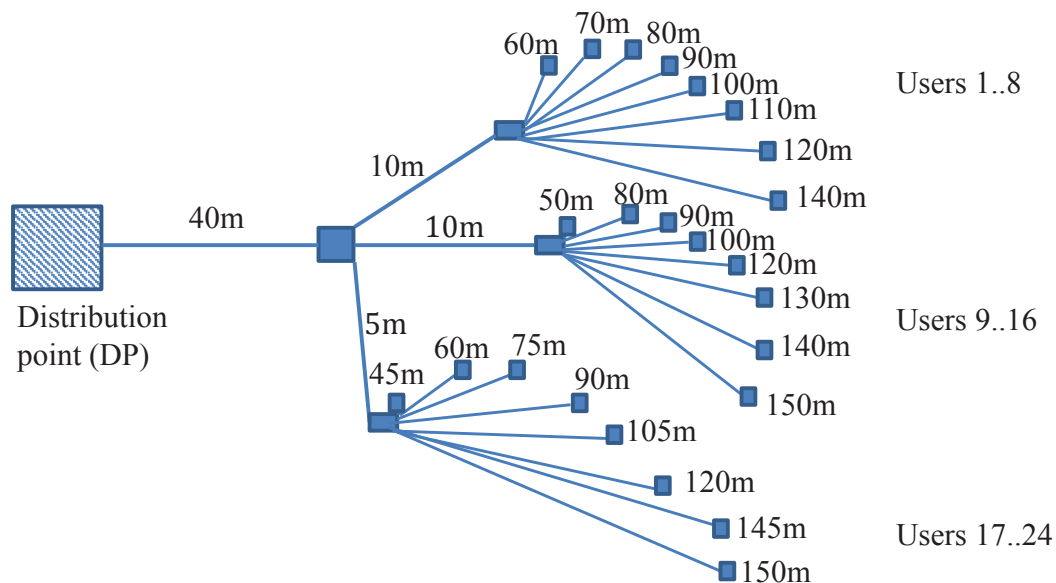
Figure 3.15: Distributed DSL access network.

I evaluate performance for two frequency bands: 2.2 MHz-106 MHz and 106 MHz-212 MHz. I consider different frequency bands because the G.fast standard recommends different DSM techniques for frequencies up to 106 MHz and 212 MHz. Thus, I show the results separately in order to give clear implementation guidelines for two G.fast frequency bands. I consider the TP100 cable model [76] while the simulated G.fast parameters are

given in Table 3.2. I use the crosstalk model proposed in [98] with dispersion parameters $X(f) = 3\,\mathrm{dB}$ and $\varphi(f) = 0\,\mathrm{dB}$ (cf. (3.42)). Furthermore, interference alignment is achieved by independently aligning the interference on K_s sub-bands. I assume $\triangle K_s > 1$ and $K_s = \lceil K / \triangle K_s \rceil$, where $\triangle K_s$ is found by exhaustive search and the last sub-band may have less than $\triangle K_s$ tones.

3.5.3.2   Results for the Frequency Band $2.2\,\mathrm{MHz}$-$106\,\mathrm{MHz}$

Table 3.2 shows the sum rates for different numbers of vectoring groups and for different interference mitigation techniques. Results are compared to network capacity (i.e. interference free scenario) where achievable sum rates are limited only by background noise. Results show that in case when vectoring is feasible over all users (one vectoring group) we are able to achieve $98\,\%$ of network capacity. Furthermore, it can be noticed that in scenario where vectoring is not feasible IA achieves the highest sum rate and it is outperforming ISB and TDMA by $11.5\,\%$ and $222\,\%$, respectively. For comparison I also evaluate IA and ISB performance on lower frequencies ($\leq 30\,\mathrm{MHz}$) where currently deployed DSL systems are operating, VDSL2. In my simulation I consider three VDSL2 band plans: B7-1, B8-4, and B8-15 [100] which use frequencies up to $8\,\mathrm{MHz}$, $17\,\mathrm{MHz}$, and $30\,\mathrm{MHz}$, respectively. Simulation results reveal that in lower frequencies where the SINR is still considerably high (cf. Figure 3.16) ISB performs better than IA achieving $64\,\%$, $58\,\%$, and $30\,\%$ higher sum rates for B7-1, B8-4, and B8-15 band plans, respectively. For partial vectoring, I notice that the effect of crosstalk originating

Figure 3.16: The received power of direct channels and crosstalk channels in $2.2\,\mathrm{MHz}$ to $106\,\mathrm{MHz}$ band for user 1 (cf. Figure 3.15) and different number of vectoring groups (N_g).

Table 3.2: Simulation results for the 2.2 MHz-106 MHz band.

Vectoring	Interference mitigation	N_g	Sum rate [Mbps]	% of network capacity
N	-	-	2391.8	9.3
N	TDMA	-	1064.8	4.2
N	ISB	-	3077.9	12
N	IA	-	3433.8	13.5
Y	-	1	25013.8	98
Y	-	2	3524.9	13.8
Y	TDMA	2	12777.7	50
Y	ISB	2	12763.9	50
Y	IA	2	12545.6	49
Y	-	3	3005.2	11.8
Y	TDMA	3	8518.4	33
Y	ISB	3	8330.2	32.6
Y	IA	3	6744.5	26.4

from different vectoring groups is in large extent mitigated by interference mitigation techniques. I also notice that there is a substantial drop in achievable sum rates when the number of vectoring groups increases from two to three groups. More precisely, the sum rates drop from 50 % to 30 % depending on the interference mitigation scheme applied. Thus, for partial vectoring in G.fast, the number of vectoring groups should be kept as small as possible. Furthermore, the results from Table 3.2 show that sum rates under joint vectoring/ISB and joint vectoring/IA are equal or even (slightly) lower than those under simple joint vectoring/TDMA implementation. This is somehow contrary to conclusions made for previous DSL systems where joint vectoring/ISB (or its alternatives) was shown to be effective solution for partial vectoring [19]. For comparison I also evaluate the performance of joint vectoring/ISB for three VDSL2 band plans: B7-1, B8-4, and B8-15 [100]. Simulation results show that joint vectoring/ISB achieves 58 %, 54 %, and 52 % of network capacity for two groups and 55 %, 42 %, and 33 % of capacity for three groups and VDSL2 band plans B7-1, B8-4, and B8-15, respectively. Thus, we see that in lower frequencies ($\leq$30 MHz) joint vectoring/ISB performs better or eventually equal as TDMA. This can be explained as follows. In higher frequencies the noise power received over crosstalk channels becomes stronger while the power received over the direct channel decreases due to the stronger attenuation at higher frequencies, which results in lower SINR in higher frequencies, cf. Figure 3.16. For low SINR the optimal solution for interference mitigation starts to resemble a simple solution where each group uses one portion of the available bandwidth. In fact, this is exactly the working principle of TDMA.
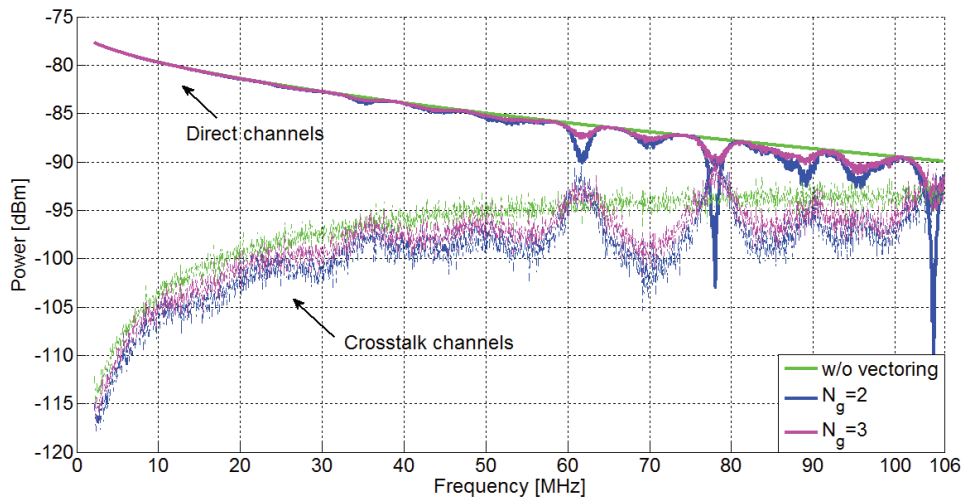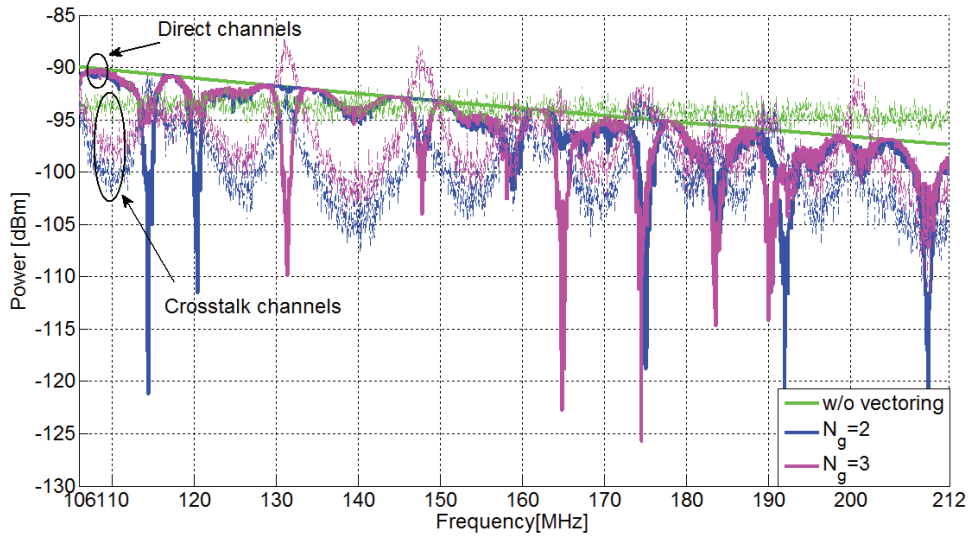
Figure 3.17: The received power of direct channels and crosstalk channels in 106 MHz-212 MHz band for user 1 (cf. Figure 3.15) and different number of vectoring groups (N_g).

3.5.3.3 Results for the Frequency Band 106 MHz-212 MHz

In Table 3.3 I show simulation results for the second frequency band, i.e., 106 MHz-212 MHz band. The results indicate that when vectoring is feasible over all users we are able to achieve 93 % of the network capacity. For the 2.2 MHz-106 MHz band (cf. Section 3.5.3.2) vectoring achieved 98 % of network capacity. The higher bit-rate loss in 106 MHz-212 MHz band is explicable by the higher transmit power scaling (ζ_k) on higher frequencies due to the stronger crosstalk noise as shown in [101]. Furthermore, when vectoring is not feasible IA again achieves the highest sum rates. More precisely, for this frequency band IA achieves 95 % and 202 % higher sum rates compared to ISB and TDMA, respectively. This should be compared with results obtained for the 2.2 MHz-106 MHz band where IA achieved 11.5 % higher sum rates compared to ISB. Figure 3.17 shows how the power received over crosstalk channels becomes dominant with respect to the power received over the direct channel for frequencies above 106 MHz. This results in lower SINR received in the 106 MHz-212 MHz band compared to 2.2 MHz-106 MHz band. Combining this with the results from Section 3.5.3.2 I conclude that IA benefits from strong interference unlike ISB and, therefore, becomes more efficient interference mitigation technique than ISB (and TDMA) for G.fast frequencies, especially for the 106 MHz-212 MHz band. For partial vectoring and without interfer-

Table 3.3: Simulation results for the $106\,\mathrm{MHz}$-$212\,\mathrm{MHz}$ band.

Vectoring	Interference mitigation	N_g	Sum rate [Mbps]	% of network capacity
N	-	-	0	0
N	TDMA	-	714	4.2
N	ISB	-	1103.4	6.4
N	IA	-	2156.3	12.6
Y	-	1	15927.2	93
Y	-	2	65.6	0.4
Y	TDMA	2	8568.4	50
Y	ISB	2	8085.4	47.2
Y	IA	2	7828.8	45.7
Y	-	3	0.2	0
Y	TDMA	3	5712.2	33
Y	ISB	3	5128.5	30
Y	IA	3	5517.1	32.2

ence mitigation mechanisms applied, the achievable sum rates drop compared to the $2.2\,\mathrm{MHz}$-$106\,\mathrm{MHz}$ band, approaching approximately $0\,\mathrm{Mbps}$ for three vectoring groups (meaning that $106\,\mathrm{MHz}$-$212\,\mathrm{MHz}$ band is not usable). ISB and IA improve the achievable sum rate in case of partial vectoring. However, the best results are again achieved using jointly vectoring and TDMA. Except achieving the highest sum rate, TDMA is also less complex compared to ISB and IA. Furthermore, it is inherently present in G.fast systems and, therefore, does not require any additional implementation changes unlike IA.

To summarize, the results indicate that IA achieves better performance compared to ISB and TDMA in case when vectoring is not feasible. From the presented results I also conclude that as crosstalk noise power increases IA gains over ISB and TDMA increase. For partial vectoring, the joint vectoring/TDMA approach yields the highest sum rates compared to the considered interference mitigation techniques.

3.6 Conclusions

In this Section, I analyzed the performance of linear and non-linear vectoring under a G.fast compliant setup, taking into consideration different assumptions: additional dynamic spectrum management level 2 (DSM-L2) optimization, channel state information (CSI) errors, and different FEXT levels. Simulation results show that while there is a considerable gap in achievable bit-rates under the $212\,\mathrm{MHz}$ profile when using non-optimized linear and non-optimized non-linear vectoring, additional spectrum optimiza-

tion, i.e., DSM-L2 improves the performance of both vectoring schemes and reduces the difference to negligible. This is especially visible on shorter loop lengths (<100 m) which represent the actually useful range of the G.fast 212 MHz profile. Furthermore, results also show that both linear and non-linear vectoring are very sensitive to CSI errors, losing up to 16% and 18%, respectively, for 99.9% accurate CSI (i.e. only 0.1% estimation error). Taking optimized vectoring design into account, sensitivity to CSI errors of both linear and non-linear vectoring is mitigated. However, optimized non-linear vectoring shows slightly higher sensitivity than optimized linear vectoring. The results also show that scaling the FEXT coupling coefficients by -10 dB significantly reduces the performance gap between non-optimized linear and non-linear vectoring and their sensitivity to CSI errors.

In this Chapter, I also studied the bit-rates achievable by G.fast when linear vectoring is not feasible or only applied within groups of users (partial vectoring). For the mitigation of crosstalk among groups I considered iterative spectrum balancing (ISB), interference alignment (IA), and time division multiple access (TDMA). Simulation results show that in the case when vectoring is not feasible, IA achieves higher sum rates than ISB and TDMA. For partial vectoring, the results show that the achievable bit-rates drop substantially as the number of vectoring groups increases. Thus, for partial vectoring in G.fast the number of groups should be kept as small as possible. Furthermore, the results show that in case of partial vectoring TDMA achieves the best results among the considered crosstalk mitigation techniques.

4. INTER-CARRIER AND INTER-SYMBOL INTERFERENCE (ICSI) MODELING FOR MULTI-USER DSL

The deployment of G.fast will be gradual and therefore it is realistic to expect that it will share the infrastructure with legacy DSL technologies like vectored very high speed digital subscriber line 2 (VDSL2). G.fast and VDSL2 use discrete multi-tone (DMT) modulation with *different parameters* such as multiplexing schemes (G.fast uses time division duplexing while VDSL2 uses frequency division duplexing), tone spacings, and sampling rates, resulting in inter-carrier and inter-symbol interference (ICSI). ICSI makes crosstalk signals between different G.fast and VDSL2 tones coupled together and consequently per-tone vectoring (discussed in Chapter 3) between the two systems is not practical. Furthermore, dynamic spectrum management level 2 (DSM-L2) algorithms can potentially improve achievable bit-rates of both DSL systems when coexisting by dynamically optimizing transmission power spectra. If estimation of all crosstalk channels is impractical, ICSI model can be used as surrogate for centralized DSM-L2 schemes. The problem of ICSI in asynchronous DSL systems with *identical modulation parameters* has been studied in [57, 58]. A frequency-domain crosstalk cancelation model between *synchronous* VDSL2 systems with different tone spacing has been presented in [59]. The authors in [47] analyze coexistence of G.fast and VDSL2 taking FEXT and NEXT into account, but neglecting the effects of ICSI. The problem of ICSI due to time and frequency offsets has also been well studied in the wireless literature. Exemplary studies modeling and dealing with ICSI originating from wireless channel variations can be found in [60–64] while the authors in [70–72] address ICSI due to carrier frequency offsets. Models for ICSI produced jointly by frequency and time variations have been studied in [65–69]. However, all these ICSI models do not take differences in modulation parameters such as tone spacings and sampling rates into account and therefore can not be used for characterization of ICSI coefficients in G.fast/VDSL2 coexistence scenarios. In this Chapter I define a novel ICSI model for asynchronous DMT systems with different tone spacing and sampling rate which also includes the influence of realistic receive (RX)

and transmit (TX) filters [102, 103]. More precisely, the developed ICSI model provides an upper bound on the ICSI coefficients and therefore allows for a prediction of the minimum achievable bit-rates in coexistence scenarios.

This Chapter is organized as follows. In Section 4.1 I briefly review the DMT system models without and with ICSI. In Sections 4.1.1 and 4.1.2 I derive and analyze the ICSI models for asynchronous DMT systems capturing also modulation differences and the influence of filtering. Note that as an exemplary DSL technologies I assume G.fast and VDSL2. Furthermore, Section 4.2 includes the verification of the proposed ICSI model by time-domain simulations.

4.1 ICSI Signal Model

The achievable bit-rate of user u on tone k for synchronized DMT transmission with identical modulation parameters on all U transmitters is given by (2.12b). Under ICSI the achievable bit-rate of user u on tone k in (2.12b) needs to be modified as [57]

$$\breve{b}_k^u = \log_2\left(1 + \frac{|H_k^{u,u}|^2 p_k^u}{\Gamma(\sum_{j\in\mathcal{U}\setminus u}(\sum_{\bar{k}\in\mathcal{K}}\gamma_{k,\bar{k}}^{u,j}|H_{\bar{k}}^{u,j}|^2 p_{\bar{k}}^j) + \sigma_k^u)}\right), \qquad (4.1)$$

where $\gamma_{k,\bar{k}}^{u,j}$ represents the ICSI coefficient from user j to user u, and from tone $\bar{k}$ to tone k. Note that the received ICSI depends on the PSD allocation of all users on all tones.

4.1.1 Influence of VDSL2 on G.fast

When VDSL2 interferes with G.fast there are two possible scenarios depending on whether one or two VDSL2 symbols influence a G.fast symbol. I start by analyzing the scenario where one VDSL2 symbol interferes with one G.fast symbol, cf. Figure 4.1a.
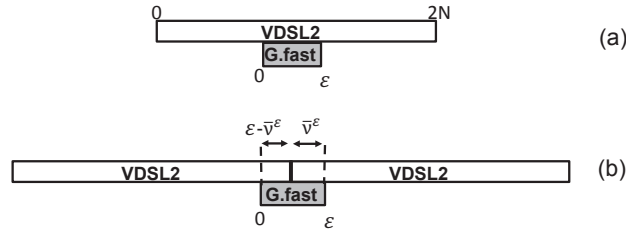

Figure 4.1: Possible time alignments between VDSL2 and G.fast symbols for a DFT block size of ε non-zero samples: a) full alignment and b) partial alignment.

The inverse discrete Fourier transform (IDFT) of a transmitted VDSL2 symbol is given

by

$$y_n = \sum_{k=0}^{2N-1} Y_k e^{j\frac{2\pi nk}{2N}} = \sum_{k=0}^{N-1} Y_k e^{j\frac{2\pi nk}{2N}} + \sum_{k=0}^{N-1} Y_{(2N-k)} e^{j\frac{2\pi n(2N-k)}{2N}}, \qquad (4.2)$$

where n and k denote the VDSL2 time and tone indices, respectively, while $2N$ is the IDFT/DFT block size and N is the number of used VDSL2 tones. Note that in (4.2) I use $Y_N e^{j\frac{2\pi nN}{2N}} = Y_{2N} e^{j\frac{2\pi n2N}{2N}}$. Furthermore, Y_k represents the Hermitian symmetric DFT coefficient at tone k [75]. Assuming Nyquist sampling, G.fast has a higher sampling rate than VDSL2, i.e., $\bar{f}_s > f_s$, where $M = \frac{\bar{f}_s}{f_s}$ is assumed to be an integer. In the folowing I model a VDSL2 transmitter in the digital domain using M-times oversampling followed by low-pass filtering. Therefore, the VDSL2 signal is first upsampled at the VDSL2 transmitter by a factor of M, i.e.,

$$y_{\bar{n}}^{\uparrow} = \begin{cases} y_{\frac{\bar{n}}{M}}, & \text{if } \bar{n} = mM, m \in [0, 1, ..., 2N-1], \\ 0, & \text{otherwise}, \end{cases} \qquad (4.3)$$

where $\bar{n}$ denotes the sample index at sampling rate $\bar{f}_s$. VDSL2 and G.fast use different carrier spacings Δf and $\overline{\Delta f}$, where $\overline{\Delta f} > \Delta f$ and $L = \frac{\overline{\Delta f}}{\Delta f}$ which is assumed to be an integer. The number of VDSL2 tones N and G.fast tones $\bar{N}$ are therefore related as $N = \frac{L\bar{N}}{M}$, i.e., $\frac{N}{L} = \frac{\bar{N}}{M}$. As explained later, upsampling introduces spectral images of the original VDSL2 spectrum. In order to remove those replicas, a low-pass (anti-image) filter with a passband gain of M is used after upsampling. Therefore, the $2\bar{N}$-point DFT of the upsampled and filtered VDSL2 symbol is given as

$$\bar{Y}_{\bar{k}} = \frac{1}{2\bar{N}} \sum_{\bar{n}=0}^{2\bar{N}-1} (y_{\bar{n}}^{\uparrow} * \bar{q}_{\bar{n}}) e^{-j\frac{2\pi \bar{n}\bar{k}}{2N}}, \qquad (4.4a)$$

$$= \frac{1}{2\bar{N}} \sum_{\bar{n}=0}^{2\bar{N}-1} \sum_{\bar{l}=0}^{2\bar{N}-1} y_{\bar{l}}^{\uparrow} \bar{q}_{(\bar{n}-\bar{l})} e^{-j\frac{2\pi \bar{n}\bar{k}}{2N}}, \qquad (4.4b)$$

$$= \frac{1}{2\bar{N}} \sum_{\bar{l}=0}^{2\bar{N}-1} y_{\bar{l}}^{\uparrow} e^{-j\frac{2\pi \bar{l}\bar{k}}{2N}} \sum_{\bar{n}=0}^{2\bar{N}-1} \bar{q}_{(\bar{n}-\bar{l})} e^{-j\frac{2\pi (\bar{n}-\bar{l})\bar{k}}{2N}}, \qquad (4.4c)$$

$$= \frac{\bar{Q}_{\bar{k}}}{2\bar{N}} \sum_{\bar{n}=0}^{\frac{2NM}{L}-1} y_{\bar{n}}^{\uparrow} e^{-j\frac{2\pi \bar{n}L\bar{k}}{2NM}}, \qquad (4.4d)$$

where $*$ denotes the convolution operator while $\bar{q}_{\bar{n}}$ and $\bar{Q}_{\bar{k}}$ are the time and frequency filter taps of the low-pass filter with frequency granularity $\overline{\Delta f}$. Note that in (4.4d) index

$\bar{l}$ was replaced with index $\bar{n}$. Using the definition in (4.3) I can rewrite (4.4d) as

$$\bar{Y}_{\bar{k}} = \frac{\bar{Q}_{\bar{k}}}{\frac{2N}{L}} \sum_{\bar{n}=0}^{\frac{2NM}{ML}-1} y_{M\bar{n}}^{\uparrow} e^{-j\frac{2\pi M\bar{n}L\bar{k}}{2NM}}, \tag{4.5a}$$

$$= \frac{\bar{Q}_{\bar{k}}}{\frac{2N}{L}} \sum_{\bar{n}=0}^{\frac{2N}{L}-1} \left(\sum_{k=0}^{N-1} Y_k e^{j\frac{\pi\bar{n}L\bar{d}_1}{N}} + \sum_{k=0}^{N-1} Y_{(2N-k)} e^{j\frac{\pi\bar{n}L\bar{d}_2}{N}} \right), \tag{4.5b}$$

where $y_{M\bar{n}}^{\uparrow} = y_n$ and y_n is defined in (4.2). The two terms in brackets in (4.5) account for the interference induced from the positive and the negative sides of the VDSL2 spectrum, where $\bar{d}_1 = \frac{k}{L} - \bar{k}$ denotes the spacing between VDSL2 tone k and G.fast tone $\bar{k}$, and $\bar{d}_2 = \frac{(2N-k)}{L} - \bar{k}$ denotes the spacing between VDSL2 tone $2N - k$ and G.fast tone $\bar{k}$. Note that the summation over $\bar{n}$ in Equation (4.5) can only go over an integer number of samples. For example, the VDSL2 profile 17a and the G.fast profile 106a result in $L = 12$ and $N = 4096$, and $\frac{2N}{L}$ is not an integer. In this case the DFT size varies between $\lfloor \frac{2N}{L} \rfloor$ and $\lceil \frac{2N}{L} \rceil$ non-zero samples rather than being a constant value for every DFT block, where $\lceil \cdot \rceil$ and $\lfloor \cdot \rfloor$ denote the ceiling and flooring operators, respectively. Therefore, I define the DFT coefficient at tone $\bar{k}$ for DFT block size ε as

$$\bar{Y}_{\bar{k}}^{\varepsilon} = \frac{\bar{Q}_{\bar{k}}}{\frac{2N}{L}} \sum_{\bar{n}=0}^{\varepsilon-1} \left(\sum_{k=0}^{N-1} Y_k e^{j\frac{\pi\bar{n}L\bar{d}_1}{N}} + \sum_{k=0}^{N-1} Y_{(2N-k)} e^{j\frac{\pi\bar{n}L\bar{d}_2}{N}} \right), \tag{4.6}$$

where $\varepsilon \in \{\lceil \frac{2N}{L} \rceil, \lfloor \frac{2N}{L} \rfloor\}$.[1] From (4.6) I extract contribution from disturber tone k on victim tone $\bar{k}$ as:[2]

$$\bar{Y}_{\bar{k},k}^{\varepsilon} = \frac{\bar{Q}_{\bar{k}}}{\frac{2N}{L}} \left(Y_k \frac{\sin(\frac{\pi L\bar{d}_1}{2N}\varepsilon)}{\sin(\frac{\pi L\bar{d}_1}{2N})} e^{j\frac{\pi L\bar{d}_1}{2N}(\varepsilon-1)} + Y_{(2N-k)} \frac{\sin(\frac{\pi L\bar{d}_2}{2N}\varepsilon)}{\sin(\frac{\pi L\bar{d}_2}{2N})} e^{j\frac{\pi L\bar{d}_2}{2N}(\varepsilon-1)} \right), \tag{4.7}$$

where $\bar{Y}_{\bar{k}}^{\varepsilon} = \sum_{k=0}^{N-1} \bar{Y}_{\bar{k},k}^{\varepsilon}$. The squared magnitude of $\bar{Y}_{\bar{k},k}^{\varepsilon}$ in (4.7) becomes

$$|\bar{Y}_{\bar{k},k}^{\varepsilon}|^2 = W^2 + 2WJ\cos(\phi_W + \phi_J) + J^2, \tag{4.8}$$

where $W = |Y_k| \frac{\sin(\frac{\pi L\bar{d}_1}{2N}\varepsilon)}{\sin(\frac{\pi L\bar{d}_1}{2N})}$, $J = |Y_{2N-k}| \frac{\sin(\frac{\pi L\bar{d}_2}{2N}\varepsilon)}{\sin(\frac{\pi L\bar{d}_1}{2N})}$, $\phi_W = \frac{\pi L\bar{d}_1}{2N}(\varepsilon - 1) + \psi_k$, and $\phi_J = \frac{\pi L\bar{d}_2}{2N}(\varepsilon - 1) - \psi_k$, with ψ_k being the phase encoded in DFT coefficients Y_k and Y_{2N-k}, respectively . Furthermore, I express the ICSI coefficients between tones k and $\bar{k}$ and between users u and $\bar{u}$ as $\bar{\gamma}^{\varepsilon}((\bar{k}, \bar{u}), (k, u)) = \frac{p_{\bar{k}}^{\bar{u}}}{p_k^u}$. I assume that the ICSI

---

[1] Note that ε is an index and not an exponent.

[2] In this step I use the reformulation: $\sum_{n=0}^{N-1} e^{inx} = \frac{\sin(\frac{1}{2}Nx)}{\sin(\frac{1}{2}x)} e^{\frac{ix(N-1)}{2}}$.

coefficients are user independent and therefore omit the user indexing in the following:

$$\bar{\gamma}^{\varepsilon}(\bar{k}, k) = \frac{\mathbb{E}\{|\bar{Y}_{\bar{k},k}^{\varepsilon}|^2\}\frac{1}{\bar{R}}\frac{1}{\overline{\Delta f}}}{\mathbb{E}\{|Y_k|^2\}\frac{1}{R}\frac{1}{\Delta f}},$$ (4.9a)

$$= \frac{(\mathbb{E}\{W^2\} + 2\,\mathbb{E}\{WJ\cos{(\phi_W + \phi_J)}\} + \mathbb{E}\{J^2\})\frac{1}{\bar{R}}\frac{1}{\overline{\Delta f}}}{\mathbb{E}\{|Y_k|^2\}\frac{1}{R}\frac{1}{\Delta f}},$$ (4.9b)

$$= \frac{\bar{Q}_{\bar{k}}^2}{(\frac{2N}{L})^2 L}\left(\frac{\sin^2(\frac{\pi L}{2N}\varepsilon\bar{d}_1)}{\sin^2(\frac{\pi L}{2N}\bar{d}_1)} + \frac{\sin^2(\frac{\pi L}{2N}\varepsilon\bar{d}_2)}{\sin^2(\frac{\pi L}{2N}\bar{d}_2)}\right) \triangleq \bar{\gamma}^{\varepsilon}(\bar{d}_1, \bar{d}_2),$$ (4.9c)

where $\mathbb{E}\{\cdot\}$ is the expectation operator, and R and $\bar{R}$ denote VDSL2 and G.fast refrence resistance, respectively. I assume that both systems use the same reference resistance, i.e., $R = \bar{R}$. Furthermore, to obtain (4.9c) I assume a modulation with symmetrical constellation, $\mathbb{E}\{WJ\cos{(\phi_W + \phi_J)}\} = 0$ since $\cos(\varrho + \pi) = -\cos(\varrho)$. From (4.9c) I can show that ICSI coefficients are $\frac{2N}{L}$ periodic with respect to $\bar{k}$. Specifically, the interval $\bar{k} \in [0, \frac{2N}{L}]$ corresponds to G.fast tones within the VDSL2 spectrum. Due to the ICSI periodicity, G.fast tones outside the VDSL2 spectrum are influenced by ICSI originating from VDSL2 out-of-band spectral images. In order to reduce unwanted spectral images, a low pass filter with taps $\bar{Q}_{\bar{k}}$ has been applied after upsampling to model the out-of-band filter at the DSL TX. As mentioned earlier, when $\frac{2N}{L}$ is not an integer we will have alternating DFT block sizes. Therefore, I define the average ICSI coefficients as

$$\bar{\gamma}(\bar{d}_1, \bar{d}_2) = \alpha\bar{\gamma}^{\varepsilon=\lfloor\frac{2N}{L}\rfloor}(\bar{d}_1, \bar{d}_2) + \beta\bar{\gamma}^{\varepsilon=\lceil\frac{2N}{L}\rceil}(\bar{d}_1, \bar{d}_2),$$ (4.10)

where $\alpha = \text{mod}(\frac{2N}{L}, 1)$ and $\beta = 1 - \alpha$ are the fractions of symbols with length equal to $\lfloor\frac{2N}{L}\rfloor$ and $\lceil\frac{2N}{L}\rceil$, respectively. For overlapping tones I evaluate the limit as

$$\bar{\gamma}(0, \bar{d}_2) = \lim_{\bar{d}_1 \to 0} \bar{\gamma}(\bar{d}_1, \bar{d}_2) = \frac{\bar{Q}_{\bar{k}}^2(\beta\lceil\frac{2N}{L}\rceil^2 + \alpha\lfloor\frac{2N}{L}\rfloor^2)}{(\frac{2N}{L})^2 L} +$$
$$\frac{\bar{Q}_{\bar{k}}^2}{(\frac{2N}{L})^2 L}\left(\beta\frac{\sin^2(\frac{\pi L}{2N}\lceil\frac{2N}{L}\rceil\bar{d}_2)}{\sin^2(\frac{\pi L}{2N}\bar{d}_2)} + \alpha\frac{\sin^2(\frac{\pi L}{2N}\lfloor\frac{2N}{L}\rfloor\bar{d}_2)}{\sin^2(\frac{\pi L}{2N}\bar{d}_2)}\right),$$ (4.11)

where $\bar{\gamma}(\bar{d}_1, 0)$ is defined analogously as in (4.11). Next, I consider the second symbol alignment scenario (see Figure 4.1b) where ε - $\bar{\nu}^{\varepsilon}$ samples of a VDSL2 symbol and $\bar{\nu}^{\varepsilon}$ samples of the following VDSL2 symbol affect one G.fast symbol. Two interfering VDSL2 symbols can be represented as truncated versions of the full-length VDSL2 symbols. The truncation is equivalent to a multiplication with a rectangular window in the time domain. Hence, analogously to (4.4)-(4.7) I obtain the ICSI contributions as

follows:

$$\bar{Y}_{\bar{k},k}^{\varepsilon,I} = \frac{M}{2\bar{N}} \sum_{\bar{n}=0}^{2\bar{N}-1} \left((y_{\bar{n}}^{\uparrow} * \bar{q}_{\bar{n}}) w_{\bar{n}}^{\bar{\nu}^{\varepsilon}} \right) e^{-j\frac{2\pi\bar{n}\bar{k}}{2\bar{N}}}, \tag{4.12a}$$

$$= \frac{\bar{Q}_{\bar{k}}^2}{\frac{2N}{L}} \sum_{\bar{n}=0}^{\bar{\nu}^{\varepsilon}-1} y_{\bar{n}} e^{-j\frac{2\pi\bar{n}\bar{k}L}{2N}}, \tag{4.12b}$$

$$= \frac{\bar{Q}_{\bar{k}}^2}{\frac{2N}{L}} \left(Y_k \frac{\sin(\frac{\pi\bar{\nu}^{\varepsilon}\bar{d}_1 L}{2N})}{\sin(\frac{\pi L\bar{d}_1}{2N})} + Y_{(2N-k)} \frac{\sin(\frac{\pi\bar{\nu}^{\varepsilon}\bar{d}_2 L}{2N})}{\sin(\frac{\pi L\bar{d}_2}{2N})} \right), \tag{4.12c}$$

$$\bar{Y}_{\bar{k},k}^{\varepsilon,II} = \frac{M}{2\bar{N}} \sum_{\bar{n}=0}^{2\bar{N}-1} \left((y_{\bar{n}}^{\uparrow} * \bar{q}_{\bar{n}}) w_{\varepsilon-\bar{n}}^{(\varepsilon-\bar{\nu}^{\varepsilon})} \right) e^{-j\frac{2\pi\bar{n}\bar{k}}{2\bar{N}}}, \tag{4.12d}$$

$$= \frac{\bar{Q}_{\bar{k}}^2}{\frac{2N}{L}} \sum_{\bar{n}=\bar{\nu}^{\varepsilon}}^{\varepsilon-1} y_{\bar{n}} e^{-j\frac{2\pi\bar{n}\bar{k}L}{2N}}, \tag{4.12e}$$

$$= \frac{\bar{Q}_{\bar{k}}^2}{\frac{2N}{L}} \left(Y_k \frac{\sin(\frac{\pi\bar{d}_1 L}{2N}(\varepsilon - \bar{\nu}^{\varepsilon}))}{\sin(\frac{\pi L\bar{d}_1}{2N})} + Y_{(2N-k)} \frac{\sin(\frac{\pi\bar{d}_2 L}{2N}(\varepsilon - \bar{\nu}^{\varepsilon}))}{\sin(\frac{\pi L\bar{d}_2}{2N})} \right), \tag{4.12f}$$

where $w_{\bar{n}}^{\bar{\nu}^{\varepsilon}}$ are the coefficients of a rectangular window of integer width $\bar{\nu}^{\varepsilon} = \lfloor \eta\varepsilon \rfloor$ with $0 \le \eta \le 1$. I assume that VDSL2 symbols are independent. Their contributions to the ICSI coefficients' expected value are therefore additive, yielding the ICSI coefficients for the second symbol alignment scenario:

$$\bar{\gamma}^{\varepsilon}(\bar{d}_1, \bar{d}_2, \bar{\nu}^{\varepsilon}) = \frac{\mathbb{E}\{|\bar{Y}_{\bar{k},k}^{\varepsilon,I}|^2\}\frac{1}{R}\frac{1}{\Delta f}}{\mathbb{E}\{|Y_k + Y_{2N-k}|^2\}\frac{1}{R}\frac{1}{\Delta f}} + \frac{\mathbb{E}\{|\bar{Y}_{\bar{k},k}^{\varepsilon,II}|^2\}\frac{1}{R}\frac{1}{\Delta f}}{\mathbb{E}\{|Y_k + Y_{2N-k}|^2\}\frac{1}{R}\frac{1}{\Delta f}}, \tag{4.13a}$$

$$= \frac{\bar{Q}_{\bar{k}}^2}{(\frac{2N}{L})^2 L} \left(\frac{f^{\varepsilon}(\bar{d}_1, \bar{\nu}^{\varepsilon})}{\sin^2(\frac{\pi L\bar{d}_1}{2N})} + \frac{f^{\varepsilon}(\bar{d}_2, \bar{\nu}^{\varepsilon})}{\sin^2(\frac{\pi L\bar{d}_2}{2N})} \right), \tag{4.13b}$$

where

$$f^{\varepsilon}(\bar{d}_i, \bar{\nu}^{\varepsilon}) = \sin^2\left(\frac{\pi\bar{\nu}^{\varepsilon}\bar{d}_i L}{2N} \right) + \sin^2\left(\frac{\pi\bar{d}_i L}{2N}(\varepsilon - \bar{\nu}^{\varepsilon}) \right), \tag{4.14}$$

for $0 \le \bar{\nu}^{\varepsilon} \le \varepsilon$. Average ICSI coefficients are given analogously to (4.10) as

$$\bar{\gamma}(\bar{d}_1, \bar{d}_2, \bar{\nu}^{\varepsilon=\lfloor\frac{2N}{L}\rfloor}, \bar{\nu}^{\varepsilon=\lceil\frac{2N}{L}\rceil}) = \alpha\bar{\gamma}^{\varepsilon=\lfloor\frac{2N}{L}\rfloor}(\bar{d}_1, \bar{d}_2, \bar{\nu}^{\varepsilon=\lfloor\frac{2N}{L}\rfloor}) + \beta\bar{\gamma}^{\varepsilon=\lceil\frac{2N}{L}\rceil}(\bar{d}_1, \bar{d}_2, \bar{\nu}^{\varepsilon=\lceil\frac{2N}{L}\rceil}). \tag{4.15}$$

As we see from (4.15), the crosstalk spectrum depends on the offset $\bar{\nu}^{\varepsilon}$ which in practice is not available. Therefore, in the rest of the paper I consider a bound on the worst-case ICSI coefficients depending on the offset $\bar{\nu}^{*\varepsilon} = \arg\max_{0\le\bar{\nu}^{\varepsilon}\le\varepsilon}\{f^{\varepsilon}(\bar{d}_i, \bar{\nu}^{\varepsilon})\}$. The analytic expression for $f(\bar{d}_i, \bar{\nu}^{*\varepsilon})$ is rigourously derived in C and the worst-case ICSI has the following form:

Proposition 1. *A bound on the worst-case ICSI coefficients in (4.15) is given by*

$$\bar{\gamma}^*(\bar{d}_1, \bar{d}_2) = \alpha\bar{\gamma}^{*\varepsilon=\lfloor\frac{2N}{L}\rfloor}(\bar{d}_1, \bar{d}_2) + \beta\bar{\gamma}^{*\varepsilon=\lceil\frac{2N}{L}\rceil}(\bar{d}_1, \bar{d}_2), \tag{4.16}$$

where $\bar{\gamma}^{*\varepsilon}(\bar{d}_1, \bar{d}_2) = \frac{\bar{Q}_{\bar{k}}^2}{(\frac{2N}{L})^2 L}(\bar{\rho}^*(\bar{d}_1) + \bar{\rho}^*(\bar{d}_2))$, where

$$\bar{\rho}^*(\bar{d}_i) = \begin{cases} \frac{f^{*\varepsilon}(\bar{d}_1)}{\sin^2(\frac{\pi L \bar{d}_1}{2N})}, & \text{for } |\bar{d}_i| \neq 0, \\ \varepsilon^2, & \text{for } |\bar{d}_i| = 0, \end{cases} \tag{4.17}$$

and where

$$f^{*\varepsilon}(\bar{d}_i) = \max_{0 \leq \bar{\nu}^\varepsilon \leq \varepsilon} \{f^\varepsilon(\bar{d}_i, \bar{\nu}^\varepsilon)\} = \begin{cases} \sin^2(\frac{\pi L \bar{d}_i}{2N}\varepsilon), & \text{if } 0 < (\frac{\pi L |\bar{d}_i|}{2N}) < \frac{\pi}{2}, \\[2mm] 2\sin^2(\frac{\pi L \bar{d}_i}{4N}\varepsilon), & \text{if } \frac{\pi}{2} < (\frac{\pi L |\bar{d}_i|}{2N}) \bmod 2 < \frac{3\pi}{2}, \\[2mm] 2\cos^2(\frac{\pi L \bar{d}_i}{4N}\varepsilon), & \text{if } 0 \leq (\frac{\pi L |\bar{d}_i|}{2N}) \bmod 2 < \frac{\pi}{2}, \\ & \text{or } \frac{3\pi}{2} < (\frac{\pi L |\bar{d}_i|}{2N}) \bmod 2 < 2\pi, \\[2mm] 1, & \text{if } |\bar{d}_i| = F\frac{2N}{L}\varepsilon^{-1} \text{where } F \text{ is uneven integer.} \end{cases} \tag{4.18}$$

Proof. The proof is given in C.   □

Finally, average ICSI coefficients for partial symbol alignment are obtained by taking into consideration $(L-1)$ aligned VDSL2 symbols and two partially aligned VDSL2 symbols, i.e.,

$$\bar{\bar{\gamma}}(\bar{d}_1, \bar{d}_2) = \frac{(L-1)}{L}\bar{\gamma}(\bar{d}_1, \bar{d}_2) + \frac{1}{L}\bar{\gamma}^*(\bar{d}_1, \bar{d}_2). \tag{4.19}$$

A comparison of ICSI coefficients using (4.10) and (4.19) for symbol alignment and worst-case symbol offset, respectively, on G.fast tone $\bar{k} = 145$ is shown in Figure 4.2, assuming perfect TX filtering at VDSL2 transceivers[3].

---

[3] Under perfect RX or TX filtering I assume RX or TX filters with unitary amplitude over VDSL2 tones and zero amplitude elsewhere.
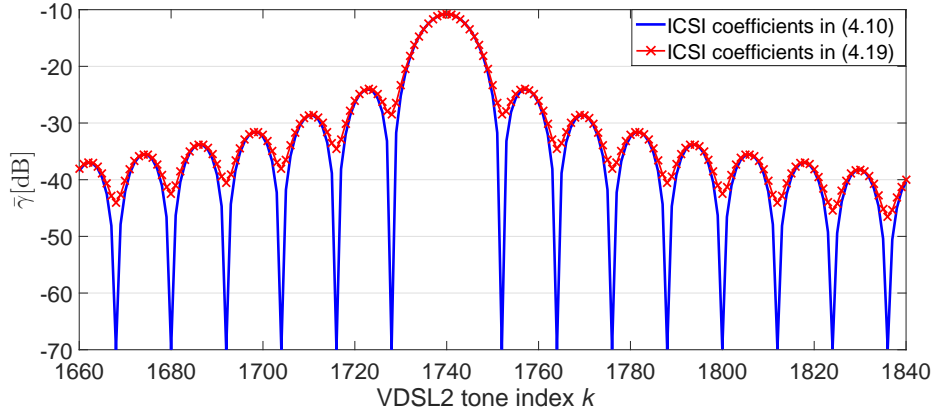
Figure 4.2: ICSI coefficients for G.fast tone $\bar{k} = 145$ calculated with (4.10) and (4.19), respectively with modulation parameters as defined in Section 5 and perfect VDSL2 TX filtering.

4.1.2   Influence of G.fast on VDSL2

Analyzing the influence of G.fast on VDSL2 I have again two possible scenarios: L entire G.fast symbols influence one VDSL2 symbol or L - 1 entire and 2 partial G.fast symbols influence one VDSL2 symbol. I begin by analyzing the earlier alignment scenario, illustrated in Figure 4.3a.
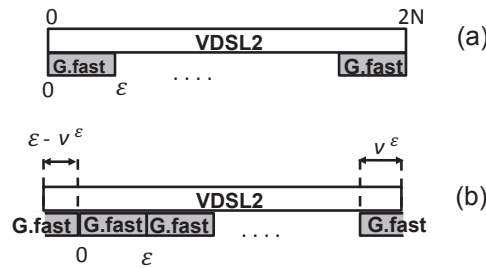
Figure 4.3: Possible time alignments between G.fast and VDSL2 symbols for a DFT block size of ε non-zero samples: a) full alignment and b) partial alignment.

The IDFT of a G.fast symbol is given by

$$\bar{y}_{\bar{n}} = \sum_{\bar{k}=0}^{2\bar{N}-1} \bar{Y}_{\bar{k}} e^{j\frac{2\pi \bar{n}\bar{k}}{2\bar{N}}} = \sum_{\bar{k}=0}^{\bar{N}-1} \bar{Y}_{\bar{k}} e^{j\frac{2\pi \bar{n}\bar{k}}{2\bar{N}}} + \sum_{\bar{k}=0}^{\bar{N}-1} \bar{Y}_{(2\bar{N}-\bar{k})} e^{j\frac{2\pi \bar{n}(2\bar{N}-\bar{k})}{2\bar{N}}}, \qquad (4.20)$$

where $\bar{Y}_{\bar{k}}$ is the DFT coefficient at tone $\bar{k}$. Due to the M times higher sampling rate, in my model I first downsample the G.fast symbol by factor of M at the VDSL2 receiver. More precisely, I model the VDSL2 receiver in the digital domain as an M-times over-sampling analog-to-digital converter followed by low-pass (anti-aliasing) filtering with filter coefficients $\bar{q}_{\bar{n}}$ and a passband gain of one followed by downsampling by a factor of

M. Therefore, the filtered G.fast symbol $\bar{\bar{y}}_{\bar{n}} = \bar{y}_{\bar{n}} * \bar{q}_{\bar{n}}$ after downsampling is denoted as $\bar{\bar{y}}_n^\downarrow = \bar{\bar{y}}_{nM}$. Since I analyze the effect of a single G.fast symbol, I use zero-padding to obtain the L-times longer VDSL2 interference symbol. The DFT of the padded G.fast symbol is given as

$$Y_k = \frac{1}{2N} \sum_{n=0}^{2N-1} \text{ZeroPad}(\bar{\bar{y}}_n^\downarrow) e^{-j\frac{2\pi nk}{2N}}, \tag{4.21a}$$

$$= \frac{1}{2N} \sum_{n=0}^{\frac{2N}{L}-1} \bar{\bar{y}}_n^\downarrow e^{-j\frac{2\pi nk}{2N}} \tag{4.21b}$$

$$= \frac{1}{2N} \sum_{n=0}^{\frac{2N}{L}-1} \bar{\bar{y}}_{nM} e^{-j\frac{2\pi nk}{2N}}, \tag{4.21c}$$

$$= \frac{1}{2N} \sum_{n=0}^{\frac{2N}{L}-1} \sum_{l=0}^{2\bar{N}-1} \bar{q}_l \bar{y}_{(nM-l)} e^{-j\frac{2\pi nk}{2N}}, \tag{4.21d}$$

$$= \frac{1}{2N} \sum_{l=0}^{2\bar{N}-1} \bar{q}_l e^{-j\frac{2\pi nk}{2N}} \sum_{n=0}^{\frac{2N}{L}-1} \sum_{\bar{k}=0}^{2\bar{N}-1} \bar{Y}_{\bar{k}} e^{j\frac{2\pi \bar{k}Ln}{2N}} e^{-j\frac{2\pi nk}{2N}}, \tag{4.21e}$$

$$= \frac{\bar{Q}_{\bar{k}}}{2N} \sum_{n=0}^{\frac{2N}{L}-1} \left(\sum_{\bar{k}=0}^{\bar{N}-1} \bar{Y}_{\bar{k}} e^{j\frac{\pi nd_1}{N}} + \sum_{\bar{k}=0}^{\bar{N}-1} \bar{Y}_{2\bar{N}-\bar{k}} e^{j\frac{\pi nd_2}{N}} \right), \tag{4.21f}$$

where $d_1 = L\bar{k} - k$ denotes the distance between tones $\bar{k}$ and k and $d_2 = L(2\bar{N}-\bar{k}) - k$ denotes the distance between tones $2\bar{N} - \bar{k}$ and k. Equivalently as in Section 4.1.1, DFT coefficients depend on the factor ε, i.e.,

$$Y_k^\varepsilon = \frac{\bar{Q}_{\bar{k}}}{2N} \left(\sum_{\bar{k}=0}^{\bar{N}-1} \bar{Y}_{\bar{k}} \frac{\sin(\frac{\pi d_1}{2N}\varepsilon)}{\sin(\frac{\pi d_1}{2N})} e^{j\frac{\pi d_1}{2N}(\varepsilon-1)} + \sum_{\bar{k}=0}^{\bar{N}-1} \bar{Y}_{2\bar{N}-\bar{k}} \frac{\sin(\frac{\pi d_2}{2N}\varepsilon)}{\sin(\frac{\pi d_2}{2N})} e^{j\frac{\pi d_2}{2N}(\varepsilon-1)} \right). \tag{4.22}$$

From (4.22) I can extract the contribution from disturber tone $\bar{k}$ to victim tone k as:

$$Y_{k,\bar{k}}^\varepsilon = \frac{\bar{Q}_{\bar{k}}}{2N} \left(\bar{Y}_{\bar{k}} \frac{\sin(\frac{\pi d_1}{2N}\varepsilon)}{\sin(\frac{\pi d_1}{2N})} e^{j\frac{\pi d_1}{2N}(\varepsilon-1)} + \bar{Y}_{(2\bar{N}-\bar{k})} \frac{\sin(\frac{\pi d_2}{2N}\varepsilon)}{\sin(\frac{\pi d_2}{2N})} e^{j\frac{\pi d_2}{2N}(\varepsilon-1)} \right), \tag{4.23}$$

where $Y_k^\varepsilon = \sum_{\bar{k}=0}^{\bar{N}-1} Y_{k,\bar{k}}^\varepsilon$. The per-symbol ICSI coefficients $\tilde{\gamma}^\varepsilon(\bar{k}, k) = \frac{p_k^u}{p_{\bar{k}}^u}$ are then calculated analogously as in Section 4.1.1 by:

$$\tilde{\gamma}^\varepsilon(\bar{k}, k) = \frac{\mathbb{E}\{|Y_{k,\bar{k}}^\varepsilon|^2\}\frac{1}{R}\frac{1}{\Delta f}}{\mathbb{E}\{|\bar{Y}_{\bar{k}} + \bar{Y}_{2\bar{N}-\bar{k}}|^2\}\frac{1}{R}\frac{1}{\Delta f}}, \tag{4.24a}$$

$$= \frac{\bar{Q}_{\bar{k}}^2 L}{(2N)^2} \left(\frac{\sin^2(\frac{\pi d_1}{2N}\varepsilon)}{\sin^2(\frac{\pi d_1}{2N})} + \frac{\sin^2(\frac{\pi d_2}{2N}\varepsilon)}{\sin^2(\frac{\pi d_2}{2N})} \right) \triangleq \tilde{\gamma}^\varepsilon(d_1, d_2). \tag{4.24b}$$

From (4.24b) we see that the ICSI coefficients are again $\frac{2N}{L}$ periodic with respect to $\bar{k}$.

As mentioned in Section 4.1.1, the interval $\bar{k} \in [0, \frac{2N}{L}]$ corresponds to G.fast tones within the VDSL2 spectrum. G.fast tones above the VDSL2 spectrum will be replicated into the VDSL2 spectrum due to the ICSI periodicity. This overlapping effect is called *aliasing* and is reduced by using a low pass filter with DFT coefficients $\bar{Q}_{\bar{k}}$ before downsampling. The average ICSI coefficients are given as:

$$\tilde{\bar{\gamma}}(d_1, d_2) = \alpha \tilde{\gamma}^\varepsilon(d_1, d_2) + \beta \tilde{\gamma}^\varepsilon(d_1, d_2). \tag{4.25}$$

For overlapping tone I again evaluate the limit as

$$\tilde{\bar{\gamma}}(0, d_2) = \lim_{d_1 \to 0} \tilde{\bar{\gamma}}(\bar{d}_1, \bar{d}_2) = \frac{L\bar{Q}_{\bar{k}}^2(\beta \lceil \frac{2N}{L} \rceil^2 + \alpha \lfloor \frac{2N}{L} \rfloor^2)}{(2N)^2} +$$
$$\frac{L\bar{Q}_{\bar{k}}^2}{(2N)^2} \left(\beta \frac{\sin^2(\frac{\pi d_2}{2N} \lceil \frac{2N}{L} \rceil)}{\sin^2(\frac{\pi d_2}{2N})} + \alpha \frac{\sin^2(\frac{\pi d_2}{2N} \lfloor \frac{2N}{L} \rfloor)}{\sin^2(\frac{\pi d_2}{2N})} \right), \tag{4.26}$$

where $\tilde{\bar{\gamma}}(d_1, 0)$ is defined analogously as in (4.26). Since I assume that G.fast symbols are independent, the average ICSI coefficients including the influence of all L interfering G.fast symbols are given by

$$\gamma(d_1, d_2) = L\tilde{\bar{\gamma}}(d_1, d_2). \tag{4.27}$$

When the G.fast symbols are only partially aligned (see Figure 4.3b), the ICSI coefficients for $L-1$ fully aligned G.fast symbols are computed according to (4.25), while the worst-case ICSI coefficients for partially aligned G.fast symbols are computed similarly as in Section 4.1.1. Thus, I again sum the contributions of two partially aligned symbols and obtain

$$\gamma^\varepsilon(d_1, d_2, \nu^\varepsilon) = \frac{\bar{Q}_{\bar{k}}^2 L}{(2N)^2} \left(\frac{g^\varepsilon(d_1, \nu^\varepsilon)}{\sin^2\left(\frac{\pi d_1}{2N}\right)} + \frac{g^\varepsilon(d_2, \nu^\varepsilon)}{\sin^2\left(\frac{\pi d_2}{2N}\right)} \right), \tag{4.28}$$

where $g^\varepsilon(d_i, \nu^\varepsilon) = \sin^2\left(\frac{\pi(\varepsilon - \nu^\varepsilon)d_i}{2N}\right) + \sin^2\left(\frac{\pi \nu^\varepsilon d_i}{2N}\right)$ for $0 \le \nu^\varepsilon \le \varepsilon$ and $i = 1,2$. The shifts ν^ε are assumed to be integer values, i.e., $\nu^\varepsilon = \lfloor \eta \varepsilon \rfloor$ with $0 \le \eta \le 1$. Average ICSI coefficients are given by

$$\gamma(d_1, d_2, \nu^{\varepsilon = \lfloor \frac{2N}{L} \rfloor}, \nu^{\varepsilon = \lceil \frac{2N}{L} \rceil}) = \alpha \gamma^{\varepsilon = \lfloor \frac{2N}{L} \rfloor}(d_1, d_2, \nu^{\varepsilon = \lfloor \frac{2N}{L} \rfloor}) + \beta \gamma^{\varepsilon = \lceil \frac{2N}{L} \rceil}(d_1, d_2, \nu^{\varepsilon = \lceil \frac{2N}{L} \rceil}). \tag{4.29}$$

We see that by replacing $\nu^\varepsilon = \frac{\hat{\nu}^\varepsilon}{L}$, $N = \hat{N}$ and $d_i = L \hat{d}_i$ the same expression as in (4.15) is obtained. Hence, the upper bound on ICSI coefficients based on the worst-case offset $\nu^{*\varepsilon}$ are obtained as in Section 4.1.1 and given by

$$\gamma^*(d_1, d_2) = \alpha \gamma^{*\varepsilon = \lfloor \frac{2N}{L} \rfloor}(d_1, d_2) + \beta \gamma^{*\varepsilon = \lceil \frac{2N}{L} \rceil}(d_1, d_2), \tag{4.30}$$

where $\gamma^{*\varepsilon}(d_1, d_2) = \frac{\bar{Q}_k^2 L}{(2N)^2}(\rho(d_1) + \rho(d_2))$, where

$$\rho(d_i) = \begin{cases} \frac{g^{*\varepsilon}(d_1)}{\sin^2(\frac{\pi d_1}{2N})}, & \text{for } |d_i| \neq 0, \\ \varepsilon^2, & \text{for } |d_i| = 0, \end{cases} \tag{4.31}$$

and where

$$g^{*\varepsilon}(d_i) = \max_{0 \leq \nu^\varepsilon \leq \varepsilon} \{g^\varepsilon(d_i, \nu^\varepsilon)\} \begin{cases} \sin^2(\frac{\pi d_i}{2N}\varepsilon), & \text{if } 0 < (\frac{\pi|d_i|}{2N}\varepsilon) < \frac{\pi}{2}, \\[2mm] 2\sin^2(\frac{\pi d_i}{4N}\varepsilon), & \text{if } \frac{\pi}{2} < (\frac{\pi|d_i|}{2N}\varepsilon) \bmod 2 < \frac{3\pi}{2}, \\[2mm] 2\cos^2(\frac{\pi}{2}\frac{|d_i|}{L}), & \text{and } 0 \leq (\frac{\pi|d_i|}{2N}\varepsilon) \bmod 2 < \frac{\pi}{2}, \\ & \text{or } \frac{3\pi}{2} < (\frac{\pi|d_i|}{2N}\varepsilon) \bmod 2 < 2\pi, \\[2mm] 1, & \text{if } |d_i| = F2N\varepsilon^{-1} \text{where F is uneven integer.} \end{cases} \tag{4.32}$$

Finally, for partial alignment the ICSI coefficients are given as

$$\gamma(d_1, d_2) = (L - 1) \cdot \tilde{\gamma}(d_1, d_2) + \gamma^*(d_1, d_2). \tag{4.33}$$

A comparison of per-symbol ICSI coefficients using (4.27) and (4.33) for VDSL2 tone $k = 2039$ is shown in Figure 4.4 assuming perfect anti-aliasing filtering at VDSL2 transceivers.
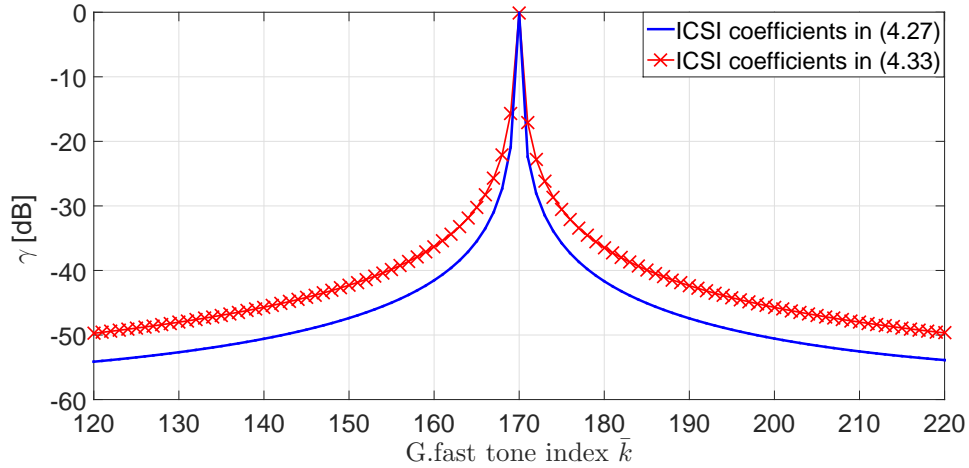
Figure 4.4: ICSI coefficients for VDSL2 tone $k = 2039$ calculated with (4.27) and (4.33), respectively with modulation parameters as defined in Section 5 and perfect VDSL2 RX filtering.

Note that for scenarios where interfering DSL technologies have the same modulation parameters, i.e., $L = M = 1$ and $\bar{N} = N$, from (4.19) and (4.33) I recover the worst-case model in [57]. Figures 4.5 and 4.6 show comparison of ICSI coefficients obtained with the worst-case model in [57][4] and ICSI models in (4.19) and (4.33). Figure (4.6) shows how G.fast spectra replicates, i.e. aliases, in case of non-identical modulation parameters due to the lack of perfect anti-aliasing filter at VDSL2 receiver.

Furthermore, the derivations (4.2) to (4.32) involve two approximations. Firstly, I
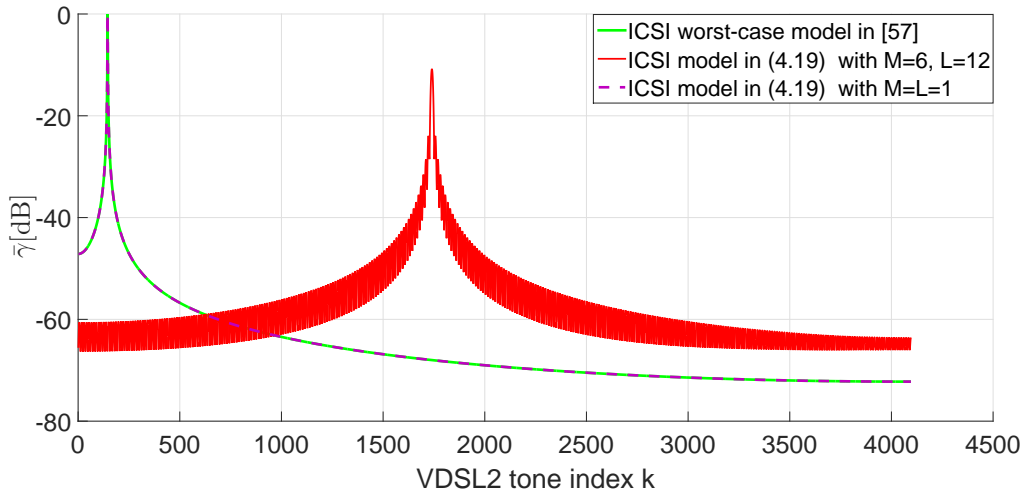
Figure 4.5: Comparison of ICSI coefficients for G.fast (victim) tone $\bar{k} = 145$ calculated with model in [57] and (4.19), with different modulation parameters (i.e., M and L) .

have assumed that the ICSI coefficients are neither user nor tone dependent (see the discussion in [58]). Hence, the derived ICSI coefficients are a function of the tone spacing between interfering and victim tone only. Secondly, the cyclic extension (CE) between consecutive symbols has not been taken into consideration.

---

[4] Worst-case model in [57] assumes that ICSI arises due to the asynchronous transmission while carrier width and sampling rate are assumed to be the same.
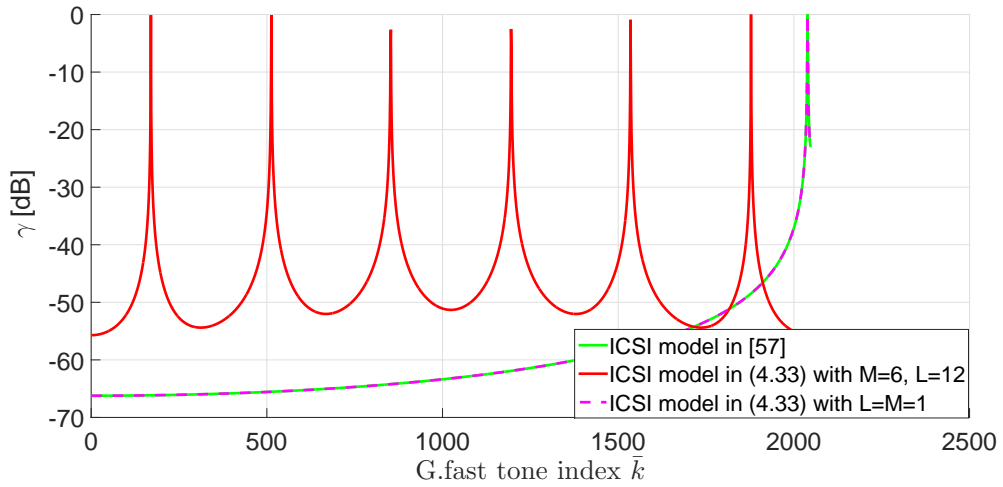
Figure 4.6: Comparison of ICSI coefficients for VDSL2 (victim) tone $k = 2039$ calculated with model in [57] and (4.33), with different modulation parameters (i.e., M and L), and without VDSL2 RX filtering.

4.2   Verification of the ICSI Model

The analytical ICSI models described in Sections 4.1.1 and 4.1.2 are verified by simulations of a simple signal chain, consisting of a IFFT/scaling, a transmit filter, resampling/time shifting, receive filter and a FFT/rescaling. Exemplary comparisons between analytical ICSI models and simulated signals are provided in Figure 4.7 and 4.8 from which we see that the derived bounds in (4.19) and (4.33) are fairly tight.
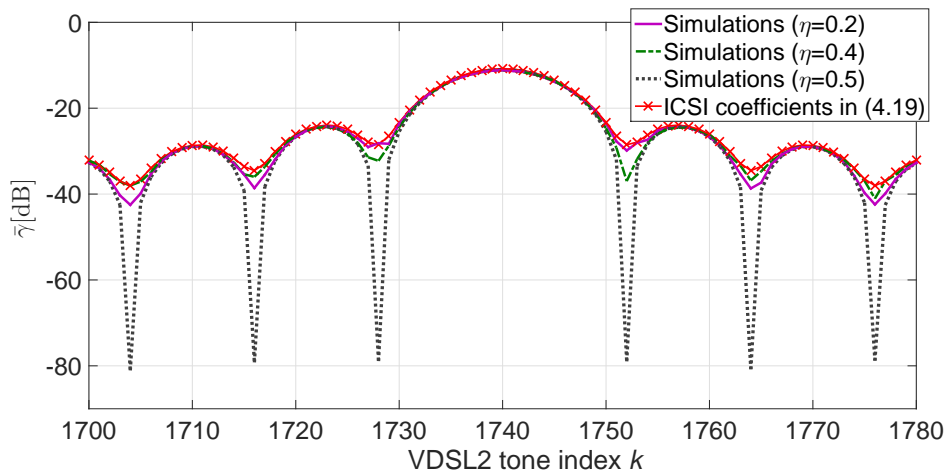
Figure 4.7: Comparison of simulated time-domain signal with different shifts η and the upper bound on ICSI coefficients in (4.19) for G.fast victim tone $\bar{k} = 145$.
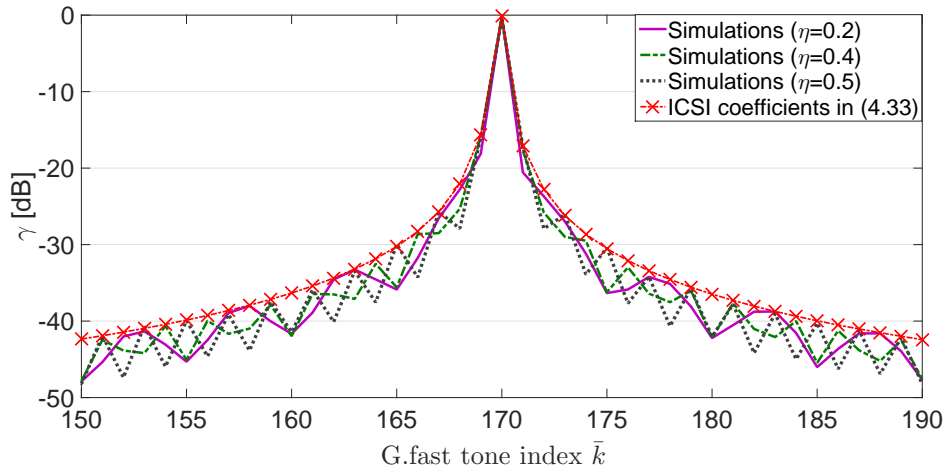
Figure 4.8: Comparison of simulated time-domain signal with different shifts η and the upper bound on ICSI coefficients in (4.33) for VDSL2 victim tone $k = 2039$.

4.3   Conclusions

In this Chapter I derived a novel analytical inter-carrier and inter-symbol interference (ICSI) model under full and partial symbol alignment that captures modulation properties such as sampling rate and carrier spacing of different multicarrier DSL systems. Differences in sampling rate causes unwanted spectral images which can be successfully removed with low-pass filtering; therefore, in this Chapter I also model impact of anti-aliasing and anti-imaging filters. The developed models are verified by time domain simulations and compared to the work in [57] showing that in the special case of identical modulation parameters the novel ICSI model and worst-case ICSI model from [57] produce the same ICSI coefficients.

5. COEXISTENCE ANALYSIS BETWEEN G.FAST AND VDSL2

In multi-user and multi-carrier digital subscriber line (DSL) access networks various DSL technologies, with or without crosstalk cancelation (vectoring) capabilities, may coexist. Among lines of different vectoring groups/technologies inter-carrier and inter-symbol interference (ICSI) occurs due to asynchronism as well as differences in modulation parameters. In Chapter 4 I have proposed a novel ICSI model, which captures the effects of different modulation parameters such as carrier width and sampling rates and also accounts for potentially asynchronism between different vectoring groups. Furthermore, as discussed in Chapter 3, the achievable bit-rates of vectored DSL systems heavily depend on the accuracy of channel state information (CSI), especially on high frequencies used by G.fast. Additionally, network providers will have new challenges to address as they embrace G.fast. They will need to ensure that their G.fast deployments can coexist with legacy DSL systems, such as very high speed digital subscriber line 2 (VDSL2). More precisely, coexistence could be defined as a deployment setup in which different DSL systems do not significantly interfere with each other. G.fast facilitates coexistence with different approaches such as providing a configurable power spectral density mask [8] and/or G.fast start frequencies [26, 27]. For example, right selection of G.fast start frequency may be a crucial performance parameter as shown in [26, 28]. More precisely, starting G.fast transmission immediately above VDSL2 may result in strong ICSI for both systems while a large spectral separation potentially incurs a significant performance penalty especially for longer ($>$ 100 m long) G.fast loops. Therefore, in order to optimize the selection of the G.fast start frequency and to estimate the achievable bit-rates of coexisting G.fast and VDSL2 a performance model which captures both effects of ICSI and erroneous CSI is required. Performance models which analyze the impact of erroneous CSI on interference cancellation techniques in different wireless and DSL technologies have been presented in [104–106] while coexistence of G.fast and VDSL2 under perfect CSI has recently been analyzed in [47]. However, to the best of my knowledge a model which captures both the impact of erroneous CSI and ICSI is still missing. In this Chapter, models presented in Chapters 3 and 4 are combined together

in order to produce a unique performance model which incorporates the effects of ICSI, linear and non-linear vectoring and CSI errors. Furthermore, measures to combat the considerable impact [23–25] of the resulting crosstalk (e.g., due to CSI errors and/or ICSI) include dynamic spectrum management (DSM), higher-layer unbundling, binder management, Vectoring across DSL Access Multiplexers (DSLAM), and cable-level Vectoring [107]. In the following analysis, I use the DSM algorithm proposed in [99] in order to mitigate the impact of uncancelled crosstalk (cf. Section 5.1.1). Similar work on power optimization inside vectoring groups with inter-user crosstalk has been published in [47, 48, 108]. Unlike the models in [47, 48] our used DSM algorithm includes multiple Vectoring groups and ICSI effects while the work in [108] optimizes transmit and receive DSL matrices under ICSI but without considering a sum-power constraint (i.e., (2.14b)) and PSD mask constraint (i.e., (2.14c)).

This Chapter is organized as follows. In Section 5.1 I combine the models from Chapters 3 and 4 in a joint performance model which encompasses the effects of ICSI, vectoring and CSI errors and shortly discuss DSM algorithm used in my performance evaluation of coexistence scenarios. A specific application of the joint model to the problem of selecting the G.fast start-frequency as well as receive and transmit filter orders for coexistence with VDSL2 is studied in Section 5 while conclusions based on the presented results are drawn in Section 5.3.

5.1   Joint Model for Linear Vectoring and ICSI

In this Section, I present a performance model which incorporates the effects of CSI errors, vectoring crosstalk cancellation matrices, ICSI as well as FEXT and NEXT. Downstream bit-rates deteriorate due to FEXT originating at the out-of-group and in-group dowsntream transmitters, as well as NEXT originating from out-of-group upstream transmitters. Differently, upstream bit-rates suffer from out-of-group and in-group FEXT upstream transmission and out-of-group NEXT downstream transmission (see Figure 5.1). In the following I exemplify the derivation of the joint model for the upstream transmission under linear vectoring discussed in Section 3.1.1. The received symbol in victim group g on victim tone k is influenced by all disturber groups $\bar{g} \in \mathcal{G}$ on disturber tone $\bar{k}$ and is given by:

$$
\begin{aligned}
\hat{\mathcal{Y}}_k^g = \hat{\mathbf{Y}}_k^g &+ \sum_{(\bar{g} \neq g)} \sum_{(\bar{k} \in K^{\bar{g}})} (\check{\mathbf{H}}_{k\bar{k},\text{NEXT}}^{(g,\bar{g})} \check{\mathbf{X}}_{\bar{k}}^{\bar{g}} + \hat{\mathbf{H}}_{k\bar{k},\text{FEXT}}^{(g,\bar{g})} \hat{\mathbf{X}}_{\bar{k}}^{\bar{g}}), \\
= \hat{\mathbf{X}}_k^g &+ \underbrace{\hat{\mathbf{R}}_k^g \hat{\mathbf{E}}_k^g \hat{\mathbf{X}}_k^g}_{\text{intra-group crosstalk}} + \hat{\mathbf{R}}_k^g \hat{\mathbf{Z}}_k^g + \underbrace{\sum_{(g \neq \bar{g})} \sum_{(\bar{k} \in K^{\bar{g}})} (\check{\mathbf{H}}_{k\bar{k},\text{NEXT}}^{(g,\bar{g})} \check{\mathbf{X}}_{\bar{k}}^{\bar{g}} + \hat{\mathbf{H}}_{k\bar{k},\text{FEXT}}^{(g,\bar{g})} \hat{\mathbf{X}}_{\bar{k}}^{\bar{g}})}_{\text{inter-group crosstalk}}, \quad (5.1)
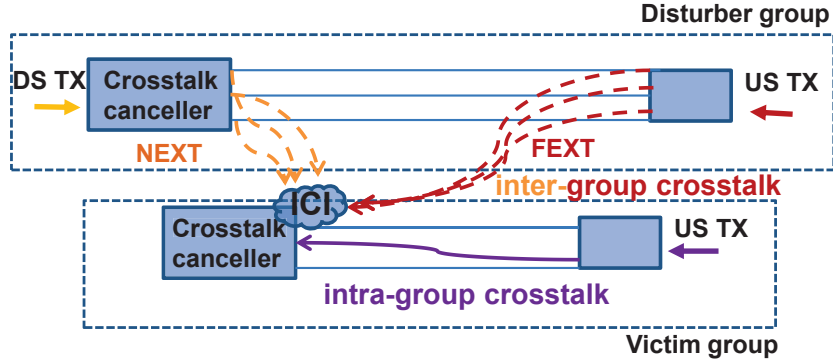\end{aligned}
$$

Figure 5.1: Effective channel between a certain pair of disturber and upstream (US) victim lines, taking upstream/downstream (US/DS) linear crosstalk canceler and ICSI between different DSL technologies into account.

where $\check{\mathbf{H}}^{(g,\bar{g})}_{k\bar{k},\mathsf{NEXT}}$ and $\hat{\mathbf{H}}^{(g,\bar{g})}_{k\bar{k},\mathsf{FEXT}}$ are effective downstream NEXT and upstream FEXT channel matrices from group $\bar{g}$ to group g and from tone $\bar{k}$ to tone k. More precisely, $\check{\mathbf{H}}^{(g,\bar{g})}_{k\bar{k},\mathsf{NEXT}} = \sqrt{\ddot{\gamma}^{g,\bar{g}}_{k\bar{k}}}(\hat{\mathbf{R}}^g_k\check{\mathbf{H}}^{(g,\bar{g})}_{\bar{k},\mathsf{NEXT}}\check{\mathbf{S}}^{\bar{g}}_{\bar{k}})$ where $\check{\mathbf{H}}^{(g,\bar{g})}_{\bar{k},\mathsf{NEXT}} \in \mathbb{C}^{|U^g| \times |U^{\bar{g}}|}$ is the downstream NEXT channel matrix on tone $\bar{k}$ between groups $\bar{g}$ and g, while the ICSI factor $\ddot{\gamma}^{g,\bar{g}}_{k\bar{k}} \in \mathbb{R}_+$ models the interaction between tones $\bar{k}$ and k and $\ddot{\gamma}^{g,\bar{g}}_{k\bar{k}}$ is given in (4.19) or (4.33) (or (4.10) or (4.27) for full symbol alignment) depending on the technology used in groups $\bar{g}$ and g. Matrices $\check{\mathbf{S}}^g_k$ and $\hat{\mathbf{R}}^g_k$ are the precoding and equalization matrices used in for linear vectoring, as defined in Section 3.1. The effective upstream FEXT channel matrix from group $\bar{g}$ to group g and from tone $\bar{k}$ to tone k is given as $\hat{\mathbf{H}}^{g,\bar{g}}_{k\bar{k},\mathsf{FEXT}} = \sqrt{\ddot{\gamma}^{g,\bar{g}}_{k\bar{k}}}(\hat{\mathbf{R}}^g_k\hat{\mathbf{H}}^{(g,\bar{g})}_{\bar{k},\mathsf{FEXT}})$ where $\hat{\mathbf{H}}^{(g,\bar{g})}_{\bar{k},\mathsf{FEXT}} \in \mathbb{C}^{|U^g| \times |U^{\bar{g}}|}$ is the upstream FEXT channel matrix on tone $\bar{k}$ and from group $\bar{g}$ to group g. The presented results can be easily adopted for downstream transmission where downstream FEXT and upstream NEXT are defined as: $\check{\mathbf{H}}^{(g,\bar{g})}_{k\bar{k},\mathsf{FEXT}} = \sqrt{\ddot{\gamma}^{g,\bar{g}}_{k\bar{k}}}(\check{\mathbf{H}}^{(g,\bar{g})}_{\bar{k},\mathsf{FEXT}}\check{\mathbf{S}}^{\bar{g}}_{\bar{k}})$ and $\hat{\mathbf{H}}^{(g,\bar{g})}_{k\bar{k},\mathsf{NEXT}} = \sqrt{\ddot{\gamma}^{g,\bar{g}}_{k\bar{k}}}(\hat{\mathbf{H}}^{(g,\bar{g})}_{\bar{k},\mathsf{NEXT}})$. Similarly as done for linear vectoring the upstream received symbol in victim group g on victim tone k for non-linear vectoring discussed in Section 3.2.1 is given as

$$\hat{\mathcal{Y}}^g_k = \hat{\mathbf{Y}}^g_k + \sum_{(\bar{g} \neq g)} \sum_{(\bar{k} \in K^{\bar{g}})} (\check{\mathbf{H}}^{(g,\bar{g})}_{k\bar{k},\mathsf{NEXT}}\check{\mathbf{X}}^{\bar{g}}_{\bar{k}} + \hat{\mathbf{H}}^{(g,\bar{g})}_{k\bar{k},\mathsf{FEXT}}\hat{\mathbf{X}}^{\bar{g}}_{\bar{k}}),$$

$$= \hat{\mathbf{Y}}^g_k\hat{\mathbf{X}}^g_k + \underbrace{(\hat{\mathbf{\Lambda}}^g_k)^\dagger\hat{\mathbf{E}}^g_k\hat{\mathbf{X}}^g_k}_{\text{intra-group crosstalk}} + (\hat{\mathbf{\Lambda}}^g_k)^\dagger\hat{\mathbf{Z}}^g_k + \underbrace{\sum_{(g \neq \bar{g})} \sum_{(\bar{k} \in K^{\bar{g}})} (\check{\mathbf{H}}^{(g,\bar{g})}_{k\bar{k},\mathsf{NEXT}}\check{\mathbf{X}}^{\bar{g}}_{\bar{k}} + \hat{\mathbf{H}}^{(g,\bar{g})}_{k\bar{k},\mathsf{FEXT}}\hat{\mathbf{X}}^{\bar{g}}_{\bar{k}})}_{\text{inter-group crosstalk}}, \quad (5.2)$$

where $\hat{\mathbf{Y}}^g_k$ and $(\hat{\mathbf{\Lambda}}^g_k)^\dagger$ are matrices obtained as defined in (3.3). Effective downstream NEXT and upstream FEXT channel matrices from group $\bar{g}$ to group g and from tone $\bar{k}$ to tone k are $\check{\mathbf{H}}^{(g,\bar{g})}_{k\bar{k},\mathsf{NEXT}} = \sqrt{\ddot{\gamma}^{g,\bar{g}}_{k\bar{k}}}((\hat{\mathbf{\Lambda}}^g_k)^\dagger\check{\mathbf{H}}^{(g,\bar{g})}_{\bar{k},\mathsf{NEXT}}\check{\mathbf{Q}}^{\bar{g}}_{\bar{k}})$ and $\hat{\mathbf{H}}^{g,\bar{g}}_{k\bar{k},\mathsf{FEXT}} = \sqrt{\ddot{\gamma}^{g,\bar{g}}_{k\bar{k}}}((\hat{\mathbf{\Lambda}}^g_k)^\dagger\hat{\mathbf{H}}^{(g,\bar{g})}_{\bar{k},\mathsf{FEXT}})$, respectively. Again the presented results can be easily adopted for downstream trans-

mission where downstream FEXT and upstream NEXT under non-linear vectoring are defined as: $\check{\mathbf{H}}_{k\bar{k},\text{FEXT}}^{(g,\bar{g})} = \sqrt{\check{\ddot{\gamma}}_{k\bar{k}}^{g,\bar{g}}}(\check{\mathbf{H}}_{\bar{k},\text{FEXT}}^{(g,\bar{g})}\check{\mathbf{\Lambda}}_{\bar{k}}^{\bar{g}})$ and $\hat{\mathbf{H}}_{k\bar{k},\text{NEXT}}^{(g,\bar{g})} = \sqrt{\check{\ddot{\gamma}}_{k\bar{k}}^{g,\bar{g}}}(\hat{\mathbf{H}}_{\bar{k},\text{NEXT}}^{(g,\bar{g})})$.

5.1.1 Modified Bit-loading Heuristic

In the following I shortly describe the DSM algorithm in [99], used in my simulation setup in Section 5.2.1, which is a modification of the greedy multi-user bit-loading heuristic in [109] applicable to the iterative power allocation in mixed vectoring group scenarios. More details can be found in [99]. Algorithm 1 describes the proposed multi-user bit-loading heuristic [99], which performs bit-loading iteratively on all the groups, and independently in upstream and downstream directions. The main modification with respect to the original algorithm in [109] is the additional check of feasibility with respect to the (precoded) power spectral density (PSD) and sum-power constraints in (2.14c) and (2.14b) (cf. Lines 4 and 8 in Algorithm 1) when calculating the cost of loading one bit on a certain tone for a specific user. Note that after the last iteration the bit-load of

---

Algorithm 1 Modified Multi-User Bit-Loading Heuristic

1: **for** all $g \in \mathcal{G}$ **do**
2:    **for** all directions $\delta \in \{\text{upstream, downstream}\}$ **do**
3:       Initialize: #Bits $B^{(g,u)} = 0$ and #Missing-Bits $R^{(g,u)}, \forall u \in \mathcal{U}^g$ (according to target rate, or infinite in case of rate-maximization)
4:       Calculate the cost (sum-PSD among users; after precoding if applicable) for loading one bit λ_k^u in direction $\varpi, \forall u \in \mathcal{U}^g, k \in \mathcal{K}^{(g,u)}$ (violations of PSD/sum-transmit power constraints incur an infinite cost)
5:       **while** $(\exists u \in \mathcal{U}^g, k \in \mathcal{K}^{(g,u)}$ with finite costs $\lambda_k^u)$ and $(R^{(g,u)} > 0$ for any $u \in \mathcal{U}^g)$ **do**
6:          Define $\bar{\mathcal{U}}^g = \{u \in \mathcal{U}^g | R^{(g,u)} > 0\}$
7:          Pick the tone k / user u pair with the lowest additional cost λ_k^u among tones $k \in \mathcal{K}^{(g,u)}, u \in \bar{\mathcal{U}}^g$ (ties among users broken a) according to the highest rate-demand $R^{(g,u)}, u \in \bar{\mathcal{U}}^g$, and b) at random)
8:          Recalculate the costs λ_k^u for loading one additional bit on tone $k, \forall u \in \bar{\mathcal{U}}^g$ (based on PSD levels after precoding, if applicable)
9:       **end while**
10:    **end for**
11: **end for**
12: **if** max. # sweeps-over-groups is not reached **then**
13:    Return to Line 1
14: **end if**

---

all groups except the last optimized group is not feasible in general (due to the updated interference). Hence, in order to obtain a feasible bit-load Algorithm 1 suggests to repeat Lines 1-11 under a PSD constraint (and corresponding crosstalk noise) given by

the PSD levels obtained in the last sweep over groups.

5.2   Simulation Results

5.2.1   Simulation Environment

In Chapter 3 I analyzed performance of linear and non-linear vectoring and I have shown that optimized linear vectoring marginally differs from optimized non-linear vectoring. Therefore in the following analysis I assume optimized linear vectoring at DSL receivers under no CSI error. I also consider Chebyshev type I filters (motivated by [110]) with different orders ($r = 6$ or 8) and 0.5 dB passband ripple at VDSL2 transceivers while no filtering is simulated at G.fast transceivers. Note that G.fast filtering can not eliminate the spectral images of VDSL2 and therefore does not have any influence on our simulation results. I also assume the same 17.7 MHz cut-off frequency for both upstream and downstream VDSL2 transmission. The simulation assumptions also include a flat background noise of -140 dBm/Hz, PSD masks according to [22] (VDSL2, profile 17a,and bandplan B8-11) and [7] (G.fast, profile 106a), an SNR gap of 10.75 dB, and an time asymmetry ratio (upstream/downstream) for G.fast of 1:4. G.fast and VDSL2 use 4 dBm and 14.5 dBm per-line sum transmit power, respectively. The values of $\overline{\Delta f}$ and Δf are equal to 51.75 kHz and 4.3125 kHz, respectively, and therefore we have $M = 6$ and $L = 12$. Furthermore, due to the different duplexing techniques used in VDSL2 and G.fast (frequency division duplexing and time division duplexing) the crosstalk power for each user is composed of FEXT and NEXT. I use British Telecom measured cable data of an underground cable of 100 m length [15] (cf. Section 2.1.2). In my simulation setup I select only the first four lines. FEXT channel gains are nonlinearly scaled to various loop lengths based on the common empirical FEXT model in [75, Eq.(3.4)](cf. Section 2.1.2). The considered measured data does not provide the NEXT couplings. Therefore, I use a common conservative European NEXT coupling model [75] for calculating NEXT gains. Furthermore, I use a mixed G.fast and VDSL2 topology, where the distance l_1 between VDSL2 DSL access multiplexer (DSLAM) and G.fast distribution point unit (DPU) varies from 0 m to 500 m and the distance l_2 between G.fast DPU and customer premises equipment (CPE) side varies from 50 m to 200 m, cf. Figure 5.2. All U lines are in a single cable binder, with number of VDSL2 and G.fast users being equal to $U_{VDSL2} = U_{Gfast} = 4$, and co-located at CPE side. In this work I focus on a lower-bound on the VDSL2 and G.fast achievable bit-rates. Therefore, all presented results in the upcoming analysis are based on the derived worst-case asynchronous ICSI models in (4.19) and (4.33).
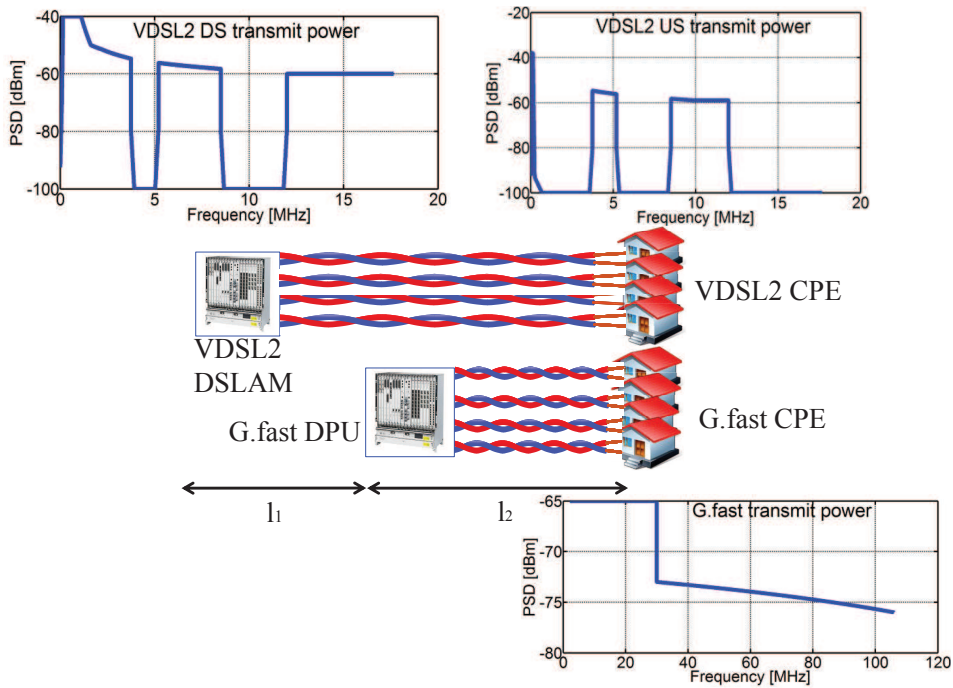
Figure 5.2: Simulated topology with considered VDSL2 and G.fast PSD masks.

5.2.2   Model Comparison with and without ICSI

In this Section I compare my ICSI model under transmit filtering with results obtained under the model in [47], which accounts for inter-group FEXT and NEXT but does not account for the influence of ICSI. In the following analysis VDSL2 and G.fast share the spectrum between 2.2 MHz and 17.67 MHz, i.e., there is no spectral separation between these two systems. Simulation results show that the largest gap between these two models in estimated mutual interference occurs for low order filtering (e.g., $r = 6$) and topologies where VDSL2 and G.fast users are collocated at both ends. This gap further increases, especially for G.fast users, for higher values of l_2, i.e., longer (FEXT) coupling lengths. In Figure 5.3 I show the total VDSL2 and G.fast downstream noise (i.e., FEXT, NEXT and background noise) estimated with our ICSI model under Chebyshev type I filtering, perfect filtering, and with the ICSI-free model in [47]. I simulate network scenario where users are collocated at both ends (i.e., $l_1 = 0$ m) and $l_2 = 200$ m. My ICSI model under *perfect filtering* and the model in [47] yield approximately the same noise levels for both VDSL2 and G.fast. A notable exception are VDSL2 frequencies below 2.2 MHz since the model in [47] omits the ICSI influence while due to the absence of G.fast (perfect) filtering there is a noise leakage (i.e., ICSI) from higher frequencies in case of VDSL2 perfect filtering. Furthermore, the ICSI interference estimated with

Figure 5.3: Total VDSL2 (left) and G.fast (right) downstream noise estimated with developed ICSI model under different types of filtering, and with ICSI-free model in [47] ($l_1 = 0$ and $l_2 = 200$ m).
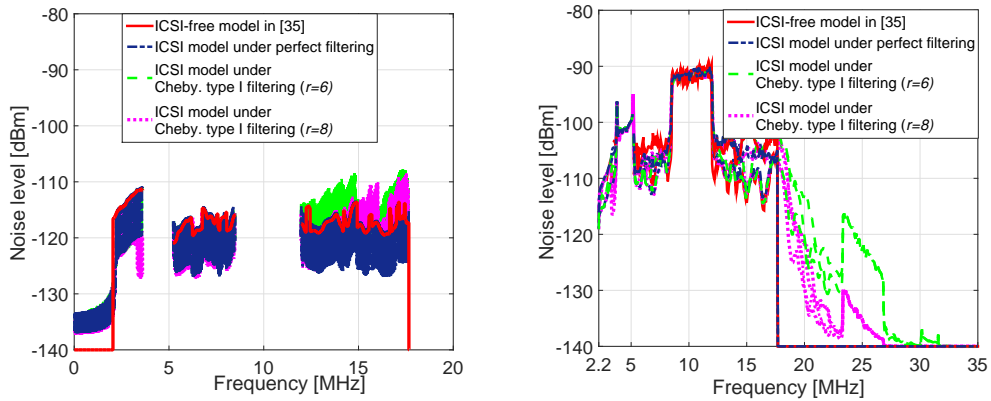
the model in [47] disappears for G.fast frequencies above 17.67 MHz while my ICSI model results in substantial noise leakage above 17.67 MHz caused by (filtered) VDSL2 spectral images. Similarly, my ICSI model results with higher noise than the model in [47] for VDSL2 frequencies between approximately 12 MHz and 17.67 MHz due to the aliased G.fast frequencies. Note, however, that difference in estimated noise between the two models is higher for G.fast than for VDSL2 due to the higher VDSL2 downstream PSD. This is also reflected in achievable bit-rates where my simulations show that the model in [47] overestimates the average G.fast and VDSL2 downstream bit-rates by approximately 18% and 7%, respectively, compared to our ICSI model under lower order filtering ($r = 6$), $l_1 = 0$ m, and $l_2 = 200$ m. For higher order filtering (i.e., $r \geq 8$) the gap in estimated noise and achievable bit-rates between these two models vanishes. The same conclusions can also be drawn for upstream transmissions.

5.2.3   Application Example: Selection of a G.fast Start Frequency for Coexistence with VDSL2

In this Section I analyze the spectral separation between G.fast and VDSL2/17a required to reduce interference between these two technologies to a negligible level. I consider two G.fast start frequencies (f_{start}): 18 MHz and 23 MHz. I start by analyzing the influence of G.fast on VDSL2. Figure 5.4 shows the noise levels at VDSL2 CPE (i.e., downstream) for $l_2 = 50$ m, different filter orders, and different G.fast start frequencies. These results indicate that starting G.fast transmission immediately above the VDSL2 in-band, i.e., at 18 MHz, causes strong noise leakage into VDSL2 downstream bands regardless of the filter order. As shown in Figure 5.5, this strong noise leakage causes
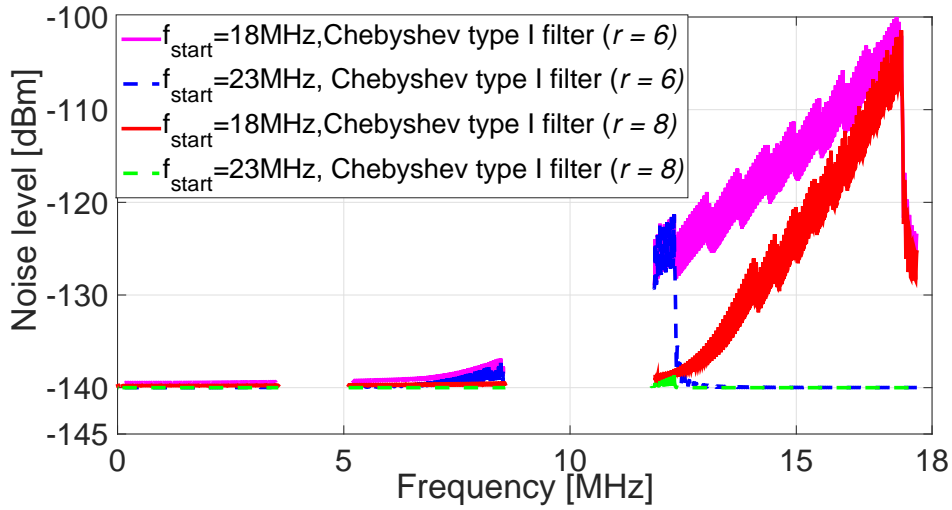
Figure 5.4: Total VDSL2 downstream noise with different filter orders and different start frequencies for collocated scenario ($l_1 = 0\,\text{m}$) and $l_2 = 50\,\text{m}$. Note that VDSL2 downstream noise does not depend on l_1.
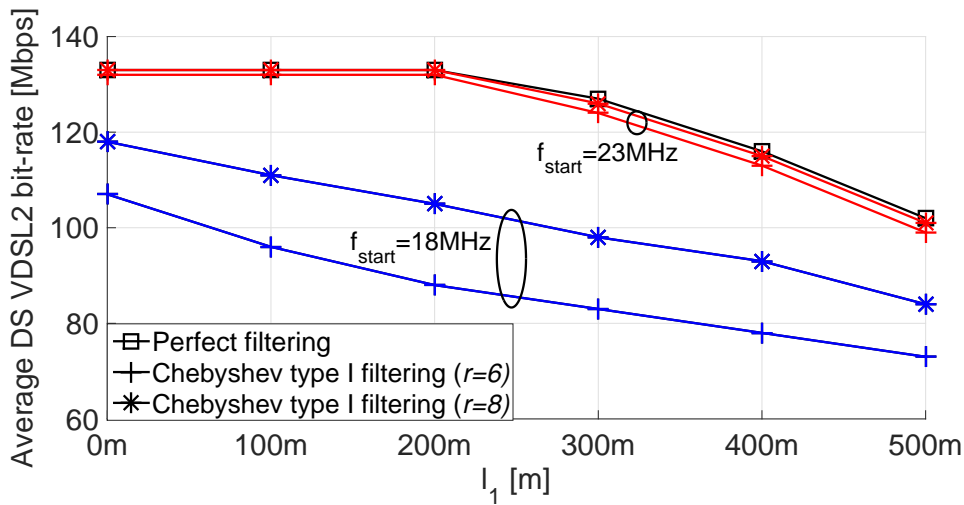
Figure 5.5: Average VDSL2 downstream (DS) bit-rates for different filter orders, different start frequencies and $l_2 = 50\,\text{m}$.

substantial VDSL2 downstream bit-rate losses compared to the bit-rates without G.fast interference, e.g., up to 30% for $r = 6$, $l_1 = 500\,\text{m}$, and $l_2 = 50\,\text{m}$ and increasing further with increasing loop length, reaching up to 40% for $r = 6$, $l_1 = 500\,\text{m}$, and $l_2 = 200\,\text{m}$. However, starting G.fast at 23 MHz notably reduces noise leakage, especially for higher order filtering ($r = 8$), keeping the noise levels below -130 dBm/Hz. Furthermore, for VDSL2 downstream transmission NEXT is the dominant noise source due to the collocation of VDSL2 and G.fast users at the CPE side. On the other hand, for VDSL2
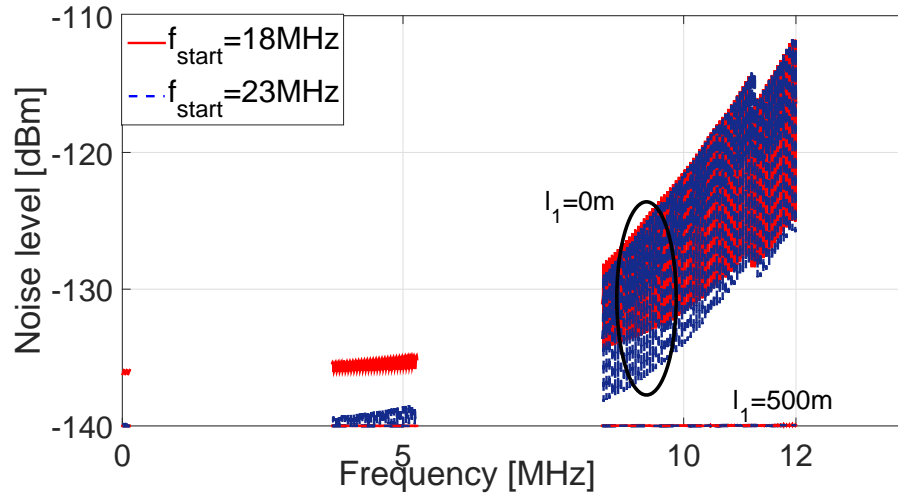
Figure 5.6: Total VDSL2 upstream noise for Chebyshev type I filtering ($r = 6$), $l_2 = 50\,\text{m}$, and different l_1.

upstream transmissions both NEXT and FEXT noise are additionally attenuated over length l_1. For example, in Figure 5.6 we see how the total VDSL2 noise at the DSLAM (upstream) decreases as l_1 increases, remaining below -130 dBm/Hz for $l_1 = 500\,\text{m}$ and $l_2 = 50\,\text{m}$ even with a low order Chebyshev type I filter ($r = 6$) and regardless of the spectral separation (i.e., f_{start}=18 MHz or f_{start}=23 MHz). Note also that the last VDSL2 downstream band (between 12 MHz and 17.67 MHz) receives the highest noise leakage from G.fast crosstalk signals while the VDSL2 upstream bands receive much lower noise levels (recall Figure 5.2 which shows the used VDSL2 downstream and upstream bands). Hence, due to the attenuated G.fast crosstalk signals over length l_1 and the tendentially decreasing noise leakage with decreasing victim tone frequency, the VDSL2 upstream bit-rate losses compared to the interference-free scenario do not exceed 6%. Furthermore, until now I assumed the same 17.7 MHz cut-off frequency for both VDSL2 downstream and upstream transmissions. However, since VDSL2 upstream bands are using frequencies up to 14 MHz (profiles B8-8 and B8-9) in the following I consider a 14 MHz cut-off frequency for VDSL2 upstream receive filters instead. [1] Figures 5.7 and 5.8 show the total VDSL2 upstream noise for different cut-off frequencies, different filter orders, and different spectral separations, i.e., G.fast start frequencies. These results indicate that a 14 MHz cut-off frequency results in substantially reduced VDSL2 upstream noise (especially for high order filtering, i.e., r=8) and therefore the (worst-case) downstream crosstalk represents the main determining factor for selecting

---

[1] The VDSL2 bandplan allows for an even smaller cut-off frequency (e.g., 12 MHz) for VDSL2 upstream receive filters, implying that the expected noise leakage from G.fast would further decrease.
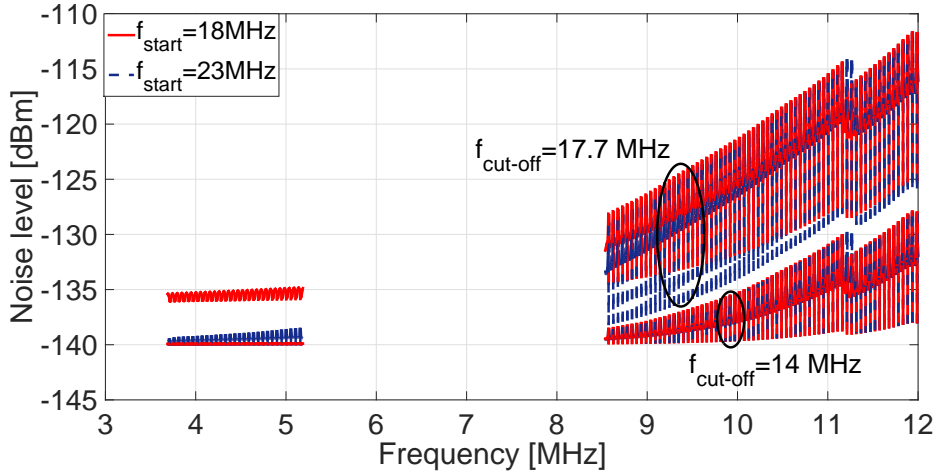
Figure 5.7: Total VDSL2 upstream noise for different cut-off frequencies ($f_{\text{cut-off}}$), different G.fast start frequencies (f_{start}), Chebyshev type I filtering ($r = 6$), and collocated scenario ($l_1 = 0\,\text{m}$) with $l_2 = 50\,\text{m}$.
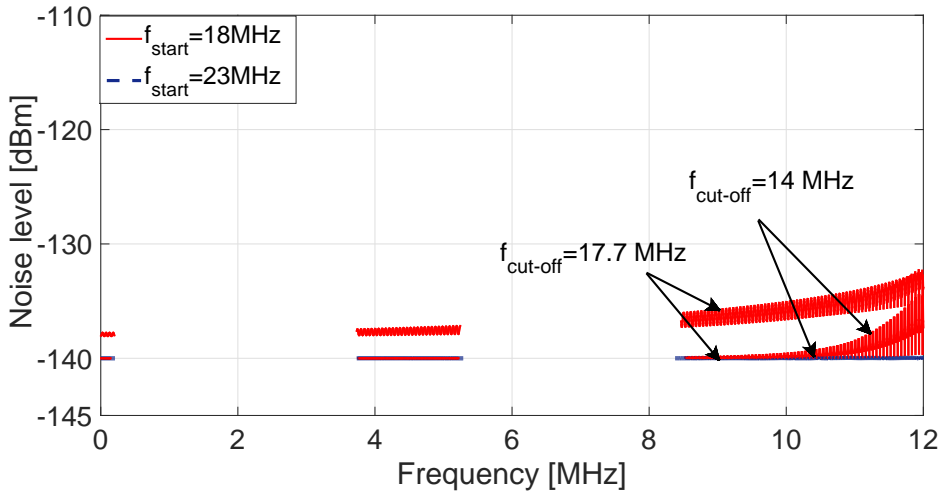
Figure 5.8: Total VDSL2 upstream noise for different cut-off frequencies ($f_{\text{cut-off}}$), different G.fast start frequencies (f_{start}), Chebyshev type I filtering ($r = 8$), and collocated scenario ($l_1 = 0\,\text{m}$) with $l_2 = 50\,\text{m}$.

the required spectral separation.

Figure 5.9 shows the total G.fast noise at the CPE side (i.e., downstream) for different filter orders, different start frequencies, and for a network scenario where $l_1 = 0\,\text{m}$, and $l_2 = 50\,\text{m}$. It can be observed that in order to guarantee noise levels below -130 dBm/Hz G.fast downstream transmission should start above 23 MHz assuming high order filtering ($r = 8$). Although the selection of non-overlapping G.fast and VDSL2 spectra mitigates mutual interference it does incur losses in G.fast bit-rates especially on longer loops (i.e.,
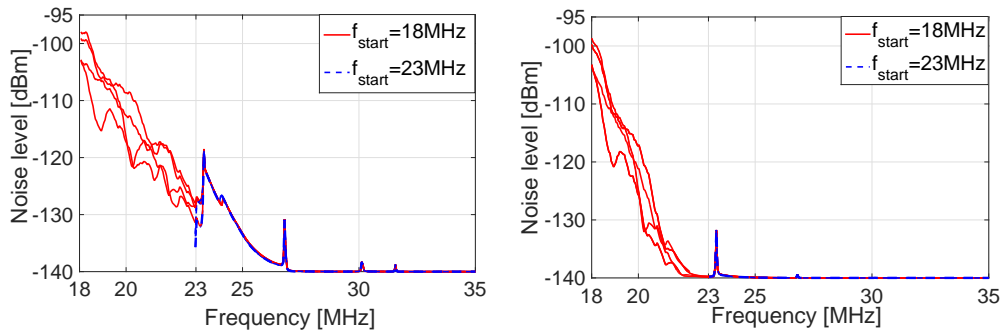
Figure 5.9: Total G.fast downstream noise for Chebyshev type I filtering with $r = 6$ (left) and $r = 8$ (right), different start frequencies, $l_1 = 0$ m, and $l_2 = 50$ m. Note that additional peak, starting at 23 MHz, arises from attenuated image of the last VDSL2 downstream band.
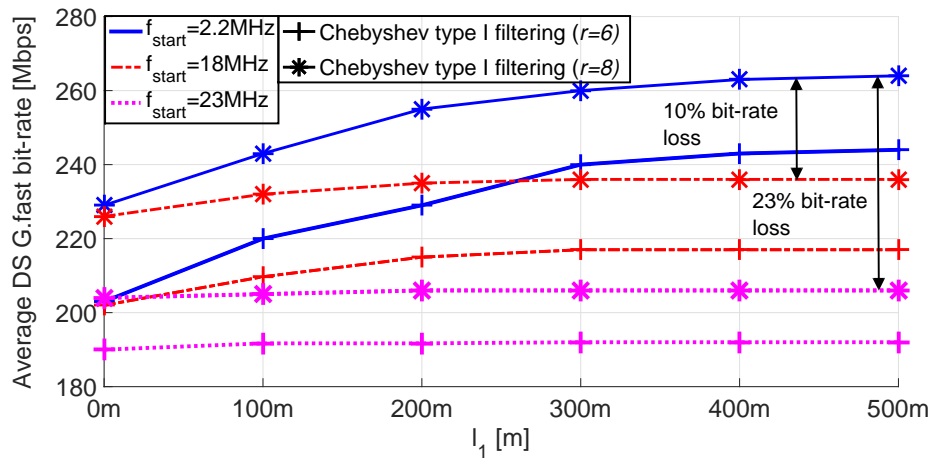
Figure 5.10: Average G.fast downstream (DS) bit-rates under VDSL2 interference for $l_2 = 200$ m, different filter orders, and different start frequencies.

high values of l_2) where high frequencies can not be used due to the strong insertion loss. Figure 5.10 shows average G.fast downstream bit-rates for $l_2 = 200$ m, different G.fast start frequencies, and different filter orders. The bit-rate curves indicate that the G.fast losses compared to the completely overlapped spectrum ($f_{start} = 2.2$ MHz) increase as spectral separation increases, reaching up to 23% for $f_{start} = 23$ MHz and $r = 8$. Similar results are found for G.fast upstream transmission. However, note that G.fast upstream transmission receives NEXT over wider VDSL2 downstream bands (cf. Figure 5.2) and correspondingly the losses are slightly higher, reaching up to 27% for $f_{start} = 23$ MHz and $r = 8$.

5.3   Conclusions

I analyzed coexistence of very high speed digital subscriber line 2 (VDSL2) and G.fast when jointly deployed in the same cable binder. These two DSL technologies use different modulation parameters which results in inter-carrier and inter-symbol interference (ICSI). I derived analytical ICSI models under full and partial symbol alignment that capture the modulation properties of both systems. By example it was shown that neglecting ICSI in simulations can potentially lead to 18% bit-rate overestimation for G.fast users. I also show that lower upstream receive filter cut-off frequencies adopted to the upstream band-plan reduce the required spectral separation with respect to upstream transmission. This leaves the downstream coexistence as the more critical test case. Furthermore, simulations of exemplary network scenarios with 8 DSL users show that in order to ensure compatibility with VDSL2 services G.fast should only utilize frequencies above $23\,\text{MHz}$ while VDSL2 transceivers should deploy high order filtering (e.g., a Chebyshev type I filter with order ≥ 8 was seen to be sufficient in simulations).

6 CONCLUSIONS

6.1 Summary of the Thesis and Key Findings

In this thesis, I analyzed the achievable bit-rates of linear and non-linear vectoring methods over frequencies up to 212 MHz and various simulations setups (e.g. different cable models, available cable measurement data, different numbers of users etc.). I also analyzed the impact of spectrum optimization on performance gap between different vectoring schemes. Furthermore, vectoring efficiency in crosstalk cancellation is only guaranteed under perfect channel state information (CSI), which is subject to errors due to the quasi-stationary properties of the DSL channel. My work in this thesis covers sensitivity of linear and non-linear vectoring on CSI errors and also provides empirical evidence which shows linear relation between CSI errors and residual crosstalk. Furthermore, vectoring requires single-side joint signal processing among the users at receiver and transmitter side for upstream and downstream transmission, respectively. However, there are scenarios where joint signal processing is practical only among groups of users, referred to as partial vectoring. In legacy DSL systems, such as very high speed digital subscriber line 2 (VDSL2), this uncancelled crosstalk was mitigated by means of dynamic spectrum management level 1 and level 2 (DSM-L1 and DSM-L2). However, an open question remained whether spectrum optimization is still the best mitigation approach for G.fast which operates over a considerably larger frequency spectrum than VDSL2 ($\leq$17 MHz) and consequently experiences much stronger crosstalk noise. Therefore, in this work I analyzed iterative spectrum balancing (ISB), as representative of DSM-L2 schemes, in a G.fast compliant setup with several vectoring groups and additionally have proposed interference alignment (IA) and time division multiple access (TDMA) as mitigation techniques for G.fast.

Coexistence between different DSL technologies, belonging to the different vectoring groups, gives a rise to the inter-carrier and inter-symbol interference (ICSI) due to the potentially unsynchronized transmissions and various modulation parameters. An ICSI model which captures all these differences is crucial for performance simulations (achievable bit-rate) of mixed DSL scenarios, such as G.fast and VDSL2. Therefore, in this thesis I developed a novel ICSI model which encompasses the impacts of asynchronous

transmission, various modulation parameters such as different sampling rates and carrier width, and the influence of realistic receive and transmit filters, unlike other ICSI models currently available in the wireless and wireline literature. The developed ICSI model is verified by time domain simulations. In this thesis, I also proposed a unique performance model which takes the impact of ICSI and (linear and non-linear) vectoring under erroneous CSI into account. I carried out a simulation study on the coexistence of G.fast and VDSL2 using the derived model and analyzed the required G.fast and VDSL2 parameters, such as G.fast start frequency and VDSL2 transmit and receiver filters, for negligible ICSI.

The contributions and key findings of my thesis are summarized as follows:

- The results for achievable bit-rates of linear and non-linear vectoring methods over frequencies up to 212 MHz indicate a higher bit-rate increase for non-linear vectoring compared to linear one especially on shorter loop lengths ($\leq$100 meters) which represents the typical deployment range for 212 MHz profile. Adding DSM-L2 on top of vectoring significantly improves the performance of both, linear and non-linear vectoring, such that both vectoring schemes achieve similar bit-rates.

- An intuition behind the CSI error model for linear downstream vectoring in [38] is given, which allows to make a sophisticated guess on the impact of estimation errors on bit-rates. More precisely, it was empirically showed that there is a linear relation between CSI errors and residual crosstalk.

- Simulations indicate that both linear and non-linear vectoring are very sensitive to CSI errors. Furthermore, spectrally optimized linear and spectrally optimized non-linear vectoring show reduced sensitivity to CSI errors compared to non-optimized ones. My results also indicate that although non-linear vectoring is more sensitive to CSI errors than linear vectoring, this difference decreases under spectral optimization.

- An analysis of ISB in case of partial vectoring in G.fast compliant setup was carried out. I also proposed IA as an alternative approach to ISB and showed that in case when vectoring is not applied IA outperforms ISB especially on frequencies above 100 MHz. However, simulations show that in case of partial vectoring for G.fast the simple TDMA outperforms both ISB and IA.

- I proposed a novel ICSI model for worst-case timing alignment in multi-carrier systems with different tone spacing and sampling rate including verification by means of time-domain simulations.

- Using the developed ICSI model, I showed that neglecting the impact of ICSI potentially leads to 18% bit-rate overestimation for G.fast users.

- I also showed by means of the developed model that in order to ensure coexistence with VDSL2 services G.fast should only utilize frequencies above 23 MHz while VDSL2 transceivers should deploy high order filtering (e.g., a Chebyshev type I filter of order 8 was seen to be sufficient in simulations).

6.2 Future Work

Despite the effort invested in this thesis, there are still some issues left that require further investigations. Tomlinson Harashima precoding (THP) and decision feedback equalizer (DFE), which were used as reference for non-linear precoding and equalization in this thesis, were implemented neglecting some design issues such as the power increase due to the modulo operation and error propagation, respectively. For more realistic evaluation of non-linear vectoring performance (i.e., achievable bit-rates) this design issues should be taken into account. Also in all my simulations I was considering sequential encoding order of THP while further investigation on optimization of encoding in THP could be performed. Furthermore, in case of partial vectoring for G.fast more advanced DSM-L2 algorithms could be analyzed while in this thesis I have considered only ISB. In this thesis I have also proposed a novel ICSI model but in my analysis I have neglected the impact of the cyclic extension (CE). Therefore, a more accurate modeling could be done by including its impact. Furthermore, the application of developed ICSI model is not restricted to DSL but it can also be used for interference analysis in other multi-carrier networks (e.g. wireless). Lastly, the developed ICSI model can not only be used for performance evaluation, but also as an interference model in autonomous spectral protection methods.

APPENDICES

A LIST OF SYMBOLS AND NOTATION

Variable	Description
Symbols	
u	User index
k	Tone index
g	Vectoring group index
K	Number of tones
$\mathcal{K}$	Set of tones
U	Number of users (lines)
$\mathcal{U}$	Set of users (lines)
G	Number of vectoring groups
$\mathcal{G}$	Set of vectoring groups
$\mathbf{X}_k$	Transmitted vector on tone k
$\mathbf{X}_k^{\text{est}}$	Estimated transmitted vector on tone k
X_k^u	Transmitted signal of user u on tone k
$X_k^{(g,u)}$	Transmitted signal of user u in group g on tone k
$\mathbf{Y}_k$	Received vector on tone k
Y_k^u	Received signal of user u on tone k
$Y_k^{(g,u)}$	Received signal of user u in group g on tone k
$\mathbf{Z}_k$	Additive white Gaussian background noise vector on tone k
Z_k^u	Additive white Gaussian background noise signal of user u on tone k
$Z_k^{(g,u)}$	Additive white Gaussian background noise signal of user u in group g on tone k
$\mathbf{H}_k$	Channel matrix on tone k
$\mathbf{H}_k^{\text{est}}$	Estimated channel matrix on tone k
$\mathbf{H}_k^{u,j}$	Channel from TX m to RX u on tone u
$\mathbf{H}_k^{u,u}$	Direct channel of user u on tone k
$\mathbf{H}_k^{g,g'}$	Crosstalk channel gains from group g' to group g on tone k ($g \neq g'$)
$\mathbf{H}_k^{g,g}$	Direct channel gains (diagonal elements) and crosstalk channel gains within group g

$\mathbf{E}_k$	Estimation error matrix on tone k
$\mathbf{I}_k$	Identity matrix
b_k^u	Number of bits of user u on tone k
R^u	Bit-rate of user u
f_s	DMT symbol rate
Γ	SNR-gap to capacity
p_k^u	Transmit PSD of user u on carrier k
$p_k^{(g,u)}$	Transmit PSD of user u in group g on tone k
$\mathbf{p}^u$	vector containing the PSD of user u over all tones
$p_{k,mask}^u$	PSD mask for user u on tone k
σ_k	Noise spectral density of user u on tone k
$\sigma_k^{(g,u)}$	Noise spectral density of user u in group g on tone k
ζ_k^{-1}	DP scaling factor on tone k
$\hat{\mathbf{R}}_k$	ZFE cancellation matrix on tone u
$\check{\mathbf{S}}_k$	DP precoding matrix on tone u
Δf	Tone spacing
L	Ratio of different tone spacings
M	Ratio of different sampling rates
$\bar{q}_{\bar{n}}$	Time filter taps of the low-pass filter with frequency granularity $\overline{\Delta f}$
$\bar{Q}_{\bar{k}}$	Frequency filter taps of the low-pass filter with frequency granularity $\overline{\Delta f}$
R	Reference resistance
n	Sample index
y_n	Transmitted symbol at time sample n
$y_n^{\uparrow}$	Upsampled signal at time sample n
$y_n^{\downarrow}$	Downsampled signal at time sample n
ε	DFT block size
ν^{ε}	Time domain shift (depending on ε)

Notation and Operators	
$\mathrm{diag}\{x\}$	Diagonal matrix with with vector x as diagonal
$\mathbb{E}\{\cdot\}$	Statistical expectation
$\|\cdot\|$	$L2$-norm
$\underset{=}{\mathrm{qr}}$	QR decomposition
$[\mathbf{H}]_{\mathrm{row}\,u}$	Row u of matrix $\mathbf{H}$
$\mathbf{H}^{\dagger}$	Hermitian transpose
$|x|$	Absolute value of scalar x
$*$	Convolution operator
$\lfloor\cdot\rfloor$	Round down to nearest integer

$\lceil \cdot \rceil$	Round up to nearest integer
$(\cdot)^\top$	Matrix or vector transpose
$\hat{x}$	Upstream parameter x
$\check{x}$	Downstream parameter x
$\mathrm{mod}(a,b)$	Modulo operation (i.e. remainder after division of a by b)

B LIST OF ACRONYMS

ADC	Analog-to-digital conversion
ADSL	Asymmetric digital subscriber line
CO	Central office
CP	Cyclic prefix
CWDD	Column-wise diagonally dominant
DAC	Digital-to-analog conversion
DFE	Decision feedback equalizer
DFT	Discrete Fourier transform
DMT	Discrete multi-tone
Dp	Distribution point
DP	Diagonalizing precoder
DS	Downstream
DSL	digital subscriber line
DSLAM	DSL access multiplexer
DSM	Dynamic spectrum management
FDD	Frequency division duplex
FEQ	Frequency domain equalizer
FEXT	Far End Crosstalk
FFT	Fast Fourier transform
FTTB	Fiber-to-the-building
FTTDp	Fiber-to-the-distribution-point
FTTH	Fiber-to-the-home
ICSI	Inter-carrier and inter-symbol interference
IA	Interference alignment
IDFT	Inverse DFT
IFFT	Inverse FFT
ISB	Iterative spectrum balancing
ITU	International telecommunication union
IWF	Iterative water filling
NEXT	Near-end crosstalk
OFDM	Orthogonal frequency-division multiplexing

OSB	Optimal spectrum balancing
PSD	Power spectral density
RWDD	Row-wise diagonal dominant
RX	Receive
TDD	Time division duplex
TDMA	Time division multiple access
THP	Tomlinson-Harashima precoding
TX	Transmit
SDSL	Symmetric digital subscriber line
SINR	Signal-to-interference noise ratio
US	Upstream
VDSL2	Very high speed digital subscriber line 2
ZFE	Zero-forcing equalizer
QAM	Quadrature amplitude modulation

C. UPPER BOUND ON ICSI GAIN: VDSL2 ON G.FAST

The definition of ICSI coefficients used in this thesis accounts for the worst possible offset $\bar{\nu}^{*\varepsilon}$ for each $\bar{d}_i$, thus, representing an upper bound on ICSI coefficients. For the sake of analytical tractability I derive the ICSI upper bound by relaxing the integer constraint on $\bar{\nu}^\varepsilon$. Furthermore, I independently search for the worst-case offsets for positive and negative frequencies and assume that consecutive symbols are independent. Therefore I maximize ICSI coefficients over two parameters: $\bar{\nu}_1^\varepsilon$ and $\bar{\nu}_2^\varepsilon$. For ε samples long symbols I have the following expression for the worst-case ICSI coefficients

$$\bar{\gamma}^{*\varepsilon}(\bar{d}_1, \bar{d}_2) = \max_{0 \leq \bar{\nu}_1^\varepsilon \leq \varepsilon} f^\varepsilon(\bar{d}_1, \bar{\nu}_1^\varepsilon) + \max_{0 \leq \bar{\nu}_2^\varepsilon \leq \varepsilon} f^\varepsilon(\bar{d}_2, \bar{\nu}_2^\varepsilon). \tag{C.1}$$

The function $f(\bar{d}_i, \bar{\nu}_i^\varepsilon)$ is $\frac{2N}{L}$ periodic with respect to $\bar{k}$. Therefore I define $\bar{\bar{d}}_1 = \frac{k}{L} - (\bar{k}) \bmod \frac{2N}{L}$ and $\bar{\bar{d}}_2 = \frac{2N-k}{L} - (\bar{k}) \bmod \frac{2N}{L}$. Taking the first derivative of $f(\bar{\bar{d}}_i, \bar{\nu}_i^\varepsilon)$ with respect to $\bar{\nu}_i^\varepsilon$ I obtain:

$$\frac{\mathbf{d}f(\bar{\bar{d}}_i, \bar{\nu}_i^\varepsilon)}{\mathbf{d}\bar{\nu}_i^\varepsilon} = 2\frac{\mathbf{d}B}{\mathbf{d}\bar{\nu}_i^\varepsilon}(-\sin(A)\cos(A) + \sin(B)\cos(B)) \tag{C.2}$$

where $A = \frac{\pi \bar{\nu}_i^\varepsilon \bar{\bar{d}}_i L}{2N}$, $B = \frac{\pi(\varepsilon - \bar{\nu}_i^\varepsilon)\bar{\bar{d}}_i L}{2N}$. There are two cases when (C.2) attains zero: $a)$ $2A \bmod 2\pi = \theta\pi - 2B \bmod 2\pi$ where $\theta \in \{1, 3\}$ and $b)$ $2A = 2B$-C2π . From case $a)$ it follows that $\bar{\bar{d}}_i = \frac{2N}{L}\varepsilon^{-1}$F where F is an uneven integer. However, in this case $f(\bar{\bar{d}}_i, \cdot)$ is constant, i.e., $f(\bar{\bar{d}}_i, \cdot) = f^{*\varepsilon}(\bar{\bar{d}}_i) = 1$. For case $b)$ and under the assumption that $\bar{\bar{d}}_i \neq 0$ I obtain that (C.2) attains zero when $\tilde{\bar{\nu}}_i^\varepsilon = \frac{\varepsilon}{2} + \frac{CN}{L\bar{\bar{d}}_i}$ where C is a positive integer and I obtain from (4.14)

$$f(\bar{\bar{d}}_i, \tilde{\bar{\nu}}_i^\varepsilon) = \left(\sin\left(\frac{\pi}{2}\bar{\bar{d}}_i\right)\cos\left(\frac{\pi}{2}C\right) - \cos\left(\frac{\pi}{2}\bar{\bar{d}}_i\right)\sin\left(\frac{\pi}{2}C\right)\right)^2 + \\ \left(\sin\left(\frac{\pi}{2}\bar{\bar{d}}_i\right)\cos\left(\frac{\pi}{2}C\right) + \cos\left(\frac{\pi}{2}\bar{\bar{d}}_i\right)\sin\left(\frac{\pi}{2}C\right)\right)^2. \tag{C.3}$$

Note that for $C = 0$ or even integer $f(\bar{\bar{d}}_i, \tilde{\bar{\nu}}_i^\varepsilon) = 2\sin^2(\frac{\pi\bar{\bar{d}}_i L}{4N}\varepsilon)$ and for $C = 1$ or any other uneven integer $f(\bar{\bar{d}}_i, \tilde{\bar{\nu}}_i^\varepsilon) = 2\cos^2(\frac{\pi\bar{\bar{d}}_i L}{4N}\varepsilon)$. Hence, it is sufficient that in the following analysis I consider $C \in \{0, 1\}$. In order to select the maximum value I use the second

derivative test, i.e.,

$$\left.\frac{\mathbf{d}^2 f^{\varepsilon}(\bar{\bar{d}}_i, \bar{\nu}_i^{\varepsilon})}{\mathbf{d}(\bar{\nu}_i^{\varepsilon})^2}\right|_{\bar{\nu}_i^{\varepsilon} = \tilde{\bar{\nu}}_i^{\varepsilon}} = 4 \left.\left(\frac{\mathbf{d}B}{\mathbf{d}\bar{\nu}_i^{\varepsilon}}\right)^2\right|_{\bar{\nu}_i^{\varepsilon} = \tilde{\bar{\nu}}_i^{\varepsilon}} \cos\left(\frac{\pi \bar{\bar{d}}_i L}{2N}\varepsilon\right) \cos(C\pi). \qquad (C.4)$$

The first term is always positive under the assumption that $\bar{\bar{d}}_i \neq 0$. Therefore, I find offsets $\bar{\nu}_i^{*\varepsilon}$ and consequently $f^{*\varepsilon}(\bar{\bar{d}}_i) = f(\bar{\bar{d}}_i, \bar{\nu}_i^{*\varepsilon})$ by analyzing the sign of the cosine terms in different quadrants as done in (4.18). For overlapping tones I have $\bar{d}_i = 0$ and applying $\lim_{x\to 0} \frac{\sin^2(ax)}{\sin^2(bx)} = \frac{a^2}{b^2}$ in (4.13b) it follows that $\left.\frac{f(\bar{\bar{d}}_i, \bar{\nu}_i^{*\varepsilon})}{\sin^2(\frac{\pi \bar{d}_i}{2N})}\right|_{\bar{\bar{d}}_i \to 0} = \varepsilon^2$.

BIBLIOGRAPHY

[1] A. Holley. Broadband copper cable models (TR-285). Technical report, Broadband Forum, February 2015.

[2] A. Carrick and T. Bongrad. G.fast: Dual slope ELFEXT behaviour on Swiss cabels. ITU-T Study Group 15/Q4a, Contribution 2013-01-4A-042, Geneva, Switzerland, January 2013.

[3] B. van den Heuvel, P. Trommelen, and R. F. M. van den Brink. G.fast: Preliminary analysis of the transfer characteristics of the 104 m KPN access cable. ITU-T Study Group 15/Q4a, Contribution 2013-03-Q4-026, Red Bank, New Jersey, March 2013.

[4] J. R. Schneir and Y. Xiong. Cost assessment of FTTdp networks with G.fast. *IEEE Communications Magazine*, 54(8):144–152, August 2016.

[5] J. R. Schneir and Y. Xiong. Cost analysis of network sharing in FTTH/PONs. *IEEE Communications Magazine*, 52(8):126–134, August 2014.

[6] P. Ödling, T. Magesacher, S. Höst, P. O. Börjesson, M. Berg, and E. Areizaga. The fourth generation broadband concept. *IEEE Communications Magazine*, 47(1):62–69, January 2009.

[7] ITU-T. Fast access to subscriber terminals (G.fast) - Physical layer specification. Study Group 15/, ITU-T Recommendation G.9701, Geneva, Switzerland, December 2014.

[8] ITU-T. Fast access to subscriber terminals (G.fast) - Power spectral density specification. Study Group 15, ITU-T Recommendation G.9700, Geneva, Switzerland, April 2014.

[9] V. Oksman, R. Strobel, X. Wang, D. Wei, R. Verbin, R. Goodson, and M. Sorbara. The ITU-T's new G.fast standard brings DSL into the gigabit era. *IEEE Communications Magazine*, 54(3):118–126, March 2016.

[10] J. Neckebroek, M. Moeneclaey, W. Coomans, M. Guenach, P. Tsiaflakis, R. B. Moraes, and J. Maes. Novel bitloading algorithms for coded G.fast DSL transmission with linear and nonlinear precoding. In *IEEE International Conference on Communications (ICC)*, pages 945–951, London, UK, June 2015.

[11] R. Strobel, A. Barthelme, and W. Utschick. Zero-Forcing and MMSE Precoding for G.fast. In *IEEE Global Communications Conference (GLOBECOM)*, pages 1–6, San Diego, California, USA, December 2015.

[12] M. Timmers, M. Guenach, C. Nuzman, and J. Maes. G.fast: evolving the copper access network. *IEEE Communications Magazine*, 51(8):74–79, August 2013.

[13] L. Humphrey. G.fast: On dual slope fext observations. ITU-T Study Group 15/Q4a, Contribution 2012-05-4A-021, Geneva, Switzerland, May 2012.

[14] R. F. M. van den Brink and B. van den Heuvel. G.fast: Dual slope behaviour of EL-FEXT. ITU-T Study Group 15/Q4a, Contribution 2012-02-4A-038, Geneva, Switzerland, February 2011.

[15] BT plc. G.fast: Release of BT cable (20 pair) measurements for use in simulations). ITU-T Study Group 15/Q4, Contribution TD-2015-02-Q4-053, Geneva, Switzerland, February 2015.

[16] D. Statovci, T. Magesacher, M. Wolkerstorfer, and E. Medeiros. Analysis of fast initialization for vectored wireline systems. In *IEEE Global Communications Conference (GLOBECOM)*, pages 2846–2851, Houston, Texas, USA, December 2013.

[17] E. Medeiros, T. Magesacher, P. Ödling, D. Wei, X. Wang, Q. Li, P. E. Eriksson, C. Lu, J. Boschma, and B. van den Heuvel. Modeling alien-line impedance mismatch in wideband vectored wireline systems. *IEEE Communications Letters*, 18(9):1527–1530, September 2014.

[18] Y. Huang, T. Magesacher, E. Medeiros, C. Lu, P. E. Eriksson, and P. Ödling. Mitigating disorderly leaving events in G.fast. In *IEEE International Conference on Communications (ICC)*, pages 939–944, London, UK, June 2015.

[19] AR. Forouzan, M. Moonen, J. Maes, and M. Guenach. Joint Level 2 and 3 Dynamic Spectrum Management for Downstream DSL. *IEEE Transactions on Communications*, 60(10):3111–3122, October 2012.

[20] AR. Forouzan, M. Moonen, J. Maes, and M. Guenach. Joint Level 2 and 3 Dynamic Spectrum Management for Upstream VDSL. *IEEE Transactions on Communications*, 59(10):2851–2861, October 2011.

[21] J. Maes, M. Guenach, M. B. Ghorbel, and B. Drooghaag. Managing unvectored lines in a vectored group. In *IEEE Global Communications Conference (GLOBECOM)*, pages 2840–2845, Atlanta, Texas, USA, December 2013.

[22] ITU-T. Very high speed digital subscriber line transcievers (VDSL2). Study Group 15, ITU-T Recommendation G.993.2, Geneva, Switzerland, July 2002.

[23] M. Guenach, J. Meas, M. Timmers, O. Lamparter, J. C. Bischoff, and M. Peeters. Vectoring in DSL Systems: Practices and Challenges. In *IEEE Global Telecommunications Conference (GLOBECOM)*, pages 1–6, Houston, Texas, USA, December 2011.

[24] F. Mazzenga, R. Giuliano, M. Petracca, M. Vari, and F. Vatalaro. A Downstream Power Back-Off Procedure for Mixed FTTC and FTTDp Scenarios. *IEEE Communications Letters*, 18(6):965–968, June 2014.

[25] D. Acatauassú, M. Monteiro, F. Müller, and A. Klautau. Experimental evaluation of fourth generation DSL in different DSM scenarios. In *IEEE Latin-American Conference on Communications*, pages 1–6, Belem, Brazil, October 2011.

[26] M. Kuipers and F. Chu. G.fast: Flexible start frequencies and PSD shaping. ITU-T Study Group 15/Q4a, Contribution 2013-05-Q4-069, Geneva, Switzerland, May 2013.

[27] M. Tilocca, F. Marigliano, T. Starr, H. Mariotte, J. Guy, D. Tjernberg, W. Bo, and G. Clerckx. G.fast:Multi-operators requirements for G.fast. ITU-T Study Group 15/Q4a, Contribution 2012-05-4A-033, Geneva, Switzerland, May 2015.

[28] L. Humphrey and A.Mohsin. G.fast: Immunity of VDSL2 to out of band interference from G.fast. ITU-T Study Group 15/Q4a, Contribution 2014-10-Q4-027, Geneva, Switzerland, October 2014.

[29] ITU-T. Integrated services digital network (ISDN). Study Group 13, ITU-T Recommendation I.120, Helsinki, Finland, March 1993.

[30] ITU-T. Asymmetric digital subscriber line (ADSL) transceivers. Study Group 15, ITU-T Recommendation G.992.1, Geneva, Switzerland, July 1999.

[31] ITU-T. Asymmetric digital subscriber line 2 (ADSL2) transceivers. Study Group 15, ITU-T Recommendation G.992.3, Geneva, Switzerland, July 2002.

[32] ITU-T. Asymmetric digital subscriber line 2 transceivers (ADSL2)- Extended bandwidth ADSL2 (ADSL2plus). Study Group 15, ITU-T Recommendation G.992.5, Geneva, Switzerland, May 2003.

[33] ITU-T. Very high speed digital subscriber line transceivers (VDSL). Study Group 15, ITU-T Recommendation G.993.1, Geneva, Switzerland, June 2004.

[34] ITU-T. Self-FEXT cancellation (vectoring) for use with VDSL2 transceivers. Study Group 15, ITU-T Recommendation G.993.5, Geneva, Switzerland, January 2015.

[35] W. Coomans, R. B. Moraes, K. Hooghe, and J. Maes. The 5th Generation Broadband Copper Access. In *ITG Symposium: Broadband Coverage in Germany*, pages 1–5, Berlin, Germany, April 2015.

[36] D. Acatauassú, F. C. B. F. Müller, and A. Klautau. Capacity of MIMO DSL systems using 100 MHz measured channel data. In *IEEE International Conference on Telecommunications (ICT)*, pages 266–269, Marrakech, Morocco, May 2009.

[37] J. Maes, M. Guenach, K. Hooghe, and M. Timmers. Pushing the limits of copper: Paving the road to FTTH. In *IEEE International Conference on Communications (ICC)*, pages 3149–3153, Ottawa, Canada, June 2012.

[38] G. Marrocco, M. Wolkerstorfer, T. Nordström, and D. Statovci. Energy-efficient dsl using vectoring. In *IEEE Global Telecommunications Conference (GLOBECOM)*, pages 1–6, Houston, Texas, USA, December 2011.

[39] K. Kerpez and M. Mohseni. G.fast: Signal processing for the G.fast 212 MHz profile. ITU-T Study Group 15/Q4a, Contribution 2016-04-Q4-024,Geneva, Switzerland, April 2016.

[40] S. Singh and M. Sorbara. G.fast: 212 MHz simulations with non-linear pre-coding. ITU-T Study Group 15/Q4a, Contribution 2016-06-Q4-052, Geneva, Switzerland, June 2016.

[41] V. Oksman. G.fast:use of linear precoding on frequencies above 106 MHz. ITU-T Study Group 15/Q4a, Contribution 2016-05-Q4-023, Geneva, Switzerland, May 2016.

[42] V. Oksman and R. Strobel. G.fast:comparing guaranteed bit rates for linear and non-linear precoding. ITU-T Study Group 15/Q4a, Contribution 2016-06-Q4-063R1, Geneva, Switzerland, June 2016.

[43] V. Oksman and R. Strobel. G.fast:rate-reach comparison for linear and non-linear precoding up to 212 MHz. ITU-T Study Group 15/Q4a, Contribution 2016-06-Q4-072R, Geneva, Switzerland, June 2016.

[44] D. Van Bruyssel and J. Maes. G.fast: Perspectives on nonlinear precoding. ITU-T Study Group 15/Q4a, Contribution 2016-06-Q4-041, Geneva, Switzerland, June 2016.

[45] D. Van Bruyssel and J. Maes. G.fast:comparison of linear and non-linear precoding. ITU-T Study Group 15/Q4a, Contribution 2013-01-Q4-046, Geneva, Switzerland, January 2013.

[46] D. Van Bruyssel and J. Maes. G.fast:perspectives on nonlinear precoding. ITU-T Study Group 15/Q4a, Contribution 2016-06-Q4-041, Geneva, Switzerland, June 2016.

[47] R. Strobel and W. Utschick. Coexistence of G.fast and VDSL in FTTdp and FTTC Deployments. In *European Signal Processing Conference (EUSIPCO)*, pages 1103–1107, Nice, France, August 2015.

[48] M. Guenach, C. Nuzman, P. Tsiaflakis, and J. Maes. Power optimization in vectored and non-vectored G.fast transmission. In *IEEE Global Communications Conference (GLOBECOM)*, pages 2229–2233, Austin, Texas, USA, December 2014.

[49] F. C. B. F. Müller, C. Lu, P. E. Eriksson, S. Höst, and A. Klautau. Optimizing power normalization for G.fast linear precoder by linear programming. In *IEEE International Conference on Communications (ICC)*, pages 4160–4165, Sydney, Australia, June 2014.

[50] R. Strobel, M. Joham, and W. Utschick. Achievable rates with implementation limitations for G.fast-based hybrid copper/fiber networks. In *IEEE International Conference on Communications (ICC)*, pages 958–963, London, UK, June 2015.

[51] W. Lanneer, M. Moonen, P. Tsiaflakis, and J. Maes. Linear and Nonlinear Precoding Based Dynamic Spectrum Management for Downstream Vectored G.fast Transmission. In *IEEE Global Communications Conference (GLOBECOM)*, pages 1–6, San Diego, California, USA, December 2015.

[52] M. Hekrdla, A. Matera, W. Wang, D. Wei, and U. Spagnolini. Ordered Tomlinson-Harashima Precoding in G.fast Downstream. In *IEEE Global Communications Conference (GLOBECOM)*, pages 1–6, San Diego, California, USA, December 2015.

[53] D. Wei, A. Fazlollahi, G. Long, and E. Wang. G.fast for FTTdp: Enabling gigabit copper access. In *IEEE Globecom Workshops (GC Workshops)*, pages 668–673, Austin, Texas, USA, December 2014.

[54] J. Maes, C. Nuzman, and P. Tsiaflakis. Sensitivity of nonlinear precoding to imperfect channel state information in G.fast. In *European Signal Processing Conference (EUSIPCO)*, pages 290–294, Budapest, Hungary, August 2016.

[55] S. Huberman and T. Le-Ngoc. Interference alignment for DSL. In *IEEE Global Communications Conference (GLOBECOM)*, pages 3092–3097, Anaheim, California, USA, Dec 2012.

[56] H. E. Khaleqdadi, A. R. Forouzan, and M. F. Sabahi. On interference alignment for crosstalk mitigation in VDSL2. In *Iranian Conference on Electrical Engineering (ICEE)*, pages 51–55, Teheran, Iran, May 2016.

[57] V. M. K. Chan and W. Yu. Multiuser spectrum optimization for discrete mutltitone systems with asynchronous crosstalk. *IEEE Transactions on Signal Processing*, 55:5425–5435, November 2007.

[58] R. B. Moraes, P. Tsiaflakis, and M. Moonen. Intercarrier interference in DSL networks due to asynchronous DMT transmission. In *IEEE International Conference on Acoustics, Speech and Signal Processing (ICASSP)*, pages 4678–4682, Vancouver, Canada, May 2013.

[59] S. Schelstraete. Frequency domain crosstalk canceling between VDSL2 systems with different symbol rates. In *IEEE Sensor Array and Multichannel Signal Processing Workshop (SAM)*, pages 221–224, Jerusalem, Israel, October 2010.

[60] Wen-Sheng Hou and Bor-Sen Chen. ICI cancellation for OFDM communication systems in time-varying multipath fading channels. *IEEE Transactions on Wireless Communications*, 4:2100–2110, September 2005.

[61] H. Steendam and M. Moeneclaey. Analysis and optimization of the performance of OFDM on frequency-selective time-selective fading channels. *IEEE Transactions on Communications*, 47:1811–1819, December 1999.

[62] A. Stamoulis, S. N. Diggavi, and N. Al-Dhahir. Estimation of fast fading channels in OFDM. In *IEEE Wireless Communications and Networking Conference (WCNC)*, volume 1, pages 465–470, Orlando, Florida, USA, Mar 2002.

[63] Ye Li and L. J. Cimini. Bounds on the interchannel interference of OFDM in time-varying impairments. *IEEE Transactions on Communications*, 49:401–404, March 2001.

[64] M. Russell and G. L. Stuber. Interchannel interference analysis of OFDM in a mobile environment. In *IEEE Vehicular Technology Conference (VTC)*, volume 2, pages 820–824, Chicago, Illinois, USA, July 1995.

[65] G. Scutari, D.P. Palomar, and S. Barbarossa. Distributed Totally Asynchronous Iterative Waterfilling for Wideband Interference Channel with Time/Frequency Offset. In *IEEE International Conference on Acoustics, Speech and Signal Processing (ICASSP)*, volume 4, pages IV–1325–IV–1328, Honolulu, Hawaii, USA, April 2007.

[66] M. Sliskovic. Carrier and sampling frequency offset estimation and correction in multicarrier systems. In *IEEE Global Telecommunications Conference (GLOBECOM)*, volume 1, pages 285–289, San Antonio, Texas, USA, 2001.

[67] A.M. Tonello, N. Laurenti, and S. Pupolin. Analysis of the uplink of an asynchronous multi-user DMT OFDMA system impaired by time offsets, frequency offsets, and multi-path fading. In *Vehicular Technology Conference (VTC)*, volume 3, pages 1094–1099, Boston, Massachusetts, USA, September 2000.

[68] M. Park, K. Ko, B. Park, and D. Hong. Effects of asynchronous MAI on average SEP performance of OFDMA uplink systems over frequency-selective Rayleigh fading channels. *IEEE Transactions on Communications*, 58(2):586–599, February 2010.

[69] F. Horlin, S. De Rore, E. Lopez-Estraviz, F. Naessens, and L. Van der Perre. Impact of frequency offsets and IQ imbalance on MC-CDMA reception based on channel tracking. *IEEE Journal on Selected Areas in Communications*, 24:1179–1188, June 2006.

[70] K. Sathananthan and C. Tellambura. Probability of error calculation of OFDM systems with frequency offset. *IEEE Transactions on Communications*, 49:1884–1888, November 2001.

[71] Yuping Zhao and S. G. Haggman. Intercarrier interference self-cancellation scheme for OFDM mobile communication systems. *IEEE Transactions on Communications*, 49:1185–1191, July 2001.

[72] J. Armstrong. Analysis of new and existing methods of reducing intercarrier interference due to carrier frequency offset in OFDM. *IEEE Transactions on Communications*, 47:365–369, March 1999.

[73] G. Cherubini, E. Eleftheriou, S. Oker, and J. M. Cioffi. Filter bank modulation techniques for very high speed digital subscriber lines. *IEEE Communications Magazine*, 38(5):98–104, May 2000.

[74] W. Henkel, G. Tauböck, P. Ödling, P. O. Börjesson, and N. Petersson. The cyclic prefix of OFDM/DMT - an analysis. In *International Zurich Seminar on Broadband Communications Access - Transmission - Networking*, pages 22–1–22–3, Zurich, Switzerland, May 2002.

[75] P. Golden, H. Dedieu, and K.S. Jacobsen, editors. *Fundamentals of DSL technology*. Auerbach Publications, 2006.

[76] R. F. M. van den Brink. Cable reference models for simulating metallic access networks. Technical report, ETSI STC TM6 Permanent document, TM6(97)02, June 1998.

[77] L. Humphrey and T. Morsman. Cable models. ITU-T Study Group 15/Q4a, Contribution 11RV-026R2, Richmond, Virginia, USA, October 2011.

[78] M. Wolkerstorfer and D. Statovci. Preliminary study on coexistence in fourth-generation DSL networks (FTW-TR-147). Technical report, Forschungszentrum Telekommunikation Wien (FTW), June 2015.

[79] P. Tsiaflakis, M. Diehl, and M. Moonen. Distributed Spectrum Management Algorithms for Multiuser DSL Networks. *IEEE Transactions on Signal Processing*, 56(10):4825–4843, October 2008.

[80] Z. Q. Luo and S. Zhang. Dynamic Spectrum Management: Complexity and Duality. *IEEE Journal of Selected Topics in Signal Processing*, 2(1):57–73, February 2008.

[81] W. Yu, G. Ginis, and J. M. Cioffi. Distributed multiuser power control for digital subscriber lines. *IEEE Journal on Selected Areas in Communications*, 20(5):1105–1115, June 2002.

[82] E. Van den Bogaert, T. Bostoen, J. Van Elsen, R. Cendrillon, and M. Moonen. DSM in practice: iterative water-filling implemented on ADSL modems. In *IEEE International Conference on Acoustics, Speech, and Signal Processing (ICASSP)*, volume 5, pages V–337–40, Florence, Italy, May 2004.

[83] R. Cendrillon, Wei Yu, M. Moonen, J. Verlinden, and T. Bostoen. Optimal multiuser spectrum balancing for digital subscriber lines. *IEEE Transactions on Communications*, 54(5):922–933, May 2006.

[84] S. Huberman, C. Leung, and T. Le-Ngoc. Dynamic Spectrum Management (DSM) Algorithms for Multi-User xDSL. *IEEE Communications Surveys Tutorials*, 14(1):109–130, January 2012.

[85] R. Cendrillon and M. Moonen. Iterative spectrum balancing for digital subscriber lines. In *IEEE International Conference on Communications (ICC)*, volume 3, pages 1937–1941, Seoul, Korea, May 2005.

[86] G. Ginis and J. M. Cioffi. A multi-user precoding scheme achieving crosstalk cancellation with application to DSL systems. In *Asilomar Conference on Signals, Systems and Computers*, volume 2, pages 1627–1631, Pacific Grove, California, USA, October 2000.

[87] G. Ginis and J. M. Cioffi. Vectored-DMT: a FEXT canceling modulation scheme for coordinating users. In *IEEE International Conference on Communications (ICC)*, volume 1, pages 305–309, Helsinki, Finland, June 2001.

[88] R. Cendrillon, G. Ginis, E. Van den Bogaert, and M. Moonen. A Near-Optimal Linear Crosstalk Canceler for Upstream VDSL. *IEEE Transactions on Signal Processing*, 54(8):3136 – 3146, August 2006.

[89] R. Cendrillon, G. Ginis, E. Van den Bogaert, and M. Moonen. A Near-Optimal Linear Crosstalk Precoder for Downstream VDSL. *IEEE Transactions on Communications*, 55(5):860–863, May 2007.

[90] ITU-T. Updated draft text for G.fast - version 11.0. ITU-T Study Group15/Q4a, Contribution 2013-12-Q4-R20R6, Geneva, Switzerland, December 2013.

[91] S. Drakulić, D. Statovci, and M. Wolkerstorfer. Performance of linear crosstalk cancelation in fourth generation wired broadband access networks. In *European Signal Processing Conference (EUSIPCO)*, pages 1–5, Marrakesh, Morroco, September 2013.

[92] S. Drakulić, D. Statovci, M. Wolkerstorfer, and T. Zemen. Comparison of interference mitigation techniques for next generation DSL systems. In *2015 IEEE International Conference on Communications (ICC)*, London, UK, June 2015.

[93] Wei Yu and J. M. Cioffi. Multiuser detection for vector multiple access channels using generalized decision feedback equalization. In *International Conference on*

Signal Processing (ICSP), volume 3, pages 1771–1777, Beijing, China, September 2000.

[94] G. Ginis and J. M. Cioffi. A multi-user precoding scheme achieving crosstalk cancellation with application to DSL systems. In *Asilomar Conference on Signals, Systems and Computers*, volume 2, pages 1627–1631, Pacific Grove, California, USA, October 2000.

[95] V.R. Cadambe and S.A. Jafar. Interference Alignment and Degrees of Freedom of the K-User Interference Channel. *IEEE Transactions on Information Theory*, 54(8):3425–3441, August 2008.

[96] K. Gomadam, V.R. Cadambe, and S.A Jafar. Approaching the Capacity of Wireless Networks through Distributed Interference Alignment. In *IEEE Global Telecommunications Conference (GLOBECOM)*, pages 1–6, New Orleans, Louisiana, USA, November 2008.

[97] R. Brandt, H. Asplund, and M. Bengtsson. Interference alignment in frequency - A measurement based performance analysis. In *International Conference on Systems, Signals and Image Processing (IWSSIP)*, pages 227–230, Vienna, Austria, April 2012.

[98] M. Sorbara, P. Duvaut, F. Shmulyian, S. Singh, and A Mahadevan. Construction of a DSL-MIMO channel model for evaluation of FEXT cancellation systems in VDSL2. In *IEEE Sarnoff Symposium*, pages 1–6, Princeton, New Jersey, USA, April 2007.

[99] M. Wolkerstorfer, D. Statovci, and S. Drakulić. Maintaining harmony in the vectoring xDSL family by spectral coordination. In *Asilomar Conference on Signals, Systems and Computers*, pages 1739–1743, Pacific Grove, California, USA, November 2015.

[100] ITU-T. Very high speed digital subscriber line transceivers 2 (VDSL2). Study Group 15, ITU-T Recommendation G.993.2, Geneva, Switzerland, July 2002.

[101] P. E. Eriksson, C. Lu, and I. Pappa. Performance study on using linear precoding (vectoring) for high frequency DSL. ITU-T Study Group 15/Q4a, Contribution COM15-C 1489-E, Geneva, Switzerland, February 2011.

[102] S. Drakulić, M. Wolkerstorfer, and D. Statovci. Coexistence analysis of asynchronous digital subscriber lines with different sampling rate and carrier frequency spacing. In *IEEE Global Communications Conference (GLOBECOM)*, pages 2234–2239, Austin, Texas, USA, December 2014.

[103] S. Drakulić, M. Wolkerstorfer, and D Statovci. Coexistence in fourth generation DSL broadband networks: Modeling and simulation results. submitted to *IEEE Transactions on Communications*, December 2016.

[104] Olmos J. Serra, A. and M.A Lema. Modelling channel estimation error in lte link level simulations. In *Scientific meeting on Cooperative radio communications for green smart environments (COST IC1004)*, Barcelona, Spain, February 2012.

[105] J. C. Ikuno, S. Pendl, M.Šimko, and M. Rupp. Accurate SINR estimation model for system level simulation of LTE networks. In *IEEE International Conference on Communications (ICC)*, pages 1471–1475, Ottawa, Canada, June 2012.

[106] R. GareUo M. Polano M. Baldi, F. Chiaraluce and M. Valentini. Simple statistical analysis of the impact of some nonidealities in downstream VDSL with linear precoding. 1:285–289, September 2010.

[107] P. Silverman. Techniques to Mitigate Uncancelled Crosstalk on Vectored VDSL2 Lines (TR-320). Technical report, Broadband Forum, March 2014.

[108] R. B. Moraes, P. Tsiaflakis, J. Maes, and M. Moonen. DMT MIMO IC Rate Maximization in DSL With Combined Signal and Spectrum Coordination. *IEEE Transactions on Signal Processing*, 61(7):1756–1769, April 2013.

[109] Jungwon Lee, R. V. Sonalkar, and J. M. Cioffi. Multi-user discrete bit-loading for DMT-based DSL systems. In *IEEE Global Telecommunications Conference (GLOBECOM)*, volume 2, pages 1259–1263, Taipei, Taiwan, November 2002.

[110] A. Carrick and T. Bongard. G.fast: Considerations regarding the choice of the duplexing scheme. ITU-T Study Group 15/Q4a Contribution, 11RV-025, Richmond, Virginia, USA, November 2011.